Ph.D. Dissertation of Engineering

A Study on the Probabilistic Determination of Gas Cloud Characteristics for Explosion Risk Analysis of Offshore Topside Process Area

해양 플랫폼 상부 공정 영역의 폭발 위험도 해석을 위한 가스 구름 특성의 확률론적 결정에 관한 연구

February 2019

Graduate School of Engineering
Seoul National University
Naval Architecture & Ocean Engineering

JIN YANLIN

A Study on the Probabilistic Determination of Gas Cloud Characteristics for Explosion Risk Analysis of Offshore Topside Process Area

해양 플랫폼 상부 공정 영역의 폭발 위험도 해석을 위한 가스 구름 특성의 확률론적 결정에 관한 연구

지도교수 장 범 선

이 논문을 공학박사 학위논문으로 제출함
2019년 2월

서울대학교 대학원
조선해양공학과
YanLin Jin

YanLin Jin 의 공학박사 학위논문을 인준함
2019년 2월

위 원 장 _____ 임 영섭 _____ (인)

부위원장 _____ 장 범선 _____ (인)

위 원 _____ 서 정관 _____ (인)

위 원 _____ 김 성희 _____ (인)

위 원 _____ 류 용희 _____ (인)

Abstract

Explosion risk analysis (ERA) is known as one of the dedicated safety studies for offshore installations and its purpose is to evaluate the explosion design accidental loads (DALs) on offshore topside structures and facilities. In general, ERA is more likely to be implemented in a probabilistic manner because it has a problem that needs to deal with a large number of explosion scenarios. In the probabilistic ERA, flammable gas cloud frequency distribution is a kind of intermediate result, which can be obtained by integrating the results of frequency analysis and gas dispersion modeling. In general, the distribution is applied to investigate a certain number of representative explosion scenarios to evaluate exceedance curves, which are commonly used to determine the DALs.

The use of Computational Fluid Dynamics (CFD) to perform the gas dispersion and associated ignition probability modeling has become a trend in recent offshore projects. In most cases, however, the gas cloud frequency distribution has not yet fully benefited from the CFD models due to the high computing costs. Therefore, the distribution is generally derived only using some particular values rather than reflecting the overall results of the CFD simulations. As a matter of fact, the consequences of explosion accidents may vary greatly, depending on variables such as ignition position, gas cloud size, position and shape etc. So far, except for the gas cloud size that can be provided by the gas cloud frequency distribution, the remaining variables are more likely to be determined by engineering

judgment and experience. Though this process follows standard guidelines or recommended practices, the determined variables can vary widely depending on engineers.

In view of this, the current research aims to develop a new type of gas cloud frequency distribution that not only reflects the overall results of the CFD simulations performed with the time-varying leak rates, but also provides the information of gas cloud position to investigate the explosion scenarios. With regard to the new distribution, a method of determining the shape of the gas cloud is also proposed in this study. Taking into account all actual gas clouds obtained from the CFD dispersion simulations, it is possible to determine a shaped equivalent gas cloud for each investigated explosion scenario. Details on how to derive the proposed distribution as well as the way to determine the shaped equivalent gas cloud is provided in this thesis. Several case studies are performed, and the limitations of the existing approach is manifested. The case studies have shown that it is important to consider the entire gas clouds shown in the dispersion simulation results and that the position and shape of the gas cloud determined by the proposed method can improve the ERA results.

Keyword : Explosion risk analysis, gas cloud frequency distribution, CFD, gas cloud position, gas cloud shape.

Student Number : 2014-30854

List of Contents

List of Figure

List of Table

NOMENCLATURE

E : Overpressure error of control volume (CV)

ER : Equivalence ratio

f_{ign} : Individual frequency (or frequency of ignited gas cloud) [/yr]

f_{leak} : Frequency of leak scenario [/yr]

f_{exp} : Explosion frequency [/yr]

F_{ESC} : Weighting factor used to calculate equivalent stoichiometric gas cloud

m_{oxygen} : Mass of oxygen [kg]

m_{fuel} : Mass of fuel [kg]

m_{cv} : Fuel mass of CV [kg]

m_c : Fuel mass of joint category [kg]

$m_{eq,s}$: Fuel mass for selected CVs [kg]

$m_{eq,tot}$: Total fuel mass for selected CVs [kg]

M : Molecular weight [kg/mole]

$MoleF$: Mole fraction of fuel in CV [mole/mole]

$MassF$: Mass fraction of fuel in CV [kg/kg]

n_V : The number of categories for gas cloud size

n_X : The number of categories for position in x direction

n_Y : The number of categories for position in y direction

n_Z : The number of categories for position in z direction

n_{ls} : The number of leak scenario

n_t : The number of time interval Δt

P_{eq} : Calculated equivalent overpressure [barg]

$\hat{P}_{eq}$: Simulated equivalent overpressure [barg]

$PORV$: Porosity

P_{ign} : Ignition probability

P_{del} : Delayed ignition probability

P_{imm} : Immediate ignition probability

P_C : Continuous ignition probability

P_D : Discrete ignition probability

ΔP_{ign} : Incremental ignition probability

S_L : Laminar flame speed (or burning velocity) [m/s]

S : Severity

T : Temperature [K]

t : Time [s]

V_{oxygen} : Volume of oxygen [m^3]

V_{fuel} : Volume of fuel [m^3]

V_{ac}^{es} : Equivalent stoichiometric volume of actual gas cloud [m^3]

V_{ac} : Volume of actual gas cloud [m^3]

V_c : Volume of equivalent stoichiometric gas cloud for cloud size category [m^3]

V_{cv} : Volume of CV [m^3]

V_{Cv}^{es} : Equivalent stoichiometric volume of CV [m^3]

$V_{eq,s}^{es}$: Equivalent stoichiometric volume for selected CVs (or shaped equivalent gas cloud) [m^3]

$V_{eq,tot}^{es}$: Total equivalent stoichiometric volume for selected CVs [m^3]

V_e : Volume expansion ratio

$[X]$: Volumetric center of control volume

$[X]_C$: Volumetric center of equivalent stoichiometric gas cloud

X : Variable for x coordinate

Y : Variable for y coordinate

Z : Variable for z coordinate

Chapter 1. Introduction

1.1. Research Background

[1]Flammable hydrocarbon leaks from offshore topside process areas can lead to explosive gas clouds, which are a major threat to offshore facilities due to destructive explosions. In general, quantitative risk assessment (QRA) is a primary option systematically identify all credible scenarios, including the process leaks, and to evaluate overall risk to human, environment and assets. Some previous studies related to the QRA of vapour cloud explosion are addressed by Khan et al. (2002); Rathnayaka et al. (2011a,b); Dan et al. (2014); Villa et al. (2016). In parallel with the QRA, however, a suite of independent risk analysis studies is conventionally carried out at the stage of project phases to provide direct inputs such as design accidental loads (DALs) for engineering design development (Total, 2011). Typically, these studies include fire risk analysis (FRA), explosion risk analysis (ERA), dropped object analysis, emergency escape, evacuation risk analysis (EERA) and so on. Due to a large number of scenarios, the ERA has been usually carried out in a probabilistic manner.

Depending on the project phases, the methodology of ERA for on/offshore process platforms can be separated into two ways, and each of them has its own capabilities and limitations. In the early stages of offshore projects, the amount of available data is scarce and hence a sophisticated consequence modelling is restrained as it requires the input of geometry details (Alghamdi, 2011). In most

[1] This chapter originates from published work (Jin and Jang, 2018a; Jin and Jang, 2018b)

cases, the ERA at this stage is carried out based on empirical or phenomenological models (HSE, 2002), but the accuracy is relatively low. This is because these models are generally lack of fundamental physics and failed to represent high-level geometry details. Nevertheless, the models have very short computing times, which implies that a huge number of explosion scenarios can be modelled quickly (HSE, 2002), and furthermore the ERA can be carried out repeatedly with various options to find an optimal design. Alonso et al. (2006) used the empirical models to develop the characteristic overpressure impulse distance curves for vapour cloud explosions. Li et al. (2014) proposed a new correlation for the empirical models using the validated CFD models. Pula et al. (2006) proposed a grid-based approach to enable better consequence and impact modelling of blast overpressures using the empirical models. Alghamdi (2011) developed an ERA methodology which adopts the empirical models to consider all credible scenarios through the use of Monte Carlo simulation, and investigated the impact of the number of leak locations and leak rate categories considered in the ERA. In addition, Ramírez-Marengo et al. (2015) proposed a similar methodology which includes probit functions to estimate the damage to humans and near buildings. Park et al. (2018) also used the empirical models to perform the ERA, and investigated structural safety of topside modules against potential VCEs.

On the contrary, a large amount of data is available in detailed design phases, which enables sophisticated consequence modelling such as CFD based gas dispersion and explosion analyses. Studies on detailed prediction of gas cloud formation and overpressure with the CFD models have been performed by Tauseef et al. (2011);

Dadashzadeh et al. (2013, 2016) ; Hansen et al. (2016). Due to the more accurate representation of underlying physics and geometry details, the capabilities of the CFD models are comparable to the actual experiment. There are many CFD models available for explosion consequence modelling in on/offshore process areas. One typical model is FLACS (Gexcon, 2015), which has been widely used and validated in previous studies (Hansen et al., 2013; Dadashzadeh et al., 2013; Azzi et al., 2016; Gupta and Chan, 2016). However, there is a heavy demand for commutating costs when using the CFD models. Although memory / processor constraints become less of an issue, it is still challenging to deal with a huge number of explosion scenarios as they are computationally expensive. As a result, all possible scenarios cannot not be considered individually, but are more often considered using categorization approaches (Alghamdi, 2011). In addition, since the decisions related to design modifications are costly at later phases of the projects, the ERA may have little impact on design engineering, which seems paradoxical in some ways.

A typical methodology of CFD-based ERA was proposed by Hansen et al. (1999), where the authors intend to bring more accurate CFD calculations into ERA in a consistent way and propose an easy-to-follow methodology that can provide fully transparent intermediate results and considerations. In this work, in order to reduce the computational effort while keeping the accuracy of the CFD models, an important concept of flammable gas cloud frequency distribution was proposed. The most significant point of this concept is that the original huge explosion scenarios can be replaced by a few representative scenarios that are probabilistically determined from the distribution. Many studies and improvements

with respect to the methodology were carried out later by Talberg et al. (2000) and (2001); Bakke and Hansen (2003); Hoorelbeke et al. (2006); Hansen and Middha (2007); Davis et al. (2011); Hansen et al. (2013); Azzi et al. (2016). These literature includes various ERA applications for different target on/offshore process areas. In view of those previous studies, however, some efforts may still be made to improve the method with regard to investigating the explosion scenarios and this motivates the current study.

In general, deriving the flammable gas cloud frequency distribution is a complex process and accounts for half of the total ERA. This involves frequency analysis, gas dispersion consequence analysis and ignition probability modelling. The gas dispersion consequence analysis requires leak scenarios as input, but the number of the leak scenarios in the real world is as tremendous as the explosion scenarios. In the CFD-based ERA methodology, the leak scenarios are identified as several to compensate for the commutating costs of the CFD models, but which may still be quite time-consuming as they need to cover a relative long physical time-span of leakage. To reduce the heavy computing costs involved in deriving the flammable gas cloud frequency distribution, in most previous studies (Talberg et al., 2000, 2001; Hoorelbeke et al., 2006; Hansen and Middha, 2007; Davis et al., 2011; Azzi et al., 2016), the gas dispersion analysis is carried out by using some simplified approaches (Gupta and Chan, 2016). However, these simplified approaches usually ignore a detailed transient footprint of gas cloud propagation, and that in return can affect the benefits of time dependent ignition probability modelling (e.g. TDIIM) (DNV, 1998) as well as the CFD model itself. Furthermore, according to the discussion provided by Bakke and Hansen (2003), Gupta and

Chan (2016), the accuracy of these approaches remains controversial which may probably result in an incorrect ERA result.

Normally, the gas clouds in real explosion scenarios are referred to inhomogeneous gas clouds formed during the gas fuel leaks. On the contrary, the investigated explosion scenarios in ERA are no longer indicative of the inhomogeneous gas clouds but are composed of four variables, including gas cloud size, shape, position and ignition position. However, all types of the gas cloud distribution presented in previous studies have concentrated only on the gas cloud size, and the reaming variables have to be determined separately from the distribution. This leads to the problem that the remaining variables can only be determined conservatively by engineering judgement and experience. In most cases, the position and shape of the gas cloud are likely to be determined largely different than those shown in the gas dispersion simulations, and therefore the explosion consequence, i.e. overpressure distribution can be estimated incorrectly. Beyond that, the conservative engineering judgment and experience can also results in various ERA results, which is problematic in terms of reliability.

1.2. Purpose of research

The purpose of this study is to improve the accuracy of the investigated explosion scenarios by developing several new methods related to the ERA to improve the limitations of existing approaches. More details on the limitations of the existing approaches are discussed in Chapter 2.

Considering the time-varying leak rates, the current study aims to propose a new type of gas cloud frequency distribution, which not only can reflect the overall results of the CFD simulations performed with the time-varying leaks, but also does not significantly increase the computing costs. The current work attaches great importance to fully reflect the transient process of gas cloud propagation, i.e. the time history of gas cloud size and ignition probability, as discussed earlier, which can be a key part of improving the accuracy of ERA. Using the proposed distribution, it is possible to look into how the ERA results can be varied depending on the number of gas clouds that are discretely selected from the transient process. Details on how to reflect the entire gas dispersion simulations to the gas cloud frequency distribution are described in Chapter 3.

Considering the gas cloud position, the current study proposes a multivariate frequency distribution (MVFD) which is designed to provide the information of the cloud position. In order to realize the idea, the most important matter is to quantify the cloud position, and the current study also proposes a method to calculate the cloud position. In consequence, the cloud position is defined by three coordinates, x, y and z, respectively, and these coordinates are integrated into the gas cloud frequency distribution in a manner similar to that of the cloud size is considered in the existing approach. When the explosion scenarios are investigated using the MVFD, the information of gas cloud position can be directly taken into account from the dispersion simulations, and thus engineering judgment and experience are no longer necessary. On the other hand, the MVFD also can accommodate transient aspects of the gas cloud size, position and ignition probability caused by time-varying

leak rates. The MVFD can be derived based on transient gas dispersion simulations which can provide the cloud size, position and the ignition probability for each time step. Details on how to derive the MVFD are described in Chapter 4.

In association with the MVFD, the present study also conceptually proposes a method for determining the shape of the gas cloud. The actual clouds shown in the gas dispersion simulation are generally represented by a number of control volumes (CV) with different mass fractions, and the cloud shapes are implicitly determined by those CVs. In considering of this, the present study proposes the concept of shaped equivalent gas cloud to account for the shape of the gas cloud. The shaped equivalent gas cloud is designed to be determined for each explosion scenario investigated by the MVFD. Since each investigated explosion scenario is indicative of multiple actual gas clouds, the shaped equivalent gas cloud should be determined by overlapping those actual clouds. The CVs used to represent the shaped equivalent gas cloud are determined by introducing the severity, which can be measured by the frequency of the actual gas cloud and the fuel concentrations of the CVs. When the explosion scenario is investigated using the proposed method, the shape of the gas cloud is automatically determined according to the actual clouds. Therefore, the conservative engineering judgment and experience are no longer necessary, and also the accuracy of the ERA may be improved. Details on how to determine the gas cloud shape are described in Chapter 5.

Chapter 2. Explosion Risk Analysis

2.1. Probabilistic approach with ERA

[2]ERA is a complicated process that should take into account the entire chain of events starting from a gas leak, via dispersion, ignition and explosion itself. For evaluating explosion consequences, one needs leak scenarios and explosion scenarios separately, both of which may include many unpredictable variables such as wind condition, leak hole diameter, leak direction, leak position, and ignition location. The changes in these variables generally lead to many potential scenarios that may challenge the ERA, and to overcome this, the ERA is usually implemented in a probabilistic manner. The basic concept of the probabilistic ERA is to manage those variables with their own probability (or frequency) distributions. For each variable, the probability distribution is divided by several intervals, and the representative values are selected at each interval and combined together to investigate a specific number of scenarios that are significantly less than the actual ones.

In general, the probability distribution can be obtained by using the historical databases such as hydrocarbon leak frequency database, wind roses, and so on. For those that cannot find a suitable probability distribution (i.e. leak location, leak direction, etc.) some simplified models or engineering judgment are applied alternatively. For offshore installations, Gexcon as a leading group in the area of the ERA, has made substantial contributions to

[2] This chapter originates from published work (Jin and Jang, 2018a; Jin and Jang, 2018b)

developing the probabilistic ERA methodology. The overall methodology is conceptually proposed in the late 1990s (Hansen et al., 1999) and later improved through many applications and related studies. By present, this methodology is most commonly used in offshore projects, which is aligned with the guidelines set out in NORSOK Z-013 (NORSOK, 2010). The outline of this methodology is presented in Fig. 1, which has been published by Hansen et al. (1999); Talberg et al. (2000, 2001) ; Hansen and Middha. (2007); Hansen et al. (2013). In current context, the "Gas cloud distribution" shown in Fig. 1 can be regarded as the gas cloud frequency distribution. The whole process can be separated into two parts based on the gas cloud frequency distribution.

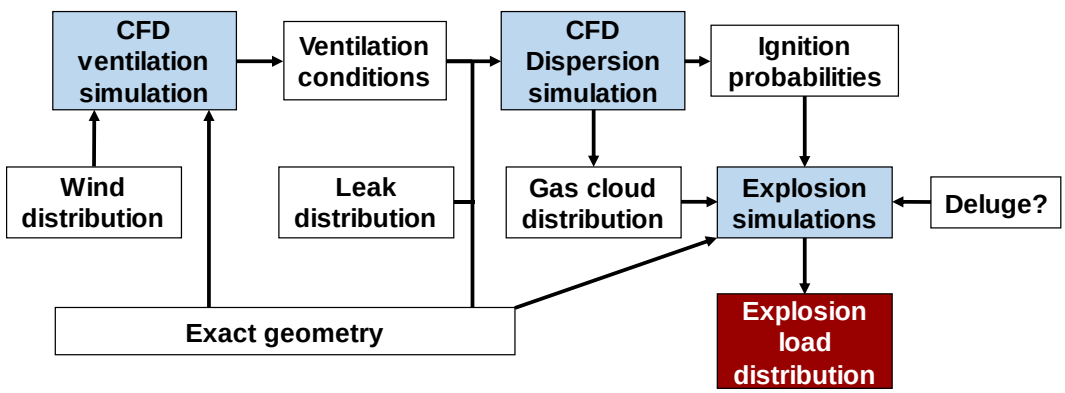

Fig. 1 Overview of the original probabilistic ERA methodology (Hansen et al., 2013).

The first part is devoted to deriving the frequency distribution by combining the results of gas dispersion simulations and leak frequency analysis. To complete this part, it is important that the leak scenarios as starting events also need to be investigated in a probabilistic manner. The second part is intended to evaluate DALs

via a probability of exceedance curve, which can be commonly obtained by combining the results of gas cloud frequency distribution, explosion simulations and ignition probability modelling.

2.2. Gas cloud frequency distribution

The reason for separating the whole process based on the gas cloud frequency distribution is that this distribution as a turning point, contributes a lot to reducing the number of explosion scenarios to a manageable level. There may be a question about why the number of explosion scenarios needs to be reduced again since the number of leak scenarios has been reduced in the first part. The answer can be found in one common characteristic of the gas clouds that occur during leaks. Physically, gas cloud propagation is a transient process regardless of whether the leak rate is time dependent or not, and hence the gas clouds are likely to ignite at any moment during the transient propagation. This indicates that, the total number of explosion scenario still increases dramatically with leak durations even if the number of leak scenarios are controlled in a probabilistic manner. If one expects accurate ERA results, the best option is to explode all of the potential gas clouds occurred during the transient process. However, another tough problem with that operation is that explosion consequences can be different depending on the location of ignition sources even for the same gas clouds. In general, a gas cloud has a non-homogeneous concentration distribution, and this distribution can also vary with time. Since the combustion reaction is strongly dependent on the gas concentration, different ignition locations may cause different pictures of the gas cloud combustion (Hansen et al.,

2013). In consequence, when considering all possible gas clouds, and the variations in ignition locations for each cloud, the total number of the explosion scenarios is almost close to infinity.

To deal with the massive explosion scenarios, the concept of gas cloud frequency distribution is introduced into the probabilistic ERA methodology. The basic idea is to derive a frequency distribution of the gas clouds, and to investigate the explosion scenarios in a probabilistic manner by using the derived frequency distribution. Such an idea is analogous to dealing with the unpredictable variables to investigate the leak scenarios (Jin and Jang, 2015; Jin and Jang, 2016). However, unlike these unpredictable variables, the gas clouds are interpreted by two different attributes, the gas cloud size and the gas concentration distribution, both of which can vary with time and affect the explosion consequences.

Generally, the gas concentration distribution is a type of field data, and thus it presents difficulties in deriving the gas cloud frequency distribution. In this regards, GexCon proposes the concept of equivalent stoichiometric cloud (ESC) (Gexcon, 2015), which can ignore the influence of the gas concentration distribution. The basic idea of the ESC is to scale the non-homogeneous gas cloud to a smaller stoichiometric gas cloud, and the size is calculated as the amount of gas in the flammable range, weighted by the concentration dependency of the flame speed and expansion. The underlying assumption is that these transformed gas clouds may give similar explosion loads as the original clouds (Gexcon, 2015). In order to enable the ESCs to give explosion loads in a conservative manner, the GexCon also provides a guideline for where to locate and ignite the clouds (Hansen et al., 2013; Gexcon, 2015). As a result, using the ESC concept, one can readily derive

the gas cloud frequency distribution by considering only the size of the ESC regardless of the aspect associated with the gas concentration distribution. The explosion scenarios are then available to be investigated. The cloud size is provided by the frequency distribution and the remaining required variables such as gas cloud shape, position and ignition location are generally determined by engineering judgment and experience according to the guidelines (NORSOK, 2010).

The overall procedure developed by GexCon is regarded as a key methodology for the probabilistic ERA, and especially, the concept of gas cloud frequency distribution is an outstanding idea, which can greatly contribute to reducing the total number of explosion scenarios. The methodology has been widely used for offshore projects and research work during the last two decades. However, since the ERA itself is a complicated process, and also every target offshore installation has a unique function, many details of the ERA are difficult to regulate consistently in practice. In particular, depending on the target offshore installation, the engineering judgment and experience provided by various analysts often lead to different applications. In addition, when considering the time-varying leak rates, it is more complicated to derive the frequency distribution, and the details are also varied depending on cases. In the following section, some practices with respect to the time-varying leak are given in more detail by reviewing the existing research.

2.3. Problem with time-varying leak rate

In general, if flammable gas leaks from a particular equipment, the rate will decrease over time due to the emergency shutdown and depressurization (ESD &EDP) system activated upon gas detections. Sometimes even if the EDP system is not activated, the portion of released gas can cause the equipment to self-depressurize as well. Normally, the system takes a certain amount of time to drain out the whole inventory contained by the equipment, and especially for small leak hole sizes, it may take longer. Such an aspect is challenging when using the CFD models to simulate the gas cloud propagation. In this section, the details of the existing research related to the time-varying leak rate are conveyed from three different perspectives on how to apply the CFD models, calculate ignition probability, and select gas clouds to derive the frequency distribution. Information is gathered from published literature (Hansen et al., 1999; Talberg et al., 2000 and 2001; Hoorelbeke et al., 2006; Hansen and Middha, 2007; Davis et al., 2001; Azzi et al., 2016), but since most of it is partially or unclearly open to the public, subsequence discussions may not account for the most correct details.

When reviewing those existing research, it can be summarized that the time-varying leak rates may or may not be considered depending on the type, function and other aspects of the target offshore installation. Without considering the time-varying leak rates, the process of deriving the gas cloud frequency distribution is less complicated. In that cases, the leak rates are assumed to be constant, and the CFD simulation covers until the volume of gas cloud inside the domain reaches a steady state. The gas cloud

frequency distribution is then derived using a group of steady-state gas cloud sizes provided by each leak scenario. In fact, until the steady state, the gas cloud builds up transiently and the volume consumes a certain amount of time to reach the steady-state magnitude. This implies that even if the leak rate is constant, a huge number of clouds can be produced with different volumes during the transient process. In existing research, however, such details are ignored since the leak rate is constant and the steady-state gas cloud is sufficient to be a representative value for each leak scenario.

Whereas, when considering the time-varying leak rates, the situation is greatly different from using a constant leak rate. The steady state no longer appears in simulations, and the gas cloud builds up first, then decays later, causing the volume to change transiently over the entire leak duration. This means that the CFD simulations are required to cover the whole leak durations by considering the time-varying leak rates. However, as well known, such simulations normally require high computing costs and lower the analysis efficiency. To make up for this, some simplified approaches are developed in previous research. For instance, one typical approach is to combine CFD-calculated results to mimic the actual time-varying aspect of the gas cloud propagation. To do so, first of all, it requires to prepare a group of steady-state results performed with constant leak rates and then combine them according to various sets of time frames, each of which is synchronized with an actual time-varying the leak rate. With such simplified approaches, the CFD gas dispersion simulations only need to be last until the steady state. Moreover, another advantage of such approaches is that based on the CFD-calculated steady-state

results, one also can implement an approximation model, e.g. frozen assumption to obtain the results for other constant leak rates without further CFD simulations (Hansen et al., 1999; Talberg et al., 2000 and 2001; FLACs, 2015; Qiao and Zhang, 2010).

However, even if a moderate reduction in the cost of computation is expected, the accuracy is still controversial as reported by Gupta and Chan (2016). The main reason is that the volume of gas cloud is dependent on the amount of leaked gas, not the leak rate. In other words, when using the steady-state results, the amount of leaked gas estimated in most cases is not equivalent to what may occur at the moment when the actual time-varying leak rate drops off to the same values as the corresponding constant leak rates. In particular, when the leak rates change rapidly with time, the accuracy problem may become more severe.

In general, it is known that frequency analysis is as important as consequence modeling in risk analysis. Ignition probability modelling, which is devoted to obtaining the frequencies of ignited gas clouds, is another tough task, especially in case of the time-varying leak rates. TDIIM (DNV, 1998) as a conventional model is the rule of thumb for calculating the ignition probability of gas cloud formation in offshore topside process areas. The greatest advantage of the TDIIM is that it takes into account of an entire transient process of gas cloud propagation and gives the ignition probability as a function gas cloud sizes varying with time. However, the approaches using a certain number of discrete gas cloud sizes, i.e. the steady-state results, to mimic the actual time-varying effect cannot afford to give the entire footprint of the gas cloud propagation and thus, under these approaches, the TDIIM may not provide its own benefits sufficiently.

2.4. Problem with gas cloud position

As a matter of fact, the consequences of explosion accidents can vary greatly depending on variables such as gas cloud size, position, and shape and ignition position. Normally, most of these variables can be readily determined from the gas dispersion simulation. In principle, the CFD models are composed of both dispersion and explosion consequence models. Therefore, it is possible to directly use the results of previous dispersion analyses when performing subsequence explosion analyses. For example, in FLACS, the results of the gas dispersion simulation, i.e. a type of dispersed inhomogeneous gas cloud can be directly applied to carry out the next explosion simulation (Gexcon, 2015). The dispersed inhomogeneous gas clouds itself is indicative of necessary information such as the gas cloud volume within flammable limits, the position or the area that the cloud covers and the boundary of the cloud at the flammable limits. Therefore, except for the ignition position, the remaining variables required for the explosion simulation can be automatically considered when using the inhomogeneous gas cloud.

However, the combined analysis is not applicable to the ERA because the number of the explosion scenarios derived from the CFD gas dispersion simulations are normally too large to be processed with the CFD models. The use of gas cloud frequency distribution can reduce the number of explosion scenarios to manageable levels, but these scenarios cannot be indicative inhomogeneous gas cloud any more. Typically, the explosion scenarios should be investigated with four variables, such as gas

cloud size, shape, position and ignition position required for the CFD explosion simulations.

Nevertheless, all types of the gas frequency distributions presented in previous studies have concentrated only on the gas cloud size, and the remaining variables have to be determined separately from the distribution. More specifically, this means that even if the size of a gas cloud can be determined with the gas cloud frequency distribution, the remaining problems associated with the gas cloud position, shape and ignition position need to be addressed further. In general, the remaining variables are not actually dealt with in a probabilistic manner but are more likely to be conservatively determined based on engineering judgment and experience. The main reason is that there are many possibilities for the variables that can be assigned to a certain cloud size, because the size read in the gas cloud frequency distribution is typically indicative of multiple leak scenarios rather than a single one. There has been some recognized literature (Talberg et al., 2001; Hoorelbeke et al., 2006; Hansen and Middha., 2007; NORSOK, 2010; Davis et al., 2011; Hansen et al., 2013) describing how to investigate the explosion scenarios in relation to the gas cloud frequency distribution, but most have been described in a qualitative manner. Though it is recommended that the selected values or cases of the variables must account for all possible explosion scenarios, such guidance is generally too ambiguous to apply specifically, and the ERA results may vary largely from engineer to engineer.

In order to comply with the qualitative guidelines, more than one combination of the variables used to be assigned to the same gas cloud size, however, in some cases this may cause the investigated

explosion scenarios to be significantly different from the real situation. In particular, such a phenomenon is dominant in specifying the gas cloud position. If the gas cloud is placed in a position other than where it should be, then the ERA results can probably be overestimated or underestimated. For convenience, this type of gas cloud is defined as a size–position mismatched cloud in the current study. As an example, if the gas cloud selected from the top cloud size category is placed in a region that is hardly exposed to that gas cloud, the explosion loads in that area is probably overestimated. Though such an extreme case seems impossible, it happens occasionally and its occurrence is subjected to engineering judgment.

2.5. Problem with gas cloud shape

The shape of the gas cloud represents the boundary of fuel mixture, which can determines the path of the flame propagation in 3D space. In order to improve the accuracy of the investigated explosion scenarios, the gas cloud position is to be determined by the proposed gas cloud distribution, i.e. MVFD in Chapter 4. However, even if the gas cloud, i.e. ESC is placed at the same position with the same volume, given a different shape of the ESC, the resulting overpressure distribution may be completely different depending on the path of the flame propagation. Different paths mean that the flame can travel different distances in different directions and therefore the overall picture of resulting overpressure will be different.

On the other side, the geometric conditions inside the cloud can also affect the overpressure distribution. If shape of the gas cloud is

given differently, the geometrical conditions inside the cloud will change. In other words, as the flames propagate along different paths, they can experience different geometric conditions. As well known, the geometric conditions are a very important factor contributing to the buildup of the overpressure in VCE. During the flame propagation, the geometric conditions affect the turbulence generation, which in return has a positive effect on the buildup of the overpressure. Normally, the geometric conditions inside the cloud become very congested, the resulting overpressure may probably be very high. Therefore, when the gas cloud is given in a shape that is significantly different from the actual shape shown in the gas dispersion simulation results, the overpressure distribution can be inaccurately estimated.

In summary, the importance of considering the shape of the gas cloud can be described in two aspects. One is the flame propagation path and the other one is the turbulence generation according to the geometric conditions surrounded by the clouds. However, there is little previous research or regulation on how to determine the shape of the ESC. In general, the shape is conservatively determined by engineering judgment and experience, such as in the case of the gas cloud position, which leads to various ERA results and can be problematic in terms of both accuracy and reliability.

Chapter 3. Ignited Gas Cloud Frequency Distribution

3.1. Existing approach

[3]A common fact that can be seen in previous studies (Gupta and Chen, 2016; Davis et al., 2011; Azzi et al., 2016) is that the cloud frequency distribution is derived by only using some specific values rather than by dealing with the entire transient process of CFD simulations. The reason for this also eventually owes to the CFD application methods, which are not able to produce the entire transient process of CFD simulations. As reviewed, these specific values are likely to be a group of maximum gas cloud sizes selected from pseudo transient processes of gas cloud propagation virtualized by combining the steady−state values (Gupta and Chen, 2016; Davis et al., 2011; Azzi et al., 2016). One of the examples is illustrated in Fig. 2. When the leak scenarios are investigated, they can be grouped by a certain number of leak rate categories. The leak rates correspond to the initial leak rates that can be calculated using the leak hole diameters and operation condition. The purpose of grouping the leak scenarios by using the leak rate category is that the scenarios in the same leak rate category have a common leak hole diameter, and thus the leak frequencies of these scenarios are identical. Through the CFD dispersion simulations, a specific gas cloud size v is attainable for each leak scenario. In previous studies, the v is selected as the steady−state result when the leak rate is assumed to be constant, otherwise it is typically selected as the maximum value.

[3] This chapter originates from published work (Jin and Jang, 2018a)

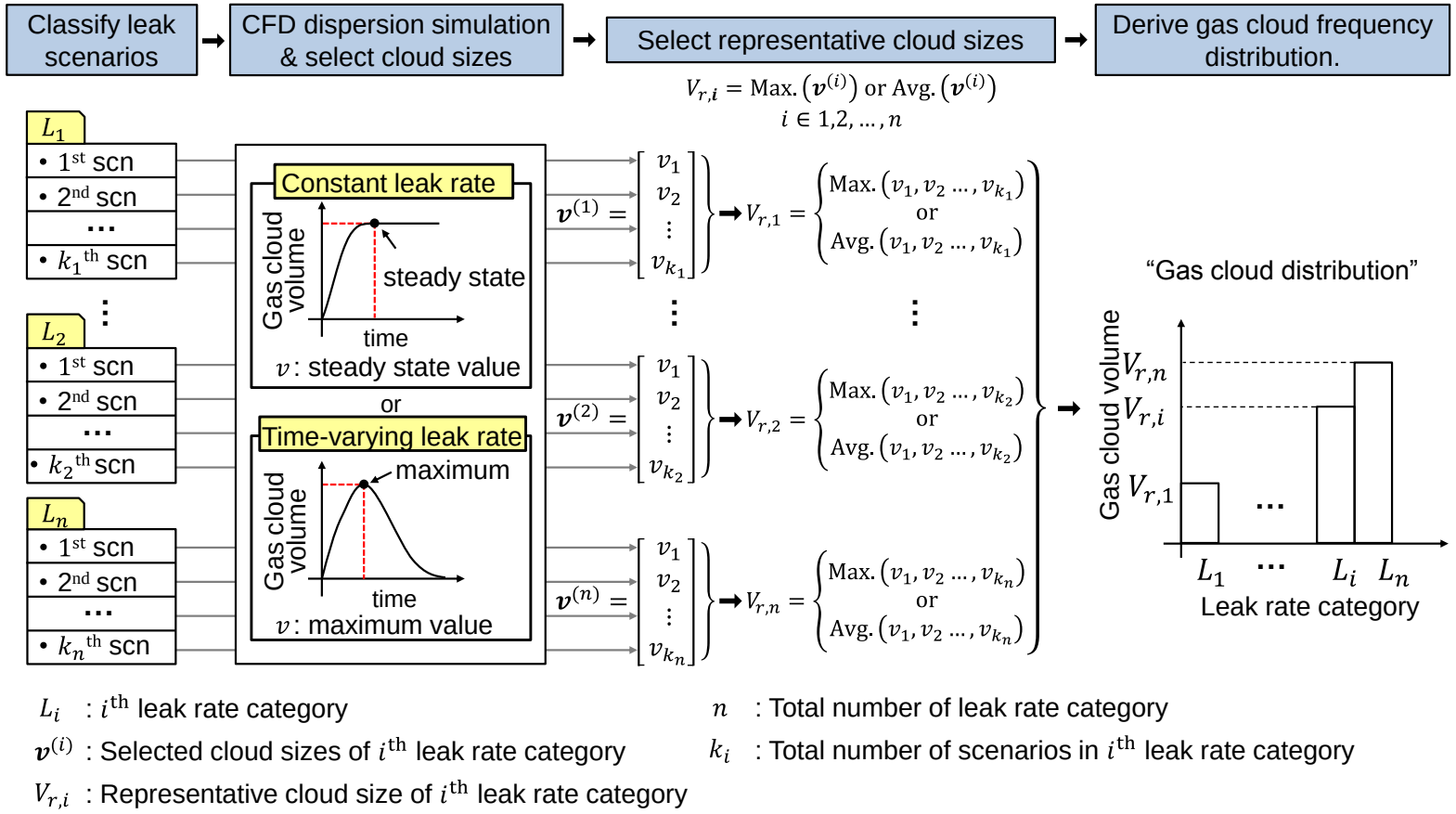

L_i : i^{th} leak rate category

$\boldsymbol{v}^{(i)}$: Selected cloud sizes of i^{th} leak rate category

$V_{r,i}$: Representative cloud size of i^{th} leak rate category

n : Total number of leak rate category

k_i : Total number of scenarios in i^{th} leak rate category

Fig. 2 Overview of deriving the original gas cloud distribution

Once the full data of $v^{(i)}$ is collected, the frequency distribution is derived using a group of representative cloud sizes, $V_{r,i}$, each of which is the maximum or average value of the $v^{(i)}$. In previous studies (Davis et al., 2011; Azzi et al., 2016), the "gas cloud distribution" is commonly expressed as the relationship between the leak rates and cloud sizes. However, given that the leak rate and the leak frequency are mutually interchangeable, the "gas cloud distribution" is consequently the same as the gas cloud frequency distribution.

The purpose of gas dispersion modeling is to figure out an overall footprint of all possible gas cloud formations. From that perspective, it is no wonder that using the maximum values is no more than a conservative manner, which is generally acceptable for dealing with such uncertain engineering problems. Nevertheless, the maximum values indicate that in the existing cases, the entire transient process for each leak rate is discarded eventually, instead, only a single gas cloud size (e.g. v in Fig. 2) is selected to derive the gas cloud frequency distribution. The approach using the maximum gas cloud sizes may be plausible, but considering it with ignition probabilities may result in overestimation of explosion frequency.

In fact, as illustrated in Fig. 1, both the "gas cloud distribution" and ignition probabilities are required for explosion simulations. More specifically, this means that the final frequency used to evaluate the explosion loads is the frequency of explosion, which should be calculated further by multiplying the leak frequency by the corresponding ignition probability. With respect to the ignition probability modeling, in Chapter 2, it has been previously discussed that the simplified approaches of CFD modelling in previous studies may affect the accuracy of ignition probability modelling due to the

incomplete foot print of gas cloud propagation. Moreover, only choosing the maximum cloud sizes, the ignition probability also may be limited to a specific value and this can be a problem in terms of the explosion frequency. The ignition probability depends on the size of the gas cloud and therefore it also generally varies with time. However, if one chooses the maximum cloud size, the ignition probability is also taken into account at a specific time, not over time. Normally, large gas clouds give a high ignition probability, and considering this, choosing the maximum cloud sizes and associated ignition probabilities can probably overestimate the ERA results. In consequence, the limitations of the existing gas cloud distribution can be summarized in three points listed below.

- Estimation of gas cloud sizes by using simplified CFD application methods which does not directly consider the effect of time-varying leak rates.
- Calculation of ignition probability using a certain number of discrete gas cloud sizes instead of dealing with the entire transient process of gas cloud propagation.
- Derivation of gas cloud frequency distributions by using only the maximum gas cloud sizes instead of considering a full set of the entire transient process for all time-varying leak rates.

To achieve highly accurate ERA results, the entire transient process of the gas cloud propagation seems necessary to calculate the ignition probability and to derive the gas cloud distribution, and meanwhile the transient process has to be modelled by taking account of the time-varying leak rates. In view of this, the work in the current chapter is to seek for a way to reflect the entire

transient process of gas cloud propagation under the time-varying leak rate conditions, whilst, without increasing the costs for CFD consequence modeling too much. To do so, a new type of gas cloud frequency distribution is proposed, as intended which can facilitate the time-varying leak rates by taking account of the whole gas cloud formations and associated ignition probabilities.

3.2. Methodology

In the current study, the entire footprint of gas cloud formations and associated ignition probabilities is considered by proposing a new type gas cloud frequency distribution. As illustrated in Fig. 3, the proposed distribution is named with ignited gas cloud frequency distribution. In order to implement the proposed distribution, most of the original methodology remains intact, but the sequence is modified and the main difference is that the cloud size and ignition probability should be considered in combination. The specific method for deriving the proposed distribution is given in detail below.

The reason for using the term “ignited” is that the gas cloud mentioned in the proposed distribution refers to a cloud that can be exploded by an ignition source rather than occurring during gas dispersion. In other words, the frequency included in the proposed distribution refers to the explosion frequency calculated using the leak frequency and ignition probability rather than the leak rate (or leak frequency) originally shown in the “gas cloud distribution”. An example of the proposed distribution is shown in Fig. 4. Instead of choosing the original leak rate categories, the cloud size categories are used directly to classify all potential gas clouds shown in gas dispersion simulations, and the explosion frequency is determined by each cloud size category.

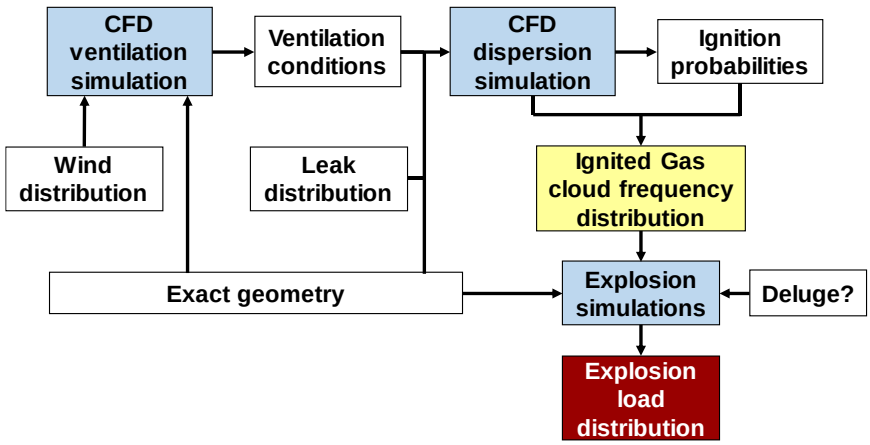

Fig. 3 ERA procedure with ignited gas cloud frequency distribution

To calculate the explosion frequency of a particular category, one needs to know how many gas clouds fall into that category, and how often each cloud can occur independently. This requires a monitoring process, during which the size and an individual frequency of each cloud can be identified. The individual frequency refers to the frequency of a gas cloud to be ignited, i.e. the frequency of an ignited gas cloud, which can be calculated by multiplying the frequency of a leak scenario that generates the cloud with the probability of an ignition event that can ignite the cloud. When the monitoring process is finished, then the explosion frequency of each category is calculated by summing the individual frequency of all clouds belonging to that category.

When monitoring the gas clouds, one must set a time interval, Δt to decide how often choose the gas clouds from the simulation results, which determines whether the transient process of gas cloud propagation is considered enough. For instance, a small Δt is likely to be better than a large one to reflect the entire footprint of gas cloud propagation. Within a large Δt, the transient process can

be missed too much and hence the accuracy may be lowered. Currently, the Δt is recommended to be set to 1s, the minimum time interval given in FLACs, to report the clouds e.g. Q6 (Gexcon, 2015) used in the calculation of the ignition probability. More details about the effect of Δt on ERA results are given in Section 3.5.

One matter to note about determining the ignition probability of a particular cloud is that the total ignition probability given by the TDIIM is a cumulative distribution with time (DNV, 1998). Therefore, a portion that each cloud deserves to have must be further identified, and this portion is given by an incremental ignition probability. Details about the way to derive the proposed frequency distribution is summarized by the following several steps.

1. For each investigated leak scenario, carry out a CFD dispersion simulation by using a time-varying leak rate profile.

2. Set a time interval for monitoring the gas clouds for all leak scenarios.

3. Calculate the total ignition probability for j^{th} leak scenario before or at time t_j, using TDIIM and gas clouds given by the FLACs dispersion modelling. (DNV, 1998)

$$P_{ign,i}(t \le t_j) = P_{imm} + (1 - P_{imm}) \cdot P_{del,i}(t \le t_j) \quad (3.1)$$

$$P_{del,i}(t \le t_j) = P_{D,i}(t \le t_j) + P_{C,i}(t \le t_j) - P_{D,i}(t \le t_j) \cdot P_{C,i}(t \le t_j) \quad (3.2)$$

where P_D and P_C is ignition probability of an intermittent and a continuous ignition source, respectively; P_{del} and P_{imm} refers

to the delayed and immediate ignition probability, respectively, and P_{ign} refers to the total igniting probability.

4. For each leak scenario, calculate the incremental ignition probability for i^{th} leak scenario in j^{th} time interval, $\Delta P_{ign,i}(\Delta t_j)$ using the total ignition probability, $P_{ign,i}(t \le t_j)$ given by TDIIM.

$$\Delta P_{ign,i}(\Delta t_j) = P_{ign,i}(t \le t_j) - P_{ign,i}(t \le t_{j-1}) \tag{3.3}$$

5. Calculate the individual frequency (or frequency of ignited gas cloud), of every monitored gas cloud for i^{th} leak scenario in j^{th} time interval, $f_{ign,i}(\Delta t_j)$.

$$f_{ign,i}(\Delta t_j) = f_{leak,i} \cdot \Delta P_{ign,i}(\Delta t_j) \tag{3.4}$$

where $f_{leak,i}$ refers to the frequency of i^{th} leak scenario.

6. Set a number of cloud size categories, $\boldsymbol{C}_m$ to classify the monitored gas clouds, where m indicates the total number of categories.

7. Classify the monitored gas clouds based on the cloud size categories. For example, if the equivalent stoichiometric volume of a certain cloud monitored at j^{th} time interval from i^{th} leak scenario, $V_{ac,i}^{es}(\Delta t_j)$ satisfies a following condition, then it can be classified into k^{th} category, $\boldsymbol{C}_k$.

$$\text{If } V_{c,k-1} \le V_{ac,i}^{es}(\Delta t_j) < V_{c,k}, V_{ac,i}^{es}(\Delta t_j) \in \boldsymbol{C}_k \tag{3.5}$$

where $V_{c,k-1}$ and $V_{c,k}$ stands for the lower and upper

boundaries of the k^{th} cloud size category.

8. For k^{th} cloud size category, calculate the explosion frequency, $f_{exp,k}$

$$f_{exp,k} = \sum_{i=1}^{n_{ls}} \sum_{j=1}^{n_{t,i}} f_{ign\_ij} \tag{3.6}$$

here, if $V_{ac,i}^{es}(\Delta t_j) \in \boldsymbol{C}_k$, $f_{ign\_ij} = f_{ign,i}(\Delta t_j)$, otherwise $f_{ign\_ij} = 0$

where n_{ls} stands for the total number of leak scenario, and $n_{t,i}$ stands for the total number of Δt in i^{th} leak scenario. In Fig. 4, $n_{t,1} = s - 3$ and $n_{t,n} = s$.

A simple example covering the whole seven steps is also presented as below for the 1st category, $\boldsymbol{C}_1$.

For 1st leak scenario:

$$\begin{aligned} f_{ign,1}(\Delta t_1) &= f_{leak,1} \cdot \Delta P_{ign,1}(\Delta t_1) \\ f_{ign,1}(\Delta t_{s-5}) &= f_{leak,1} \cdot \Delta P_{ign,1}(\Delta t_{s-5}) \\ f_{ign,1}(\Delta t_{s-4}) &= f_{leak,1} \cdot \Delta P_{ign,1}(\Delta t_{s-4}) \\ f_{ign,1}(\Delta t_{s-3}) &= f_{leak,1} \cdot \Delta P_{ign,1}(\Delta t_{s-3}) \end{aligned} \tag{3.7}$$

For n^{th} leak scenario:

$$\begin{aligned} f_{ign,n}(\Delta t_1) &= f_{leak,n} \cdot \Delta P_{ign,n}(\Delta t_1) \\ f_{ign,n}(\Delta t_{s-5}) &= f_{leak,n} \cdot \Delta P_{ign,n}(\Delta t_{s-5}) \\ &\cdots \\ f_{ign,n}(\Delta t_{s-1}) &= f_{leak,n} \cdot \Delta P_{ign,n}(\Delta t_{s-1}) \\ f_{ign,n}(\Delta t_s) &= f_{leak,n} \cdot \Delta P_{ign,n}(\Delta t_s) \end{aligned} \tag{3.8}$$

Then, the explosion frequency of category $\boldsymbol{C}_1$ is

$$f_{exp,1} = f_{ign,1}(\Delta t_1) + f_{ign,1}(\Delta t_{s-5}) + \cdots + f_{ign,1}(\Delta t_{s-3}) \ldots + f_{ign,n}(\Delta t_1) + f_{ign,n}(\Delta t_{s-4}) + \cdots + f_{ign,n}(\Delta t_s) \quad (3.9)$$

In general, the total ignition probability consists of two types of ignition probability, immediate ignition and delayed ignition, respectively. The immediate ignition refers to the simultaneous occurrence of gas leakage and ignition, and typically the portion of probability contributed by this type is given once at the beginning of leak. (DNV, 1998).

The delayed ignition, on the other hand, includes all situations where ignition sources are exposed to a gas cloud at any moment. In the TDIIM, the delayed ignition is modelled by further classifying the ignition sources into two types, i.e. intermittent sources and continuous sources, respectively. The intermittent type is related to the time and volume of the gas cloud with concentration between LFL and UFL. Whereas, the continuous type is related to the cloud volume that is newly exposed to flammable gas concentrations (DNV, 1998). Contrary to the intermittent type, the continuous ignition source contained within the flammable gas cloud at the previous time step can be still active at the next time step, therefore, the ignition probability of the continuous type increases only when there is a newly exposed volume to the flammable concentrations (DNV, 1998).

In the present study, the gas cloud volumes used to calculate the two types of ignition probabilities are obtained directly using the FLACS. During a gas dispersion simulation, the FLACS can produce various types of results with regard to the gas cloud volume or mass (Gexcon, 2015). Among those results, there are two readymade variables, i.e. “FLAM” and “Q6”, which are designed to

be interfaced with the TDIIM. The "FLAM" provides the total gas cloud volume within the flammable concentrations at the current stage of the simulation and the "Q6" provides the cloud volume at the flammable concentrations for the first time last second (Gexcon, 2015; Jin and Jang, 2018), which corresponds to the volume newly exposed to flammable concentrations.

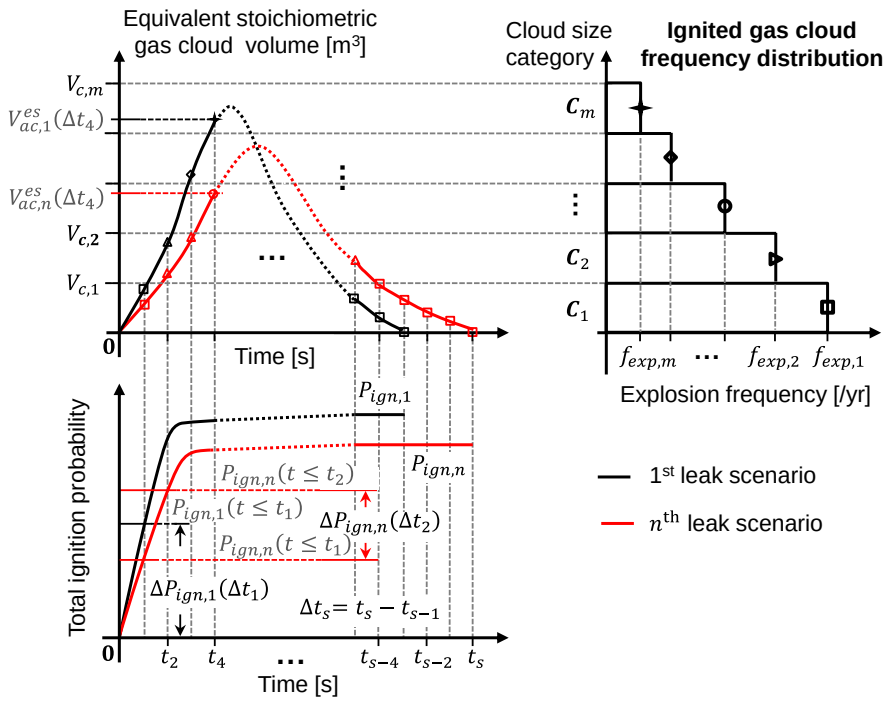

Fig. 4 Example of deriving ignited gas cloud frequency distribution

3.3. Cost of deriving the proposed distribution

In the proposed method, the CFD gas dispersion simulations are carried out with the time-varying leak rates to capture the entire transient processes of gas cloud buildup and decay. Whereas, as well known, such simulations are a major challenge in probabilistic

ERA because of the high computing costs. For example, for a moderate size of equipment, it may at least take a few minutes to blow down the whole inventory, and that even be much longer if the leak hole diameter is small. In some cases, depending on operating conditions as well as inventory components, the total time required may take up to several hours for small leak hole diameters. Given that the CFD simulations typically take a couple of hours to analyze a few minutes of transient process, the computing costs for many leak scenarios are usually considerable.

However, fortunately, the individual frequency introduced in the present study additionally provides the fact that a considerable number of gas clouds appearing after a certain moment in the transient process contribute little to the gas cloud frequency distribution due to the low individual frequencies. If such a finding is utilized properly, it may be of great value in reducing the total simulation time. Perhaps one can disregard the part of simulation where these clouds seem dominant, and expect to reduce the computational costs significantly without concerning about the accuracy of the gas cloud frequency distribution.

To demonstrate the fact, three cases of gas cloud volume-varying individual frequency are investigated in Fig. 5. The gas cloud volume in each case comes from the CFD simulations using three different time-varying leak rates as illustrated in Fig. 6, and each of the leak profile is calculated by applying different leak hole diameters, D under the same operating condition. From Fig. 5 it is clear that the individual frequencies decrease as the volume of gas cloud increases, and remains very low after a certain value of the volume. As shown by Eq. (3.4) in the previous section, the reason for the low individual frequencies can be related to the incremental

ignition probability.

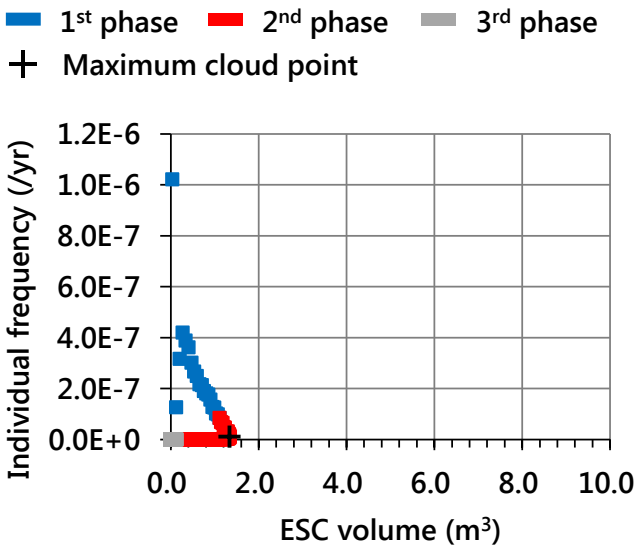

(a) D=90mm

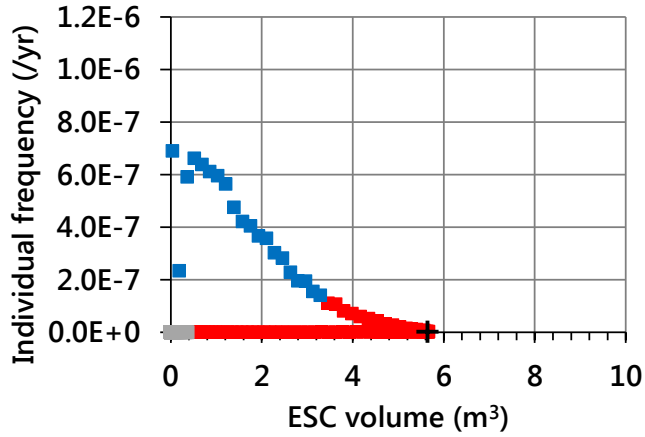

(b) D=135mm

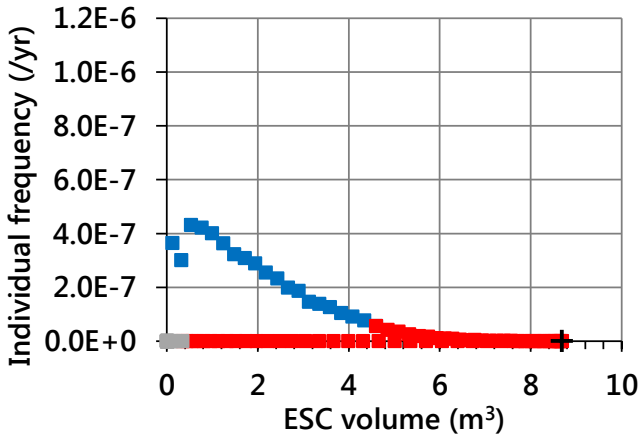

(c) D=180mm

Fig. 5 Frequency of ignited gas cloud (or individual frequency) with time-varying leak rate.

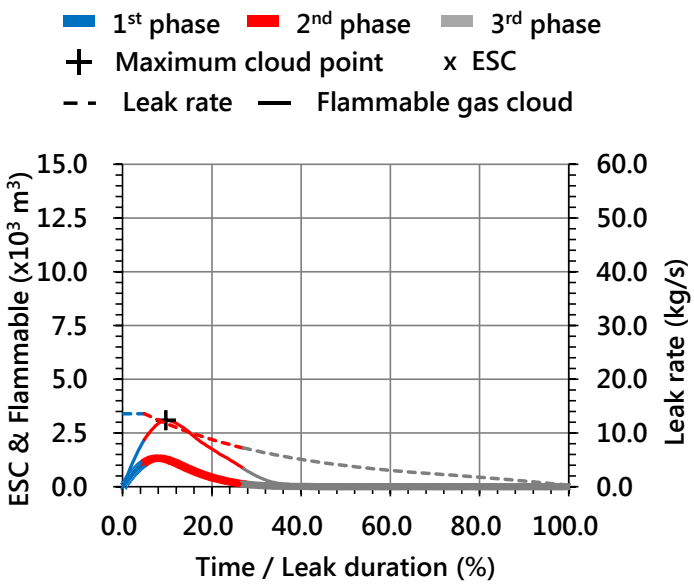

(a) D=90mm

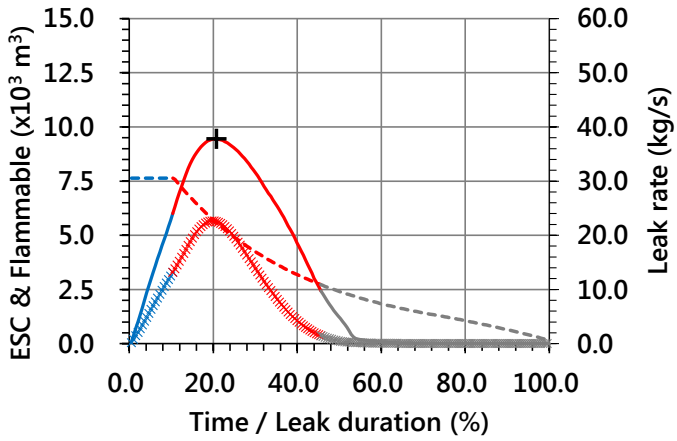

(b) D=135mm

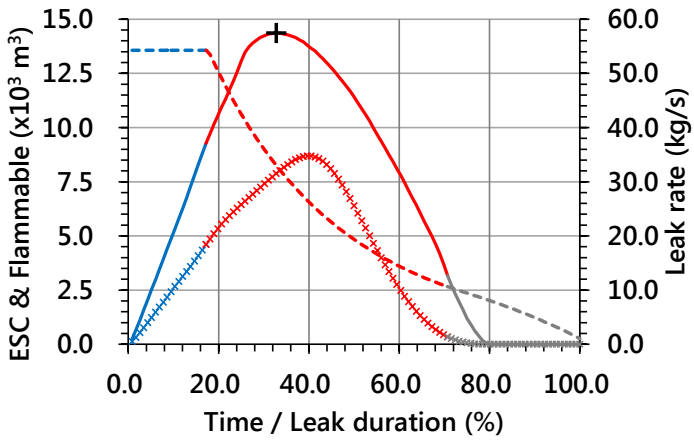

(c) D=180mm

Fig. 6 Leak rate and gas cloud volume with time-varying leak rate.

In general, the incremental ignition probability at every time interval, Δt, decreases with time, in other words, as Δt is located far away from the beginning of a leak, the ignition sources have less opportunity to allow an ignition event to take place. Such an aspect can also be interpreted physically. That is, the later phase of a transient gas dispersion has less opportunities to have an ignition event, since it may have already occurred in the previous phase. As

a result, if the gas clouds appear far away from the beginning of the leak, they have less chance to be ignited and hence have very low individual frequencies. The relevant discussions are also proven in Fig. 7 and Fig. 8. Both of the total and its incremental ignition probabilities are calculated for the three cases shown in Fig. 6

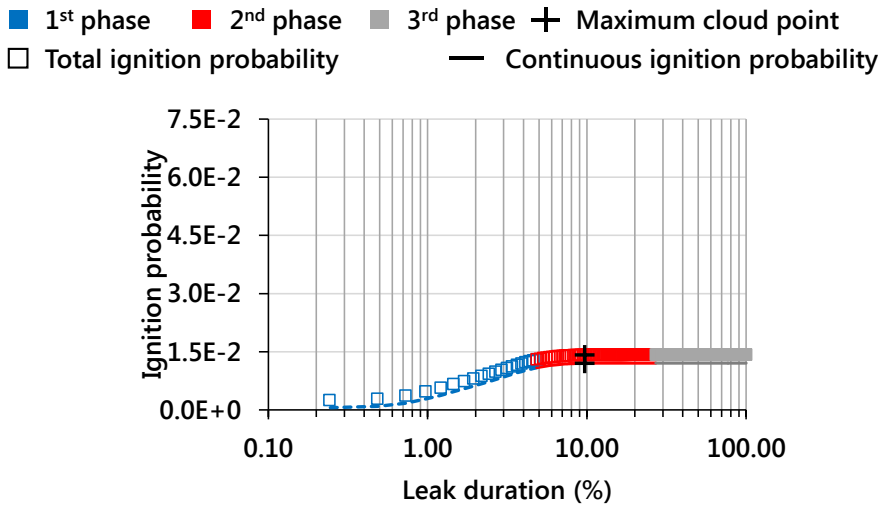

(a) D=90mm

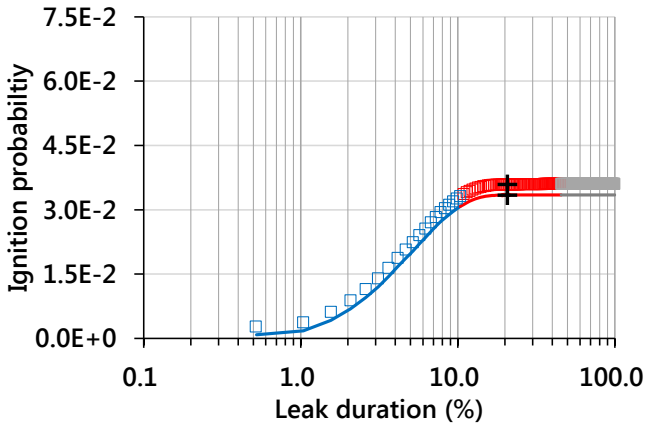

(b) D=135m

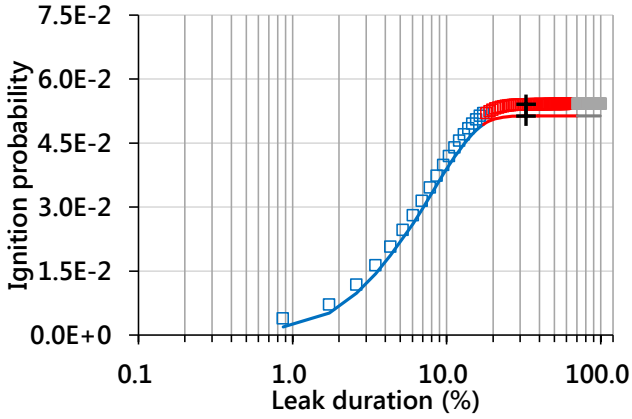

(c) D=180mm

Fig. 7 Total and continuous ignition probabilities with time-varying leak rate.

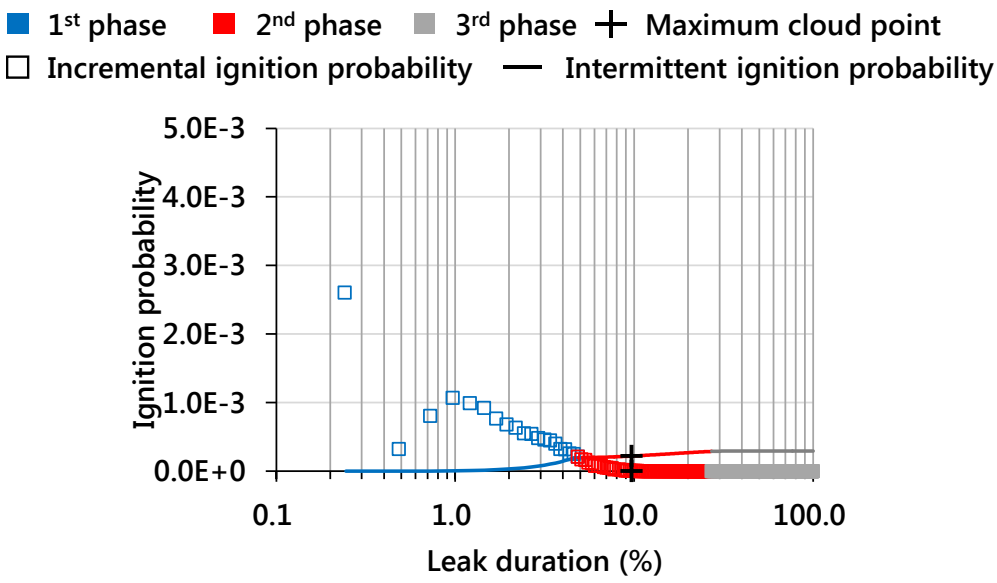

(a) D=90mm

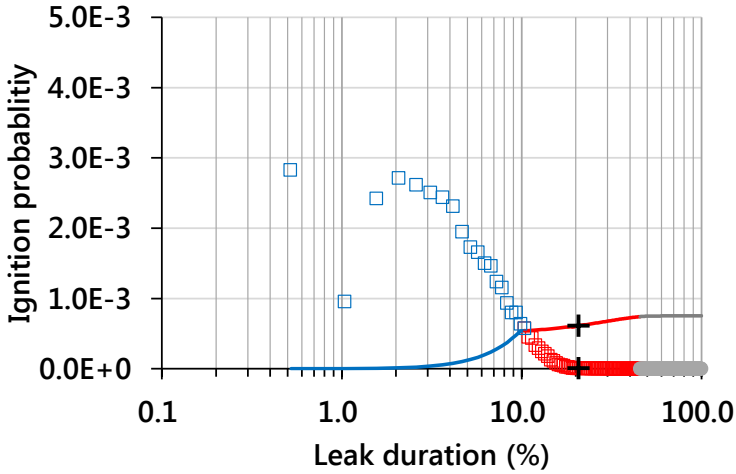

(b) D=135m

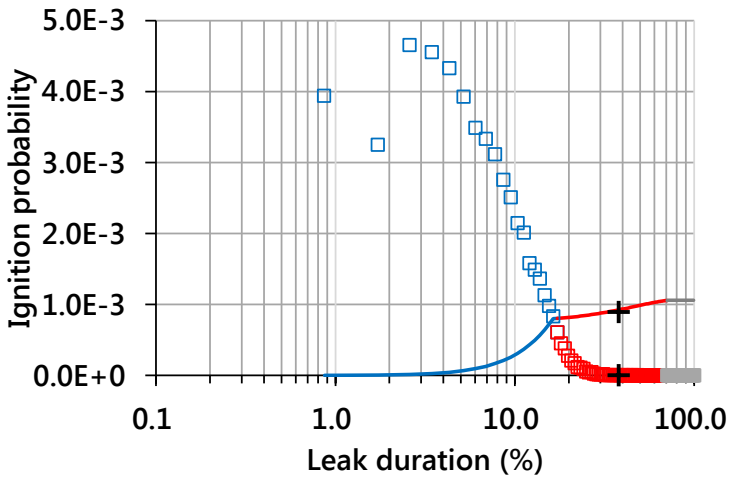

(c) D=180mm

Fig. 8 Incremental and intermittent ignition probabilities with time-varying leak rate

In order to clarify the details more clearly, in the present study, the whole transient process of gas cloud propagation is looked into by three different phases as listed in Table 1. During the 1st phase, the leak rate maintains a maximum magnitude, i.e. an initial value, and the ignition sources remain fully activated, promoting a rapid

increase in total ignition probability. When the 2nd phase begins, the gas detection triggers the ESD & EDP systems, which start to reduce the leak rate and shut down the ignition sources mostly. Consequently, the increase in total ignition probability slows down and gradually approaches to its peak value before entering into the 3rd phase. Such a process is repeated for all three cases.

On the other hand, as discussed earlier, the incremental ignition probability decreases as time passes. The phenomenon appears quickly after experiencing a few seconds from the beginning of the leak, and remains until the end of the 2nd phase. During the first few seconds, since the gas clouds suddenly appear from an absence, the incremental ignition probability may increase with time, but such a duration is very short. In addition, the reason for having a high starting value is that the contribution of the immediate ignition probability is included in the first Δt as shown in Eq. (3.1) and Eq. (3.3).

Table 1. Typical regions in gas dispersion simulation performed with time-varying leak rate

Phase No.	Description
1st phase	From the beginning of leakage to a gas detection.
2nd phase	From a gas detection to the moment when frequency of an ignited gas cloud is reduced to zero or very close to zero.
3rd phase	The remaining part, except for the 1st and 2nd phases. (The CFD simulation can be omitted in this phase.)

When a dispersion simulation steps into the 3rd phase, there is not any increment of the total ignition probability any more, in other words, it means that the incremental ignition probability is zero and the same matter occurs at the individual frequency. Therefore, there is little contribution from the gas clouds monitored in this phase to the frequency distribution, and which in return implies that the CFD gas dispersion simulations performed with time-varying leak rates do not need to cover the 3rd phase. Such a fact is meaningful for reducing the heavy CFD computing costs raised by adopting the time-varying leak rates, and hence it is worthwhile in ERA.

From Table 2, it is clear that the 3rd phase occupies a certain percentage of the total leak duration and the ratio becomes higher as the leak hole diameter or the initial leak rate decreases. In view of this, neglecting the 3rd phase for a large leak hole diameter may seem like a meaningless action on reducing the computing costs. However, the CFD simulations for the large hole diameters are inherently not too costly, as the leak durations are relatively short. For example, in Table 2, the percentage of the 3rd phase is 29.31% for D =180mm, much less than other cases, but the total duration is only 116s, which is one tenth of D=90mm. On the contrary, for a small hole diameter, the CFD simulations may be very costly due to a long leak duration, e.g. 6.9 min for D=90mm as presented in Table 2. In that case, a high portion of the 3rd phase, e.g. 72.88%, seems to be very worthwhile to be reduced for saving the computing costs.

Table 2 Summary of the three phases with different leak hole diameters.

	Leak		1st phase		2nd phase		3rd phase	
Leak hole diameter, D (mm)	Initial leak rate (kg/s)	Total duration (s)	Interval (s)	Portion (%)	Interval (s)	Portion (%)	Interval (s)	Portion (%)
45	3.55	1029	0~30	2.92	N/A*	N/A*	30~1029	97.08
62	6.31	861	0~30	3.48	30~40	1.16	40~861	95.35
90	13.57	413	0~20	4.84	20~112	22.28	112~413	72.88
135	30.53	193	0~20	10.36	20~88	35.23	88~193	54.40
180	54.27	116	0~20	17.24	20~82	53.45	82~116	29.31

*Not applicable, since the volume of gas clouds is very small, there is little increment of intermittent ignition probability after the 1st phase.

3.4. Separation of the 2nd and the 3rd phases

In the 2nd phase, once the leaked gas is detected, most of ignition sources are shut down and their intensities are greatly reduced. At the same time, the leak rate also starts to decrease, which in return to reduce the cloud volume with a certain time lag. When a gas cloud reaches its maximum value, there is not any global increment of the cloud size any more, and hence the total ignition probability almost approaches to its maximum value. However, owing to the intermittent ignition probability, as illustrated in Fig. 8, which continues to increase after passing through the maximum cloud size point, the total ignition probability can still go up further.

The intermittent type is usually related to the time and volume of the gas cloud with concentration between LFL and UFL, and hence it is still active as long as the flammable gas cloud is present. Whereas, the continuous type is related to the cloud volume that is exposed to flammable gas concentrations for the first time last second (Gexcon, 2015; DNV, 1998). If the simulation time passes the maximum cloud size point, there is no increment of the volume exposed to the flammable gas concentrations, and therefore the continuous ignition probability, indicated by the lines in Fig. 7, already reaches to its peak value. On the contrary, however, there is still a gas cloud with concentration between LFL and UFL, and the cloud continues to increase the intermittent ignition probability until the volume is reduced to a certain magnitude. As can be seen from Fig. 7, at the maximum cloud size point, the intermittent ignition probability, indicated by the lines, has not yet reached to its maximum value in each case. On average, the magnitude is around 80% of the maximum value, as presented in Table 3, and in order to

reach to the maximum value, it further needs to take around 15~30% of the total leak duration.

Table 3 Intermittent and increment of total ignition probability at the end of each phase.

Variables	Intermittent ignition probability $P_D(t \le t_e)/P_D^{Max}$ (%)				Increment of total ignition probability $\Delta P_{ign}(\Delta t_e)/\Delta P_{ign}^{Max}$ (%)			
t_e (s) / D (mm)	End of the 1st phase	Max. cloud size	End of the 2nd phase	End of the 3rd phase	End of the 1st phase	Max. cloud size	End of the 2nd phase	End of the 3rd phase
90	65.97	75.01	97.81*	100.00	8.22	0.19	0.04**	0.00
135	71.90	81.65	98.72*	100.00	20.30	0.21	0.04**	0.00
180	75.82	84.26	99.59*	100.00	13.11	0.13	0.02**	0.00

*After this moment, the value can still gradually increase to 100 % until the volume the flammable gas cloud is zero.

**After this moment, the value reduces to zero by rounding up to three decimal places.

Strictly speaking, the increase in intermittent ignition probability continues as long as the amount of flammable gas cloud is not zero, and thus the 3rd phase should not be excluded. As illustrated in Fig. 8, the volume of flammable gas cloud at end of the 2nd phase has still a certain magnitude, and it is gradually reduced to zero through the 3rd phase. Therefore, the intermittent ignition probability has not yet reached to its maximum value by the end of the 2nd phase. As presented in Table 3, the magnitude in each case is very close to the maximum value, but still can increase by about 0.4~3.0%

more during the 3rd phase. However, after the end of the 2nd phase, the incremental ignition probability is very subtle, the magnitude of which is almost zero percentage of its maximum value shown in Table. 3. The main reason can be explained by three aspects, a long time-shift from the beginning of the leak, a significant reduction of the intensity and a relatively small volume of flammable gas cloud, respectively. Also, as can be seen in Fig. 7 and Fig. 8, in general, the contributions of intermittent sources to the total ignition probability is much less than the continuous sources. In consequence, though the intermittent ignition probability can increase further in the 3rd phase, the slight increase has little effect on the incremental ignition probability. Therefore, when considering the computing costs, it is more advantageous to use the incremental ignition probability (or individual frequency) to distinguish the 2nd and the 3rd phases than the intermittent ignition probability.

In the same manner, even at the maximum cloud size point, the incremental ignition probability seems very small. As presented in Table 3, in all cases, it is less than 0.3% of the maximum value, appearing that the gas clouds after the maximum cloud size point may also contribute little to the cloud frequency distribution. Accordingly, a question then may be raised whether the region beyond the maximum cloud size point in the 2nd phase needs to be taken into consideration or not. After all, as similar to the 3rd phase, if this region is further excluded from the CFD dispersion simulation, the total computational costs can be reduced more. Before answering the question, it should remind that the proposed distribution is derived by grouping all monitored gas clouds with a certain number of cloud size categories, and the explosion frequency is calculated by summing the individual frequencies of all

monitored gas clouds in each category. As a result, even if the individual frequencies of the monitored clouds are commonly low after the maximum cloud point, the sum may not be ignored in terms of the explosion frequency. Particularly for a high-level cloud size category, the number of monitored clouds is scarce and each of them is important and may greatly have influence on the explosion frequency. Given that, it is concluded that neglecting the region beyond the maximum point in the 2^{nd} phase is restrictive, and may not be allowed for the high-level cloud size categories. For the purpose of validation, the effects of neglecting the 3^{rd} phase and the region beyond the maximum point in the 2^{nd} phase are further investigated through the case studies in Section 3.5.

3.5. Case study

As discussed earlier, using only a specific cloud size (i.e. the maximum one) or several discrete cloud sizes for evaluating the gas cloud frequency distribution may not be reasonable and the main reason is summarized by three aspects described in Section 3.1.

In the present study, case studies are conducted to demonstrate the importance of the transient process of gas cloud propagation in deriving the frequency distribution. The main focus is on two sides; one is to investigate whether the accuracy of the frequency distribution is lowered when disregarding the 3rd phase or the whole region beyond the maximum cloud size point, and the other one is to check how the number of monitored gas clouds affects the ERA results. To achieve that, a number of proposed ignited gas cloud frequency distributions are investigated in two different conditions, each of which is presented separately in the next sections.

All of the gas cloud distributions are derived from the same set of CFD dispersion simulations performed with time-varying leak rates, and for each derived distribution, a number of explosion scenarios is investigated by changing the cloud size category and cloud location. The cloud location is selected by four corners and one center to cover the entire interested area. Using the scenarios, then explosion simulations are carried out to check the pressure loads exerting on an interested target. In the current study, the target is chosen to be a firewall located between module 6 and module 7 shown in Fig. 9. At last, a number of overpressure exceedance curves are evaluated for the target, and each curve can be regarded as an ERA result for each frequency distribution.

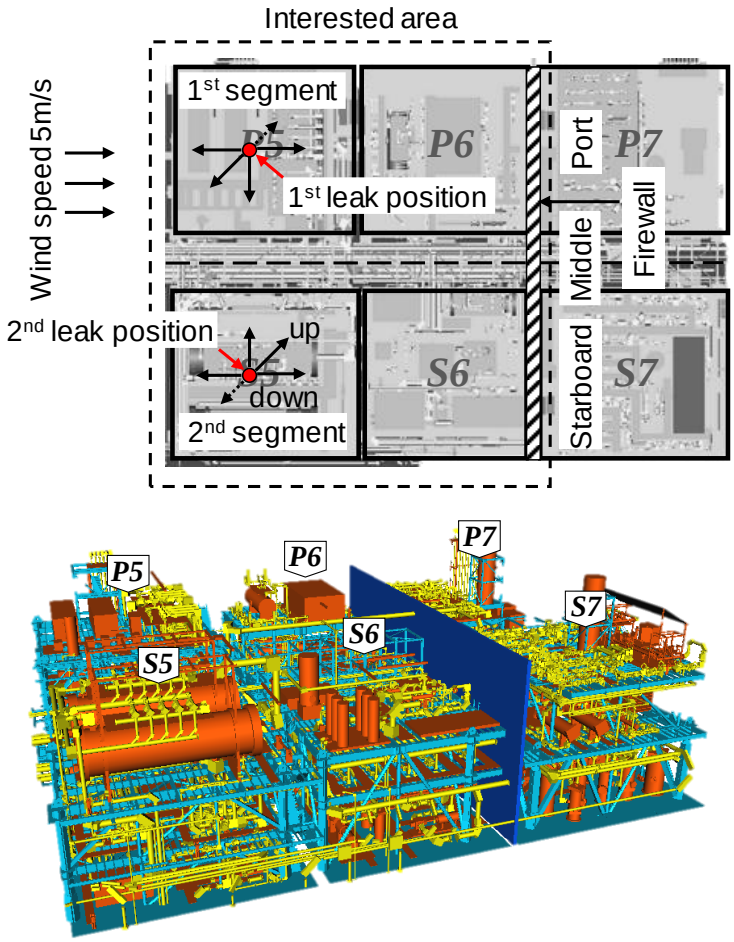

Fig. 9 Topside process model used in case studies

It is fair enough to say that investigating the leak scenarios is at least as challenging as the explosion scenarios. However, keeping in mind that the current study only focuses on the latter part of the ERA process (i.e. how to evaluate the exceedance curves when given a certain number of leak scenarios), the case studies only considers a small portion of the entire leak scenarios for simplicity. As presented in Fig. 9, totally 50 leak scenarios are investigated by including one wind speed & direction, two leak positions associated with two representative segments, five cases of time-varying leak

rate for each leak direction, and five leak directions for each position. In some cases, the ESD may not work properly and the leak rates do not decrease over time. In general, however, the failure probability of the ESD is very low and has little impact on the evaluation of DALs. In this study, the case where the ESD does not work is ignored. The time-varying leak rates are calculated purely by self-depressurization without considering the extra depressurization or blowdown functions. The two segments have the same amount of inventory, but the operating pressure of the 1st segment is twice of the 2nd segment. As a result, under the same initial leak rates, the leak durations until when the pressure drops to atmospheric pressure are higher for the 1st segment. The results of the calculation are presented in Fig. 10; five different leak hole sizes are taken into account in accordance with the five initial leak rate categories listed in Table 4.

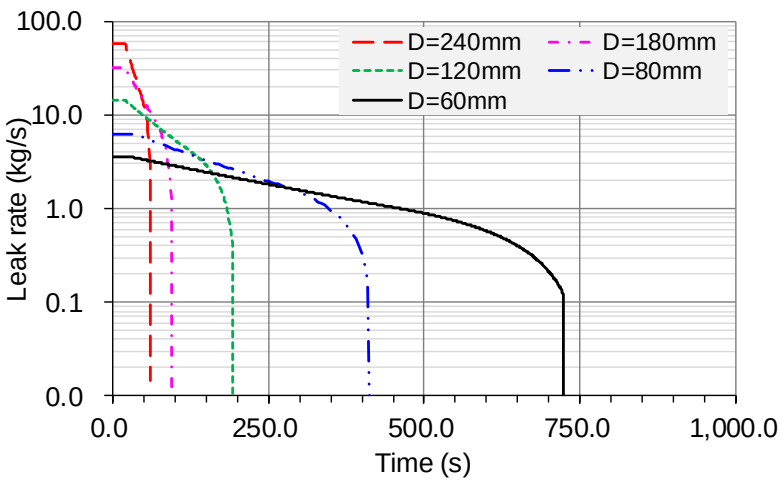

(a) 1st segment

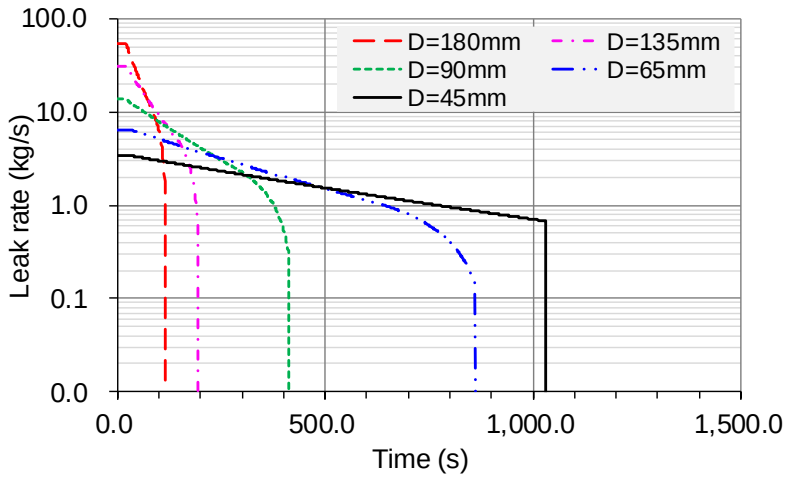

(b) 2nd segment

Fig. 10 Time-varying leak rates for case studies

Table 4 Initial leak rate categories and leak hole diameters

Initial leak rate category (kg/s)	1st segment Leak hole diameter, D (mm)	2nd segment Leak hole diameter, D (mm)
2~4	45	60
4~8	65	80
8~16	90	120
16~32	135	180
32~64	180	240

3.5.1. Case study 1: Effects of neglecting the 3rd phase or the region beyond the maximum cloud size point

To demonstrate the discussion of time-saving management using the simulation duration given in the Section 3.5, three examples of the ignited gas cloud frequency distribution are investigated here. The length of the simulation duration reflected in the distribution is given differently in the three cases. The first case considers a full length of the leak duration, and in case II the length is extended to the 2nd phase, and in case III, it is only limited to the maximum cloud size point.

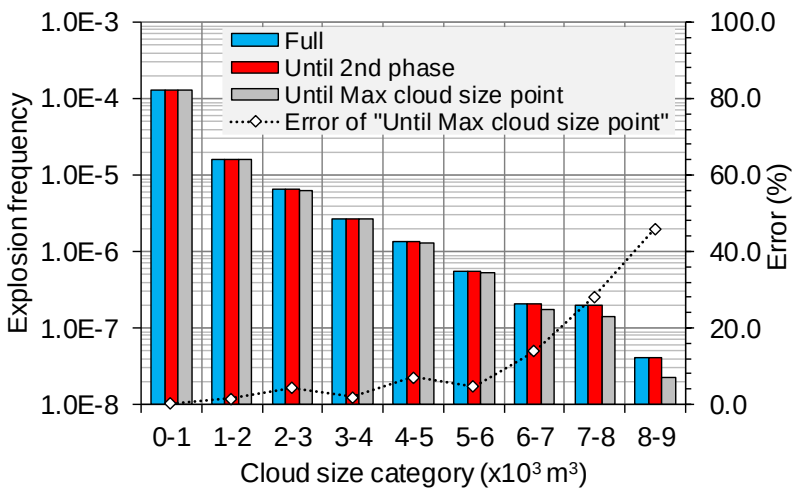

Fig. 11 Ignited gas cloud frequency distributions by different lengths of leak duration

The resulting ignited gas cloud frequency distributions are illustrated in Fig. 11. There is little difference between case I and case II, indicating that the 3rd phase has little impact in deriving the cloud frequency distribution. On the other hand, the difference between case II and case III is observable and grows up rapidly in

the high-level cloud size categories. As can be seen from the curve, the error in explosion frequency keeps less than 10 % before "5-6" category, but it starts to increase afterwards, and can reach up to 46% in the highest category. In Section 3.5, it has been argued that neglecting the region beyond the maximum point in the 2nd phase is restrictive and may only be allowed in low-level cloud size categories, and such a view is precisely proved in the present case study.

In terms of leak duration, the study also looks into the differences between case I and case III. As presented in Fig. 12, the total necessary duration for case II is 2625s, which is 12.82% of the total leak duration, while in case III that is 7.66%. The term "total" refers to a sum of the 50 investigated leak scenarios. The difference is 5.16%, which seems less significant than losing the accuracy in explosion frequency of high-level categories.

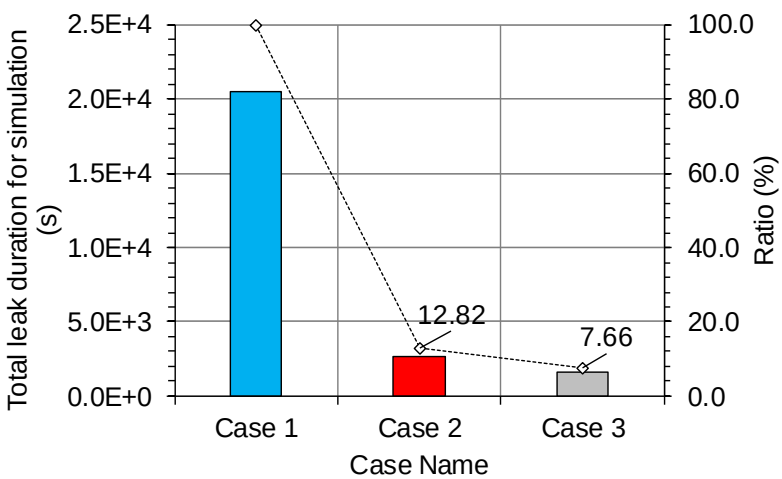

Fig. 12 Total leak durations for simulation

3.5.2. Case study 2: Effect of time interval, Δt

As discussed in Section 3.1, the main issue raised in existing ERA approach is that it does not fully reflect the entire transient process of gas cloud propagation when deriving the cloud frequency distribution. In the current case study, that issue is investigated using the proposed ignited gas cloud frequency distribution by varying the Δt. The total number of investigating cases is seven, and one of them is derived using only the maximum cloud sizes for the 50 identified scenarios as in the existing cases. Currently, the Δt can be given as smallest as 1s, thereby, when the Δt is 1s, the result is more accurate than any other cases and can be regarded as a base case to determine the error in other cases.

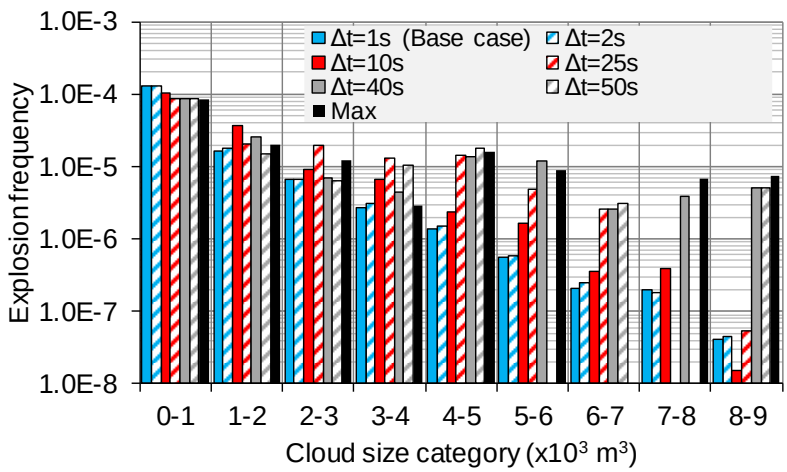

Fig. 13 Ignited gas cloud distribution by different Δt

The results are illustrated in Fig. 13. In each cloud size category, the explosion frequency varies with the Δt, and the intensities become more evident in the high-level categories. When the Δt is chosen to be greater than 1s (the base case), many gas clouds

appearing during the Δt are missed in the monitoring process, and the ignition probability portion that should be assigned those missed clouds, are then wrongly assigned to adjacent monitored clouds.

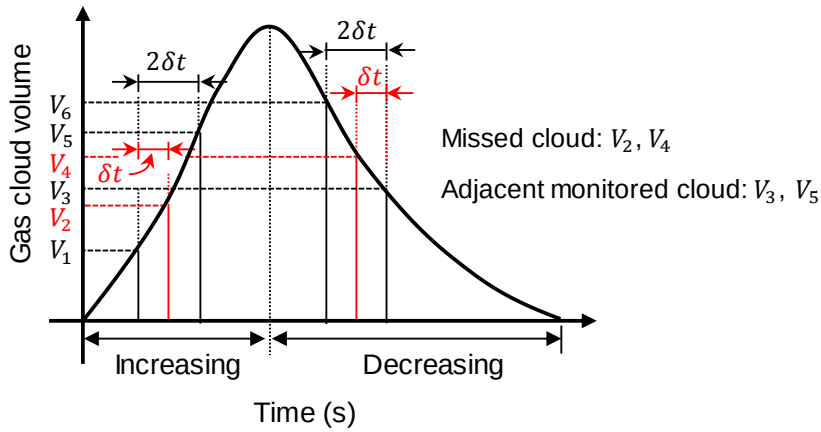

Fig. 14 Missed clouds and Adjacent monitored clouds

For example, in Fig. 14, if the Δt is chosen to be $2\,\delta\,t$, V_5 can be relatively regarded as an adjacent monitored cloud and V_2 can be a missed cloud which could have been monitored by a smaller time interval, $\delta\,t$. In this case, by choosing the larger interval, $2\,\delta\,t$, the ignition probability portion of V_2 during $\delta\,t$ is assigned to V_5, hence, the ignition probability portion of V_5 is overestimated as the duration becomes longer from the $\delta\,t$ to $2\,\delta\,t$. Consequently, the individual frequency of V_5 becomes higher than it is supposed to be.

With an overestimated individual frequency, the monitored clouds make a contribution to increasing the explosion frequency of the category to which they belong, but the missed clouds can, on the contrary, lower it. In particular, if the Δt is very large, owing to the missed clouds, some of the cloud size categories even occasionally lose the explosion frequency, and in that situation the cloud

frequency distribution is severely misinterpreted. For example, in Fig. 13, when the Δt is chosen to be 50s, the explosion frequency in "5−6" and "7−8" category is zero since the clouds of 5000~6000m^3 or 6000~7000m^3 are probably not identified during the monitoring process. However, such losses in most cases, are compensated for the overestimated explosion frequency in other categories. Again, for example, when compared to other categories, the explosion frequency of "3−4" category is evaluated much higher when Δt =50s than in the "Max" case. This implies that the explosion frequency of "3−4" category is probably overestimated, and affords for the frequency losses of the "5−6" and "7−8" categories.

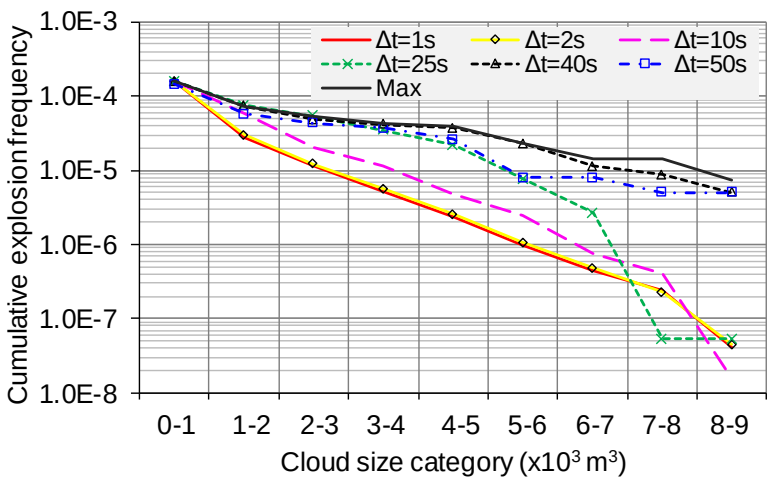

Fig. 15 Exceedance curve of cloud size category

Nevertheless, for all investigated cases, the total explosion frequency is conserved, which can be confirmed in Fig. 15. In other words, even if the Δt becomes greater, there is little global loss in explosion frequency, however, local losses are very likely available depending on the Δt.

From an overall perspective, as the Δt becoming larger, the difference in explosion frequency increases and becomes prominent in the high-level categories. As an extreme case, when only using the maximum cloud size, the differences are generally considerable in the high-level categories. If the Δt is greater than 1s, in most cases, the adjacent monitored clouds are more likely to be larger than the missed clouds, thereby, the overestimated individual frequencies tends to be assigned to the larger gas clouds than expected. The reason can be found in Fig. 12. The difference in total necessary duration between case I and case III is 5.16%, which is around half of the case II. This means that the total gas cloud size increasing period in case II, is twice as large as the decreasing period. Bearing in mind that the adjacent monitored clouds are bigger than the missed clouds during the increasing period ($V_5 > V_2$ but $V_3 < V_4$ in Fig. 14), the opportunity to have larger monitored gas clouds is very possible.

In order to investigate the effect of Δt in terms of an exceedance curve, overpressure exceedance curves are further developed for the target firewall. To do that, five cases of the derived frequency distributions are selected, and the exceedance curves are evaluated by dividing the whole firewall into three parts as presented in Fig. 9. Each of them is port side, starboard side and the middle part. The results are demonstrated in (a)-(c) of Fig. 16. As expected, the exceedance curves are also overestimated as the Δt is greater than 1s, and the difference from base case becomes greater with the Δt. In particular, when only using the maximum cloud sizes, the resultant DAL determined by a certain frequency level has the largest magnitude.

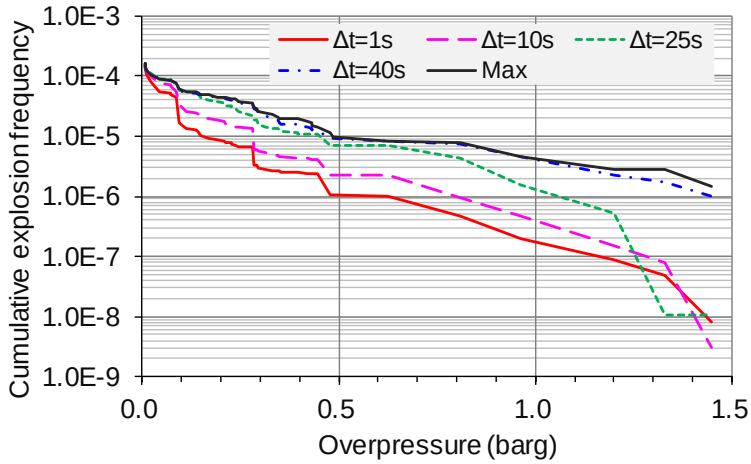

(a) Exceedance curves for portside

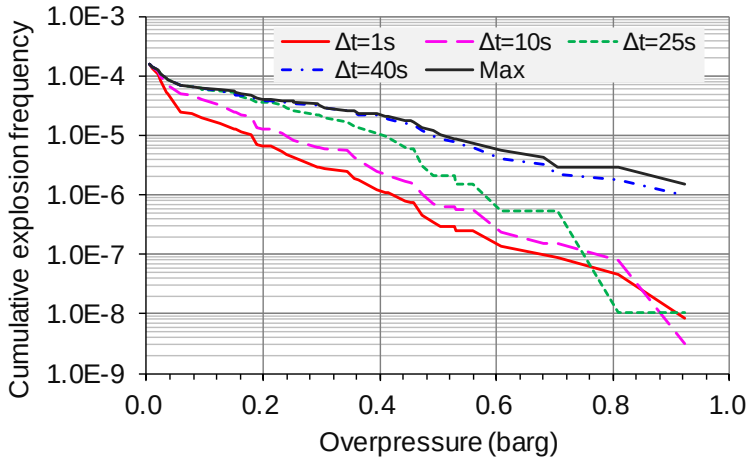

(b) Exceedance curves for starboard side

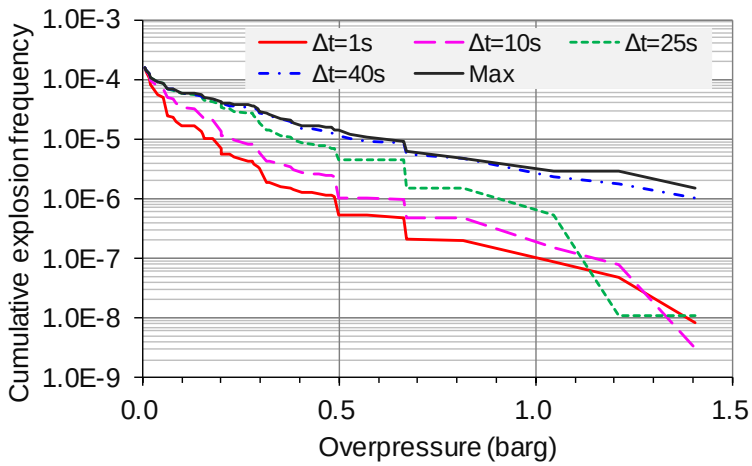

(c) Exceedance curves for the middle part

Fig. 16 Exceedance curves for target firewall

3.6. Summary

In the first case study, it proves that the proposed distribution can afford to reflect the entire transient process of gas cloud propagation under a time-varying leak rate condition, whilst, without increasing the costs for CFD consequence modeling too much. By introducing the concept of individual frequency (or ignited gas cloud frequency), it is found that the total necessary duration for deriving a gas cloud frequency distribution is far less than the total leak duration, and this is very beneficial in saving the total computing costs of the ERA. On the other hand, through the second case study, it is also concluded that if the gas clouds are monitored sparsely, i.e. $\Delta t > 1$ during the entire transient process, the ERA results may be overestimated. In particular, it is observed that the difference from the actual results becomes large when the gas cloud frequency distribution is derived using only a single maximum cloud size in each investigated scenario.

Chapter 4. Multivariate Frequency Distribution

4.1. Existing approach

[4]As already introduced, except for the cloud size, the variables needed for the explosion simulations are not actually dealt with in a probabilistic manner but are more likely to be conservatively determined based on engineering judgment and experience. The main reason is that there are many possibilities for the variables that can be assigned to a certain cloud size, since the size read in the gas cloud frequency distribution is typically indicative of multiple leak scenarios rather than a single leak scenario. Such an aspect can be found in the process of deriving the existing gas cloud distribution. A simple example is demonstrated in Fig. 17. In general, a large number of gas clouds are required to derive the gas cloud frequency distribution, but in this example only five are considered and each is assumed to be caused by a different leak scenario. Depending on the cloud size, the first three clouds belong to the 1st cloud size category, and the other two fall into the 2nd category. Normally, the gas clouds obtained from the gas dispersion simulations have an inhomogeneous fuel concentration distribution as well as an irregular shape. Such kinds of clouds are indicated by a closed dashed line in Fig. 17 and the cloud size, i.e. the volume of ESC is denoted by $V_{ac,i}^{es}$, which can be calculated using the actual volume $V_{ac,i}$, of the gas cloud within flammable limits.

[4] This chapter originates from published work (Jin and Jang, 2018b)

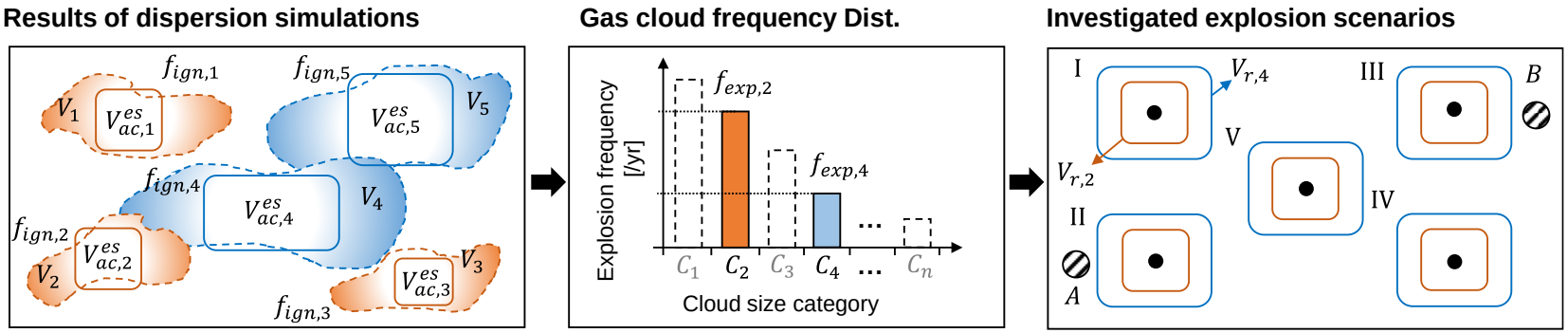

$V_{ac,1}^{es}, V_{ac,2}^{es}, V_{ac,3}^{es} \in C_2,\ V_{ac,4}^{es}, V_{ac,5}^{es} \in C_4$

$f_{exp,2} = f_{ign,1} + f_{ign,2} + f_{ign,3}$
$f_{exp,4} = f_{ign,4} + f_{ign,5}$

Non-homogeneous gas cloud

ESC ● Cloud position

Target (structure or equipment)

$f_{ign,i}$: Individual frequency of the i^{th} actual cloud, $i = 1, 2, 3, 4, 5$ [/yr]

$V_{ac,i}^{es}$: The volume of ESC for the i^{th} actual cloud [m³]

$V_{ac,i}$: The volume of the i^{th} actual cloud [m³]

C_j : The j^{th} cloud size category, $j = 1, 2, 3, 4, \cdots n$

$V_{r,j}$: Representative cloud volume for the j^{th} cloud size category [m³]

$f_{exp,j}$: Frequency of the j^{th} cloud size category [/yr]

Fig. 17 Example of existing gas cloud frequency distribution and investigated explosion scenarios.

The resultant distribution is also shown in the same figure and the frequency of the cloud size category is calculated using the individual frequency of the gas cloud. As shown in Eq.(3.6), the explosion frequency of the category C_2, $f_{exp,2}$ is obtained by summing the individual frequencies of the gas clouds (i.e. the 1st to 3rd gas clouds) whose size can be within the range of the C_2, and likewise the other two clouds are used to calculate the $f_{exp,4}$. More details on how to derive the distribution has been described in Chapter 3.

After the gas cloud distribution is derived, the explosion scenarios can be investigated by selecting a representative gas cloud size $V_{r,j}$, which used to be the upper bound of each category conservatively. However, it is obviously observed that each cloud size category represents one or more gas clouds and each gas cloud has a different position. In addition, the example illustrates that the information on the cloud position is not reflected in the derived distribution at all. Under these circumstances, to investigate the explosion scenarios, the position, shape and ignition position of each representative gas cloud must be additionally specified and that used to be determined conservatively by engineering judgment and experience.

Corresponding to such limitations of the existing gas cloud frequency distribution, guidance on how to determine the gas cloud position, shape and ignition position has been described in many previous studies (Hansen et al., 1999; Hoorelbeke et al., 2006; Hansen and Middha., 2007; Davis et al., 2011; Hansen et al., 2013), and also documented in the NORSOK standard (NORSOK, 2010). However, most guidance can only provide some qualitative recommendations and final decisions still remain for engineering

judgment. Therefore, the ERA results can vary from engineer to engineer, and the investigated explosion scenarios may be significantly different from the real conditions. In general, the guidance requires that the selected values or cases of the variables must sufficiently cover all possible explosion scenarios. In order to comply with the requirements, each variable used to be specified in multiple cases for the same selected cloud size, but some cannot match the real conditions and consequently affect the accuracy of the ERA. As a typical example, the specified ignition position may be different from the actual position of the ignition source, or the selected cloud size may be misplaced.

So far, the NORSOK standard recommends that the frequency distribution of gas cloud locations shall take into account the location of leak sources and ventilation conditions, e.g. wind rose etc. (NORSOK, 2010). According to this qualitative guidance, in most cases, the gas cloud positions have been selected based on a common practice that they should be distributed throughout the target area. The practice usually may lead to five common positions minimally, including four corners and one centre of the target area (Hansen et al., 1999; Hansen et al., 2013) but this is not always absolute, and may vary depending on the engineering judgment.

When the representative cloud size is considered with more than one positions, the frequency is evenly divided by the number of selected positions. For example, considering the common practice, both of the gas cloud size categories shown in Fig. 17 should be considered with the five indicated positions I–IV, and for any explosion scenario, for example, if the cloud size $V_{r,4}$ is placed in the position I, the explosion frequency is calculated by $f_{exp,4}/5$, and the same value is also assigned to the remaining four positions.

Multiple selections of the cloud position may be a way to effectively explain the aspect that the gas clouds can be formed anywhere due to various leak scenarios, but it does not mean that all possible gas cloud positions can be accurately described. More generally, applying the same gas cloud distribution to the entire target area may probably result in some misinterpreted explosion scenarios. For example, the contribution of the 4^{th} to 5^{th} gas clouds shown in Fig. 17 belongs to the 4^{th} cloud size category, and if the cloud positions are determined based on the existing method, the representative gas cloud of the 4^{th} category may be additionally placed at position I, II and IV. However, considering the results of dispersion simulations, these clouds are placed inaccurately and thus can affect the evaluations of explosion loads for nearby objects. In this example, the explosion load of target A may probably be overestimated because the larger gas cloud, $V_{r,4}$ is taken into account, which should not appear at position II. On the contrary, the explosion load of target B may be underestimated because those unnecessary size-position mismatched clouds can lower the frequency portion of position III, i.e. from $f_{exp,4}/2$ to $f_{exp,4}/5$.

Considering the above-mentioned example, in the current chapter, a multivariate frequency distribution (MVFD) is proposed, which aims at investigating the explosion scenarios without a concern of the size-position mismatch problems. The main endeavour is devoted to make the gas cloud frequency distribution contain the information of the gas cloud position so that the cloud size and the position are determined at the same time. To do so, two major problems need to be addressed, one is to define and quantify the cloud position and the other one is to reflect the quantified gas cloud position into the frequency distribution. The following section

is used to illustrate the solutions, and a general procedure for deriving the MVFD is to be presented.

4.2. Calculation of gas cloud position

In order to derive the propose MVFD, the gas cloud position should be quantified first. In the current study, the cloud position is defined as the volumetric center of the ESC, and calculated using the results of CFD gas dispersion simulations. The calculation is based on the original method (Gexcon, 2015) of calculating the ESC volume, Eq. (4.2) to Eq. (4.4) and finally performed by following Eq. (4.7) to Eq. (4.8). Prior to that calculation, it is necessary to first understand the physical meaning of the ESC. The ESC is designed to give explosion consequences comparable to an inhomogeneous gas cloud, and is calculated as the amount of gas in the flammable range, weighted by the concentration dependency of flame speed and volume expansion (Gexcon, 2015).

$$ER = \frac{\left(m_{fuel}/m_{oxygen}\right)_{actual}}{\left(m_{fuel}/m_{oxygen}\right)_{stoichiometric}} = \frac{\left(V_{fuel}/V_{oxygen}\right)_{actual}}{\left(V_{fuel}/V_{oxygen}\right)_{stoichiometric}} \qquad (4.1)$$

Generally, the flame speed and volume expansion of a fuel–oxygen gas mixture depend on the fuel concentration, which is typically measured by the equivalence ratio (ER) defined in Eq. (4.1) (Gexcon, 2015), where m is the mass, and V is the volume of the gas mixture. Using the ER, the volume of the ESC (or the equivalent stoichiometric volume of an actual gas cloud), V^{es}, can be calculated by considering only the gas amount within flammable ranges, which is given by Eq.(4.2)

$$V^{es} = \sum_{i=1}^{n} V_{cv,i} \cdot PORV_i \cdot F_{ESC}(ER_i) \tag{4.2}$$

Index $i = 1,2,\ldots n$ is used to indicate all control volumes (CVs) of the numerical grid inside the calculation domain where the ER is between the lower flammable limit (LFL) and the upper flammable limit (UFL) (Gexcon, 2015), i.e. $ER_{LFL} \leq ER_i \leq ER_{UFL}$. $V_{cv,i}$ is the volume of the i^{th} CV and $PORV_i$ is the corresponding porosity, which is defined as a fraction of volume open for fluid flow in the i^{th} CV. The weighting factor F_{ESC} is used to scale the original CV to a smaller volume with ER close to the stoichiometric condition, which can be calculated by Eq. (4.3). When the flame speed or the volume expansion has a maximum value, the ER is in general close to the stoichiometric condition (i.e. ER=1.0), but not exactly equal to 1.0. On the other hand, if the flame speed or the volume expansion is greatly below the maximum value, the ER is close to zero (Gexcon, 2015). Such an aspect becomes the basis for defining the factor F_{ESC}, and both the physical quantities, i.e. flame speed and volume expansion are included in the calculation. As shown in Eq. (4.3), the factor F_{ESC} is a dimensionless variable that has a value between zero and 1.0, depending on the value of ER. The function $\mathrm{ERfac}(ER_i)$ defined by Eq. (4.4) represents the effect of the flame speed, S_L, and the term $V_e(ER_i) - 1$ accounts for the effect of the volume expansion. V_e indicates the volume expansion ratio of the gas mixture before and after the combustion. By applying the ideal gas law, it can be rewritten by Eq. (4.5) in the form of the temperature T and the mean molecular weight M that varies with ER (Gexcon, 2015). When the ER of a particular CV provides the maximum of

$[V_e(ER)-1]\cdot ERfac(ER)$, then the F_{ESC} is equal to 1.0, which means that the entire CV contributes to the ESC, but if the F_{ESC} is calculated less than 1.0, the corresponding CV only contributes partially to the ESC.

$$F_{ESC}(ER_i)=\frac{[V_e(ER_i)-1]\cdot ERfac(ER_i)}{max\{[V_e(ER)-1]\cdot ERfac(ER)\}} \tag{4.3}$$

$$\mathrm{ERfac}(ER_i)=\frac{S_L(ER_i)}{max\{S_L(ER)\}} \tag{4.4}$$

$$V_e=\frac{V_{burnt}}{V_{unburnt}}=\frac{T_{burnt}/M_{burnt}}{T_{unburnt}/M_{unburnt}} \tag{4.5}$$

Based on the above-defined formulations, the following equation is proposed in the current study to calculate the volumetric center of the ESC. Both $[X]_c$ and $[X]_i$ indicate a position vector containing three components of the center coordinates. $[X]_c$ represents the ESC center and $[X]_i$ represents the i^{th} CV center.

$$[X]_c=\frac{\sum_{i=1}^{n}[X]_i\cdot V_{cv,i}\cdot PORV_i\cdot F_{ESC}(ER_i)}{\sum_{i=1}^{n}V_{cv,i}\cdot PORV_i\cdot F_{ESC}(ER_i)} \tag{4.6}$$

Considering the time aspect, Eq. (4.6) can be rewritten in the following form.

$$[X(t)]_c=\frac{\sum_{i=1}^{n}[X]_i\cdot V_{cv,i}\cdot PORV_i\cdot F_{ESC}\left(ER_i(t)\right)}{\sum_{i=1}^{n}V_{cv,i}\cdot PORV_i\cdot F_{ESC}\left(ER_i(t)\right)} \tag{4.7}$$

where $F_{ESC}\left(ER_i(t)\right)$ is determined by $ER_i(t)$, as shown in Eq. (4.8), which varies with time.

$$F_{ESC}\left(ER_i(t)\right) = \frac{\left[V_e\left(ER_i(t)\right) - 1\right] \cdot ERfac\left(ER_i(t)\right)}{max\{[V_e(ER) - 1] \cdot ERfac(ER)\}} \tag{4.8}$$

In order to perform the calculation, one needs to access each CV to collect necessary data, such as the center coordinates, volume, porosity and fuel concentration etc. As well known, the number of CVs is usually very large in a CFD simulation and manual calculations can be very challenging. In the current study, however, the calculation is automated with an in-house code. The code can interface with the commercial tool, FLACS (Gexcon, 2015) to read the necessary input data automatically and compute the center coordinates at every single time step of the CFD simulation.

The detailed calculation process is demonstrated in Fig. 18. First, it is necessary to extract the grid data from the setup files of the dispersion simulation performed by the FLACS and use it calculate the center coordinates and volume of each CV. Afterwards, the porosity distribution, $PORV_i$ and the ER distribution, $ER_i(t)$ should be extracted from the results of the dispersion simulation. The latter one is time dependent and must be extracted repeatedly. The weighting factor, $F_{ESC}\left(ER_i(t)\right)$ can be obtained using the functions, $ERfac\left(ER(t)\right)$ and $V_e\left(ER(t)\right)$, and the cloud position then can be calculated using Eq. (4.7). The whole process should be proceeded iteratively by updating the time t.

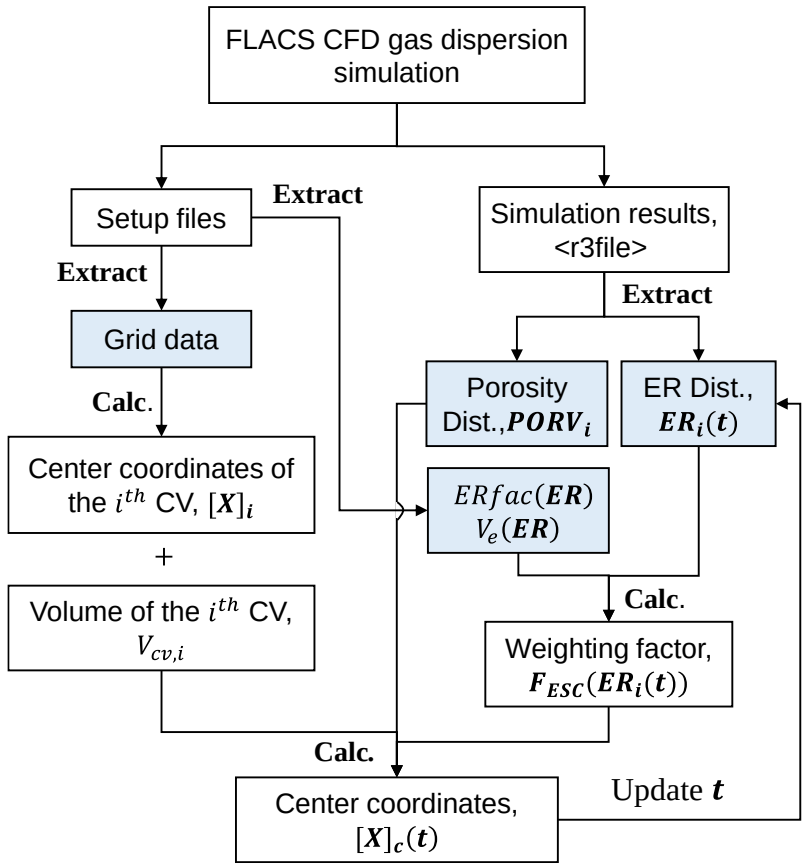

Fig. 18 Computing process of self-developed code

Fig. 19 shows an example of the gas cloud center positions calculated by Eq. (4.7) and Eq. (4.8). The results are displayed in a projected x-y plane with four different snapshots, and a full-time trajectory of the center is also presented by a zoomed plot in the lower right corner. The red solid circle indicates the current position, which is shown by an empty circle in the contour plot. The contour represents the fuel concentration, which is expressed by a normalized flammable range with an equivalent ratio (EQNFL). EQNFL=1 indicates the UFL and EQNFL=0 the LFL.

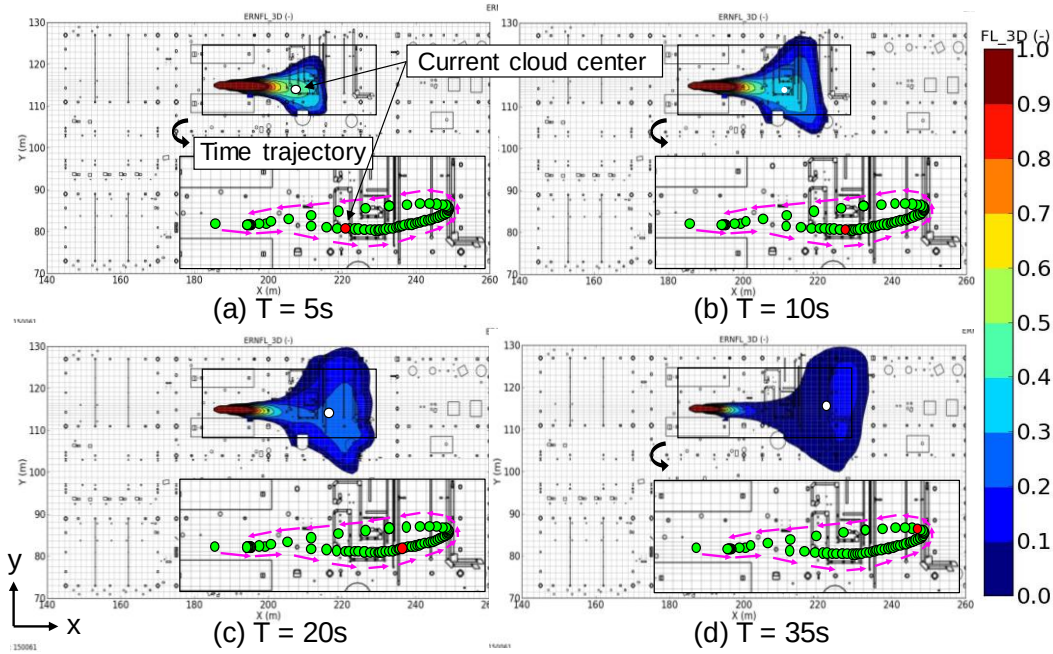

Fig. 19 Snapshots of gas cloud center position in x−y plane

4.3. Methodology of MVFD

The main idea of the proposed MVFD is to distribute the explosion frequency not only by the gas cloud size but also by the position of the corresponding gas cloud. In other words, it means that the MVFD is a 4−dimensional distribution that includes three variables X, Y and Z representing the center position and a variable V representing the cloud size. Using the equations introduced in Section 4.2, each variable is available to be calculated at any moment and the proposed distribution can be derived by gathering and summarizing the results.

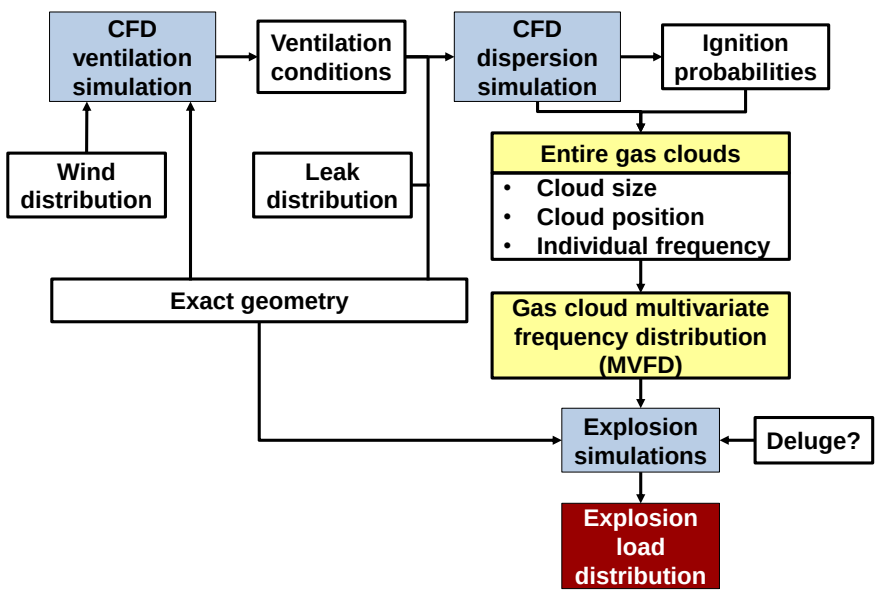

Fig. 20 ERA procedure with MVFD

The detailed procedure is given in Fig. 20 and the MVFD shown in the figure can be regarded as an extended version of the previous gas cloud frequency distribution, i.e. ignited gas cloud frequency

distribution introduced in Chapter 3. The applied methodologies are very similar but in the case of the MVFD, the previous procedure has to be extended to multi-dimensional. That is, one needs to consider the explosion frequency using a joint category consisting of four types of categories, as described in Step 6, and also use the four conditions shown in Eq. (4.13) to determine whether a monitored gas cloud belongs to the current joint category. Time-varying leak rate is still considered in the current section, as it is typical in most leak scenarios. The processes of obtaining the individual frequency of each monitored gas cloud, i.e. Steps 3 to 5, are identical to the previous procedure described in Chapter 3.

1. Perform a CFD simulation for each investigated leak scenario using a time-varying leak rate profile.

2. Set a time interval Δt to monitor the gas clouds for all leak scenarios, and meanwhile calculate the properties, i.e. $[V_{ac}^{es}, x, y, z]$ of each cloud using the equations described in Section 4.2.

3. Calculate the total ignition probability for i^{th} leak scenario before or at time t_j, using TDIIM and gas clouds given by the FLACs dispersion modelling (DNV, 1998).

$$P_{ign,i}(t \le t_j) = P_{imm} + (1 - P_{imm}) \cdot P_{del,i}(t \le t_j) \qquad (4.9)$$

$$P_{del,i}(t \le t_j) = P_{D,i}(t \le t_j) + P_{C,i}(t \le t_j) - P_{D,i}(t \le t_j) \cdot P_{C,i}(t \le t_j) \quad (4.10)$$

where P_D and P_C is ignition probability of an intermittent and a continuous ignition source, respectively; P_{del} and P_{imm} refers to the delayed and immediate ignition probability, respectively,

and P_{ign} refers to the total igniting probability.

4. For each leak scenario, calculate the incremental ignition probability for i^{th} leak scenario in j^{th} time interval, $\Delta P_{ign,i}(\Delta t_j)$ using the total ignition probability, $P_{ign,i}(t \le t_j)$ given by TDIIM.

$$\Delta P_{ign,i}(\Delta t_j) = P_{ign,i}(t \le t_j) - P_{ign,i}(t \le t_{j-1}) \qquad (4.11)$$

5. Calculate the individual frequency (or frequency of ignited gas cloud) of every monitored gas cloud for i^{th} leak scenario in j^{th} time interval, $f_{ign,i}(\Delta t_j)$, and add it as another property of the cloud.

$$f_{ign,i}(\Delta t_j) = f_{leak,i} \cdot \Delta P_{ign,i}(\Delta t_j) \qquad (4.12)$$

where $f_{leak,i}$ refers to the frequency of i^{th} leak scenario.

6. Set a number of categories for each variable including the cloud size V, and three coordinates of the cloud center, X, Y and Z to classify the monitored gas clouds. The notations n_V, n_X, n_Y and n_Z are used to indicate the total number of categories for each variable. Since the proposed distribution is a multivariate distribution, the four types of categories must be considered conjunctively, which is denoted by a joint category $\boldsymbol{C}_{klpq}$, where $k \in (0, n_V)$, $l \in (0, n_X)$, $p \in (0, n_Y)$ and $q \in (0, n_Z)$. The total number of joint categories n_{JC} is equal to $n_V \cdot n_X \cdot n_Y \cdot n_Z$.

7. Classify the monitored gas clouds based on the four types of categories defined in Step 6. For example, if the properties of a certain gas cloud monitored at j^{th} time interval in i^{th} leak scenario, $\left[V_{ac,i}^{es}(\Delta t_j), x_i(\Delta t_j), y_i(\Delta t_j), z_i(\Delta t_j), f_{ign,i}(\Delta t_j)\right]$ satisfies the following conditions simultaneously, then it can be classified into a jointed category $\boldsymbol{C}_{klpq}$.

$$\begin{cases} V_{c,k-1} \le V_{ac,i}^{es}(\Delta t_j) < V_{c,k} \\ X_{l-1} \le x_i(\Delta t_j) < X_l \\ Y_{p-1} \le \mathrm{y}(\Delta t_j) < Y_p \\ Z_{q-1} \le z_i(\Delta t_j) < Z_q \end{cases} \tag{4.13}$$

where $V_{c,k}$ and $V_{c,k+1}$ stand for the lower and upper boundaries of the k^{th} cloud size category, respectively and the same rule of notation is applied to the remaining variables.

8. Calculate the explosion frequency of the jointed category $\boldsymbol{C}_{klpq}$.

$$f_{exp,klpq} = \sum_{i=1}^{n_{ls}} \sum_{j=1}^{n_{t,i}} f_{ign\_ij} \tag{4.14}$$

here, if the gas cloud satisfies the Eq. (4.13), $f_{ign\_ij} = f_{ign,i}(\Delta t_j)$, otherwise $f_{ign\_ij} = 0$.

where n_{ls} stands for the total number of leak scenario and $n_{t,i}$ stands for the total number of Δt in i^{th} leak scenario.

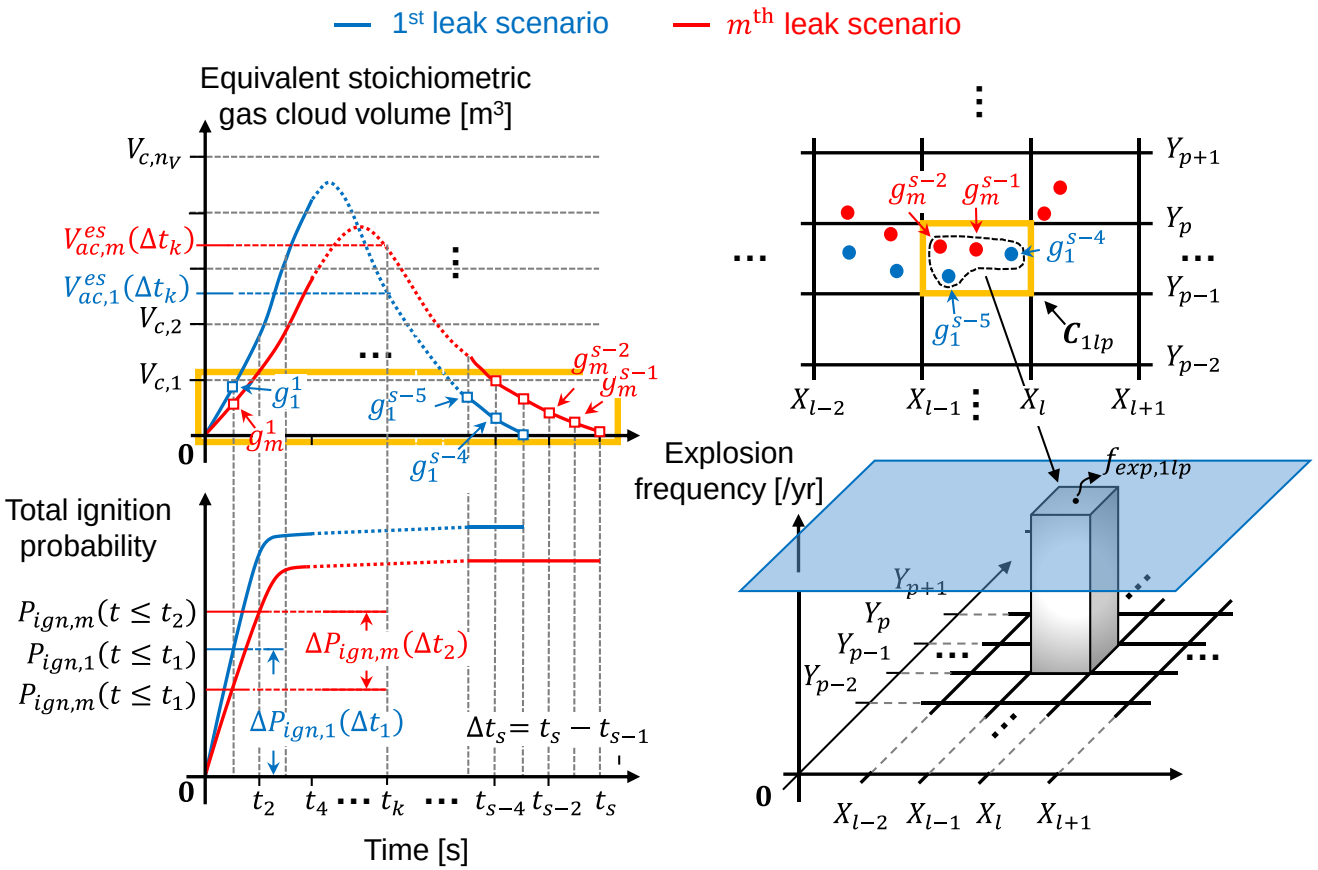

Fig. 21 Example of deriving the proposed distribution

An example covering the entire steps is presented in Fig. 21. Here, the example is demonstrated with a simplified version of the MVFD because it is impossible to display a 4−dimensional distribution graphically. The variable Z is ignored and only the 1st cloud size category including the monitored gas cloud with a size between zero and $V_{c,1}$ (i.e. the gas clouds located inside the rectangular box in Fig. 21.) is considered. The explosion frequency of the 1st cloud size category can be further divided by the position of the cloud center. For instance, the joint category $\boldsymbol{C}_{1lp}$ shown in the figure contains four monitored gas clouds (i.e. $g_1^{s-5}, g_1^{s-4}, g_m^{s-2}, g_m^{s-1}$) with a range of $V \in (0, V_{c,1})$, $X \in (X_{l-1}, X_l)$, $Y \in (Y_{p-1}, Y_p)$, and then the corresponding frequency, $f_{exp,1lp}$ can be calculated as below. The equations only represent the two leak scenarios shown in figure, and in this case n_{ls}= 2, $n_{t,1} = \mathrm{s} - 3$ and $n_{t,m} = \mathrm{s}$.

$$g_1^{s-5} \ : \ f_{ign,1}(\Delta t_{s-5}) = f_{leak,1} \cdot \Delta P_{ign,1}(\Delta t_{s-5})$$

$$g_1^{s-4} \ : \ f_{ign,1}(\Delta t_{s-4}) = f_{leak,1} \cdot \Delta P_{ign,1}(\Delta t_{s-4})$$

$$g_m^{s-2} \ : \ f_{ign,m}(\Delta t_{s-2}) = f_{leak,m} \cdot \Delta P_{ign,m}(\Delta t_{s-2})$$

$$g_m^{s-1} \ : \ f_{ign,m}(\Delta t_{s-1}) = f_{leak,m} \cdot \Delta P_{ign,m}(\Delta t_{s-1})$$

$$f_{exp,1lp} = f_{ign,1}(\Delta t_{s-4}) + f_{ign,1}(\Delta t_{s-5}) + f_{ign,m}(\Delta t_{s-1}) + f_{ign,m}(\Delta t_{s-2})$$

4.4. Case study

In the present study, case studies are conducted to demonstrate how important it is to accurately specify the gas cloud position when evaluating the explosion loads. The main focus is on two sides; one is to investigate the variations in ERA results using the existing distribution and the other one is to identify the differences in ERA results between the existing and the proposed distributions. To achieve that, the ERA is carried out with three cases (i.e. Case I-1, Case I-2 and Case II) and all are designed to evaluate the explosion design loads for the same targets using the same leak scenarios. However, the investigated explosion scenarios in each case are different. For Case I-1 and Case I-2, the scenarios are investigated by the existing gas cloud frequency distribution and the difference is given in selecting the cloud position. Whereas, for Case II, the scenarios are investigated using the proposed MVFD, and the cloud position is automatically determined. To obtain these distributions, the CFD gas dispersion simulation should be performed in advance with a certain amount of leak scenarios.

In the present study, the leak scenarios remain consistent with the previous case study introduced in Chapter 3. As shown in Fig. 9, for each leak position, one representative segment is considered with five cases of time-varying leak rate (or leak hole size), and each time-varying leak rate is simulated with five leak directions and one wind speed and direction.

One of the problems with the existing gas cloud frequency distribution is that the selected cloud positions can vary from engineer to engineer, and in the current case studies the aspect is implemented by investigating two different sets of explosion

scenarios (Case I−1 and Case I−2). The difference between Case I−1 and Case I−2 lies in the target area shown in Fig. 22, which is used for determining the gas cloud position as described in Section 4.2. Perhaps, from a conservative perspective, most engineers are likely to choose the target area I, since it includes the entire process area. However, depending on the wind condition, some experienced engineers may also prefer to choose the target area II because they believe that most of the gas clouds may be blown to the firewall. This discrepancy of engineering judgment consequently leads to different pictures of the selected gas cloud positions and each is to be separately discussed in the following sections.

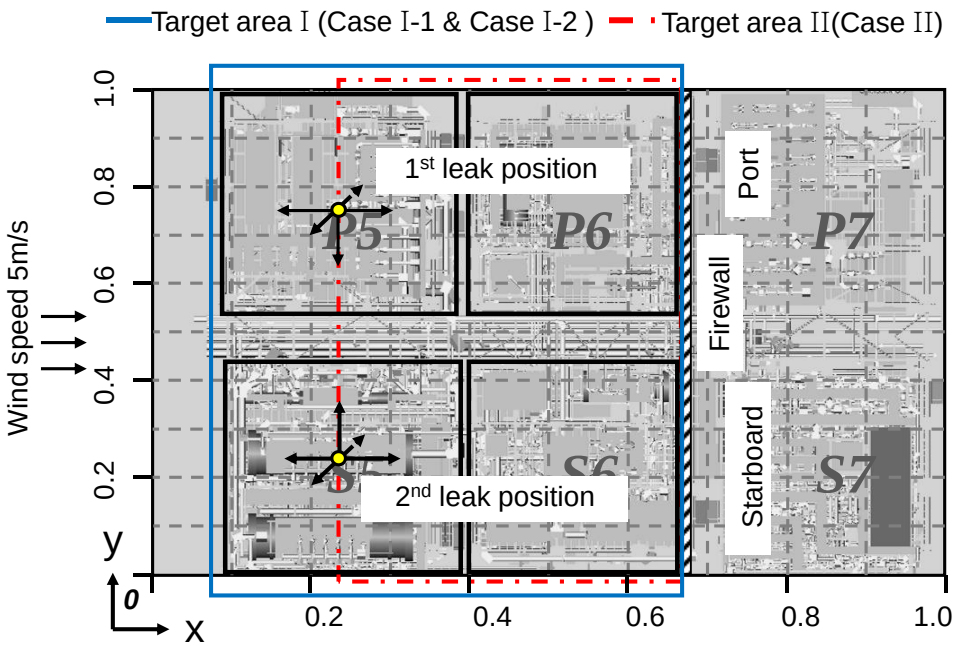

Fig. 22 Target area used for determining gas cloud position

The derived distributions are presented in following Fig. 23 and Fig. 24, respectively. As described in Section 4.3, the MVFD cannot be displayed in its entirety because it is a 4−dimensional distribution, but can only be displayed by reducing the number of dimensions. Using the same method shown in Fig. 21, the total number of the simplified version of the MVFD for Case II is nine, which is the same as the number of the cloud size categories shown in Fig. 23.

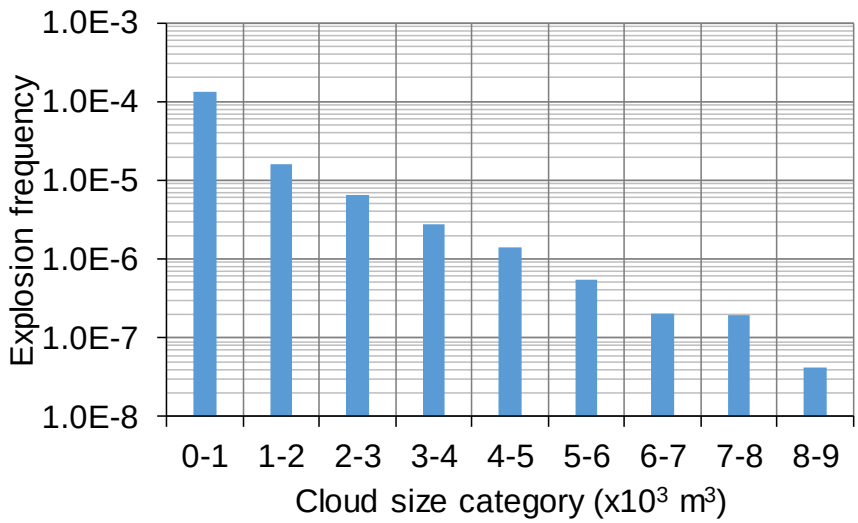

Fig. 23 Existing gas cloud frequency distribution for Case I−1 & Case I−2

As an example, only two of them are presented in Fig. 24, each representing the categories of 0−1000 m^3 and 7000−8000 m^3, respectively. In other words, it means that the explosion frequency of each cloud size category in the existing distribution is further distributed by the cloud position categories in the MVFD. Comparing the two distributions, it can also be found that the cloud size is dependent on the cloud position. For example, if the cloud size belongs to the 0−1000 m^3 category, the corresponding position is

typically close to the leak positions. According to the Fig. 22, the 1st the leak positions is located in 0.2−0.3 (x) ∩ 0.2−0.3 (y) (former represents the x direction and latter represents the y direction), the other one is located in 0.2−0.3 (x) ∩ 0.7−0.8 (y). It should also be noted that the category not only includes the clouds that appear at the early stages of a leak, but also those appearing in the later stages of the leak. On the other hand, if the cloud size falls within the 7000−8000 m^3 category, the corresponding cloud is relatively far away from the leak positions, and all of these phenomena are both self−evident. That is, the cloud size within flammable limits is small at the beginning of a leak, and grows as the gas mixture moves outward. When the gas mixture spreads much wider and at the same time the leak rate drops significantly, the fuel concentration is diluted, causing the cloud size to decrease and the position to approach the leak positions again. However, such dynamic aspects cannot be manifested by the existing distribution.

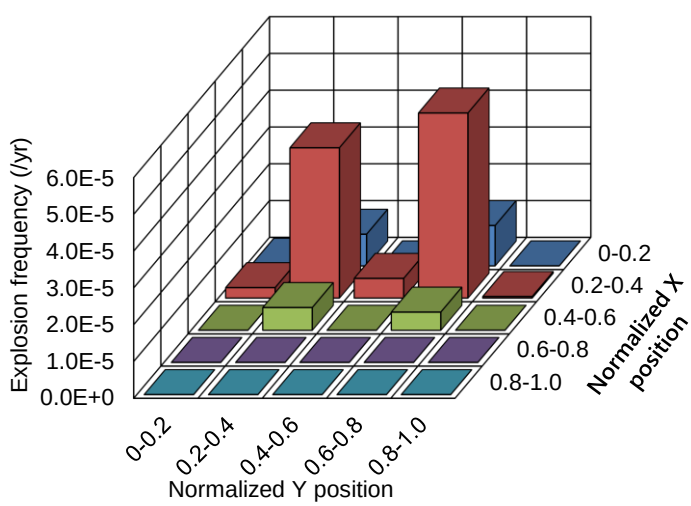

(a) Cloud size category, 0−1000 m^3

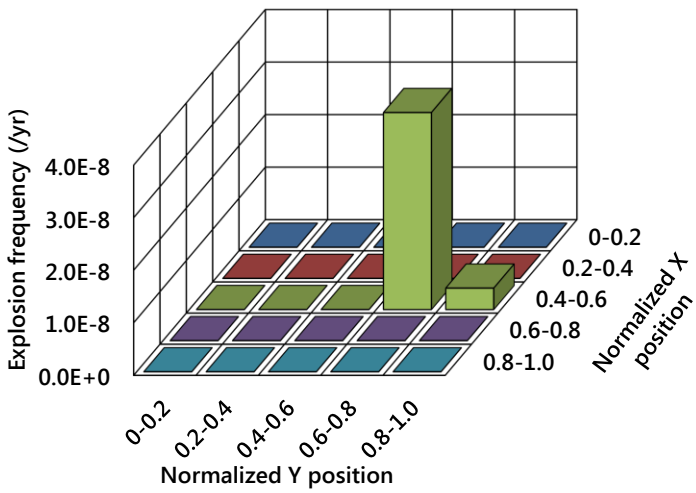

(b) Cloud size category, 7000 −8000 m^3

Fig. 24 MVFD for Case II (Displayed by a simplified version)

Using the derived distributions, the explosion scenarios are investigated for each case, and then explosion simulations are carried out to evaluate the design explosion loads. Further details are provided in the following sections. In general, for a single target of interest, the design explosion load is determined via a probability of exceedance curve. The targets used in the case studies include all deck spaces inside the modules illustrated in Fig. 22, and these deck spaces are shown Fig. 26. For example, “P6_M_T” is the space between the mezzanine deck and top deck of module P6 and “S5_P_U” is the space between the process deck and upper deck of module S5. For each investigated explosion scenario, the resulting overpressure distribution inside each deck space is measured by using a certain number of monitoring points. For each deck space, monitoring points are arranged at regular intervals and the peak

overpressure as shown in Fig. 25 of each monitoring point is selected to calculate the average peak overpressure. The average peak overpressure for each explosion scenario is then collected to evaluate the exceedance curve.

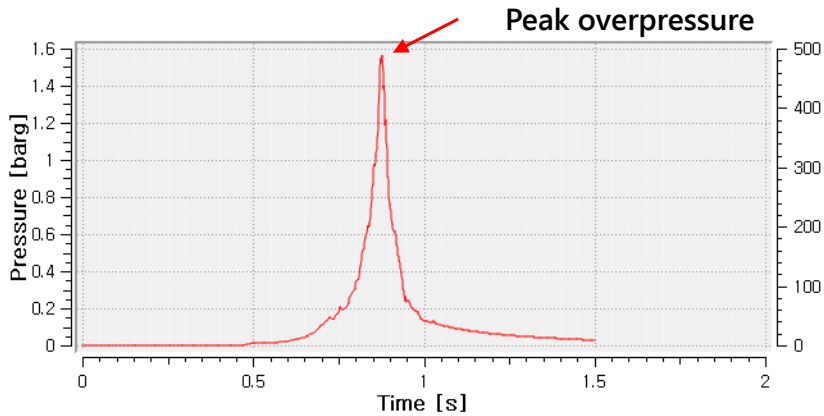

Fig. 25 Example of peak overpressure

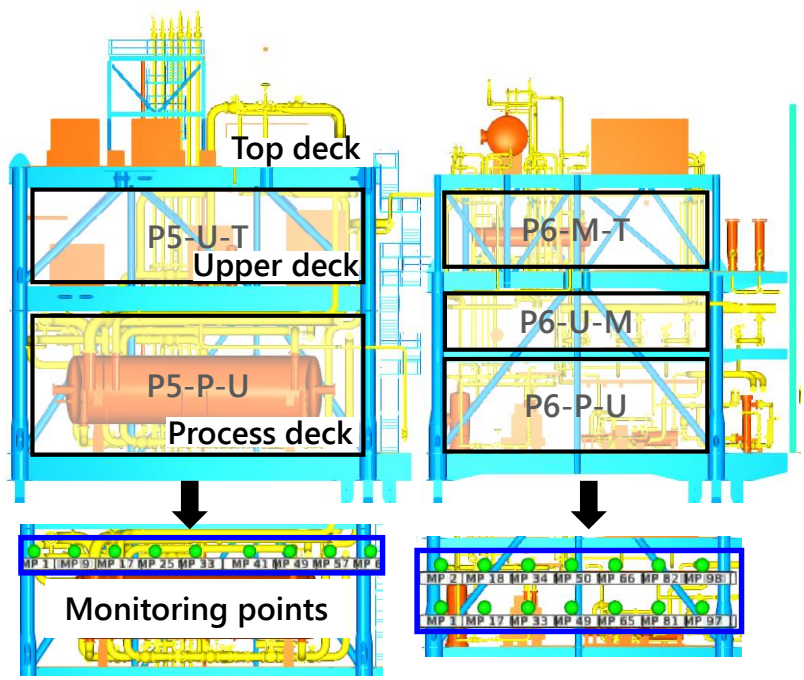

(a) Port side

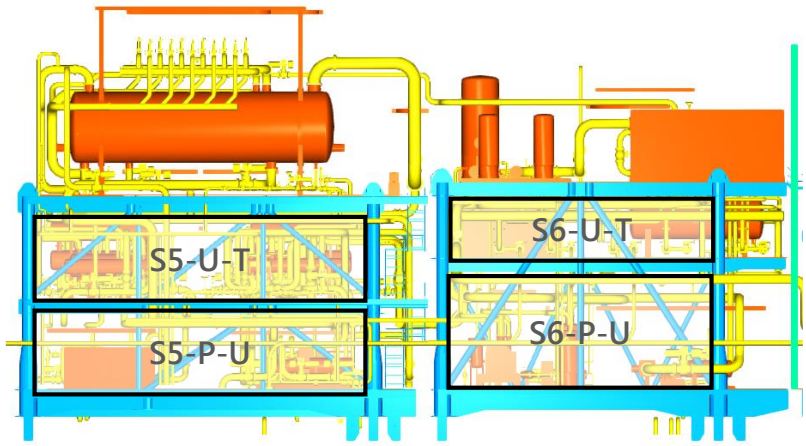

(b) Starboard side

Fig. 26 Target deck spaces used for case studies

4.4.1. Case study I: Variations in ERA results with the existing g as cloud frequency distribution.

To demonstrate the variations in the ERA results caused by selecting different gas cloud positions, Case I−1 and Case I−2 are compared in this section. The investigated explosion scenarios for each case are provided in Fig. 27. The figure displays a projected view of a normalized x−y plane, which is consistent with the Fig. 22 and Fig. 24. In the figure, the shaded area represents the deck plates, and the four empty circles connected by a dotted line indicate the main columns of each module. The colored rectangles indicate calculated ESCs and each color represents a different cloud size category. The ESCs are placed at five different positions numbered from 1 to 5 in the target areas, including four corners and one center as described in Section 4.1. Among them, position 1 and position 3 represent the back two corners, position 2 and position 4 represent the front two corners, and position 5 represents the center. It is observed that the two back corners and the center position of Case I−2 are placed closer to the firewall than Case I−1, because of the different targets areas.

The resultant overpressure exceedance curves are presented in Fig. 28 − Fig. 31. Comparing the two cases, the exceedance curves are evaluated lower in Case I−1 than Case I−2 for the deck spaces in S6 and P6 modules. This is because, as shown in Fig. 27, the targets are closer to the ESCs in Case I−2 and higher overpressure loads can act on them. On the contrary, in Case I−2, the deck spaces in S5 and P5 modules are farther away from the ESCs than Case I−1, therefore the exceedance curves are evaluated lower in Case I−2.

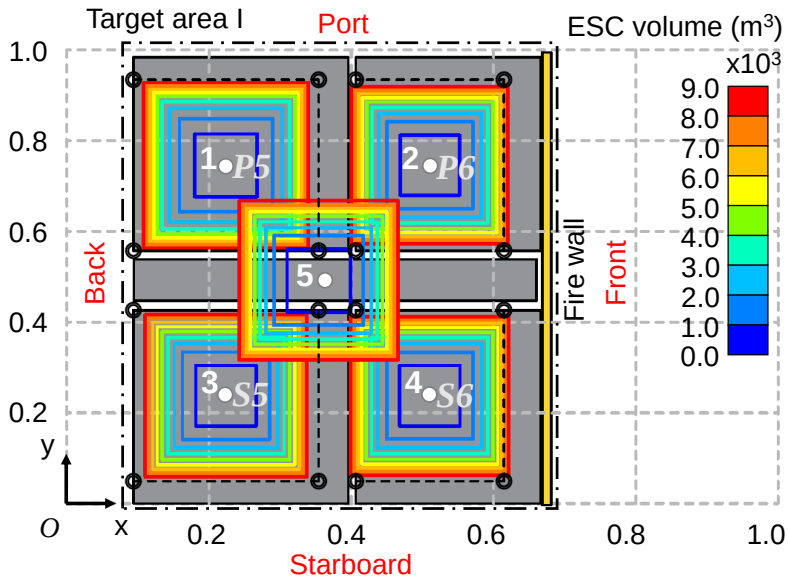

(a) Case I-1

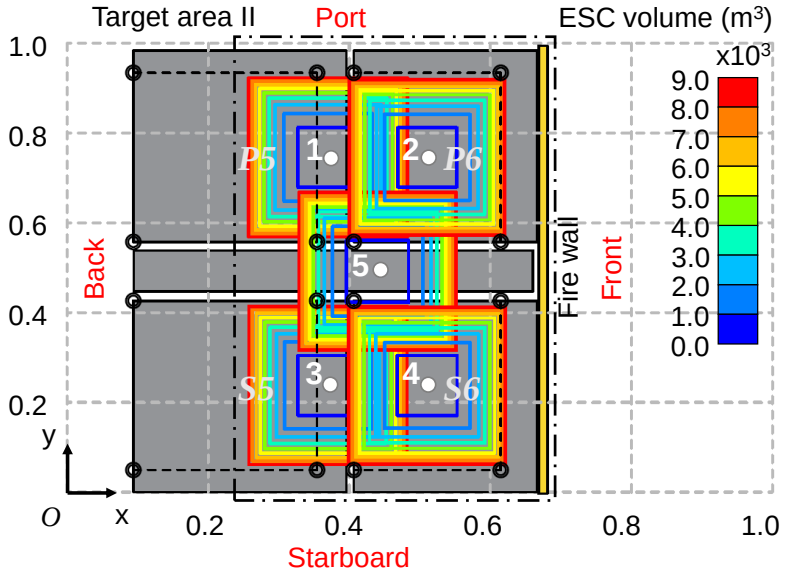

(b) Case I-2

Fig. 27 Investigated explosion scenarios (ESC sizes & positions)

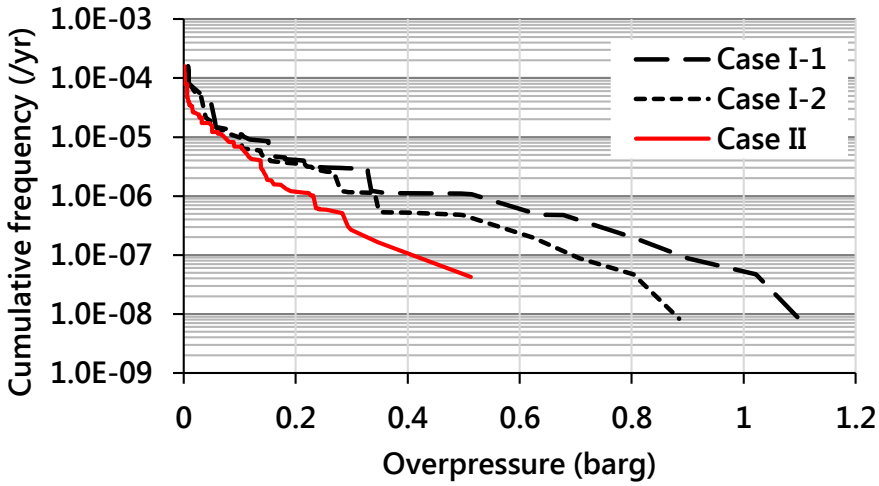

(a) S5-P-U

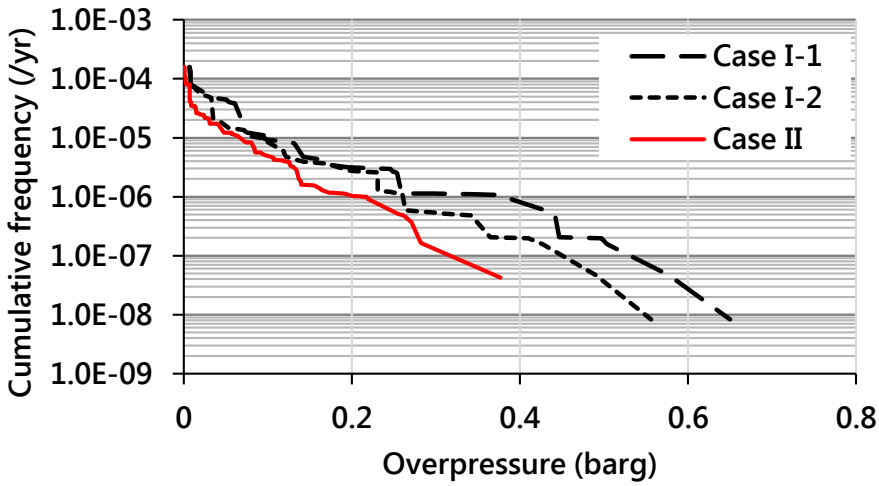

(b) S5-U-T

Fig. 28 Overpressure exceedance curves for deck spaces in S5 module[5]

[5] Since the explosion simulations are updated by adding initial turbulence, the results are different from the original version published in Jin and Jang (2018b).

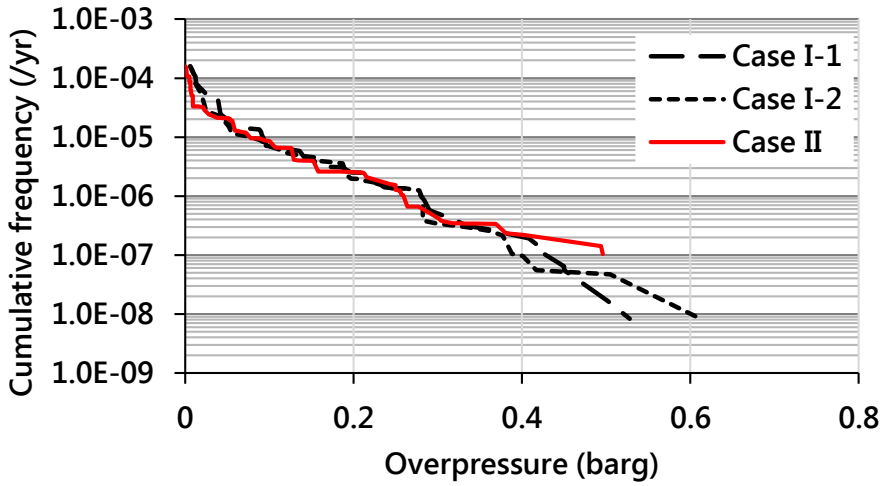

(a) P5_P_U

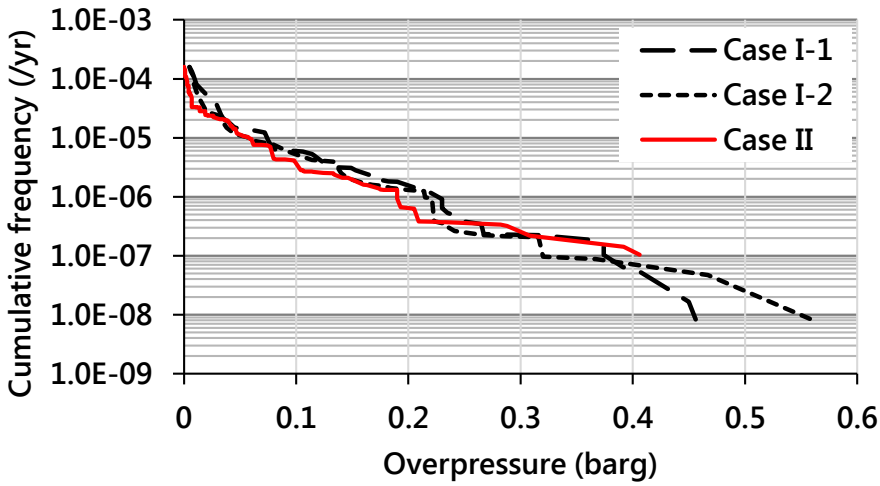

(b) P5_U_T

Fig. 29 Overpressure exceedance curves for deck spaces in P5 module[6]

[6] Since the explosion simulations are updated by adding initial turbulence, the results are different from the original version published in Jin and Jang (2018b).

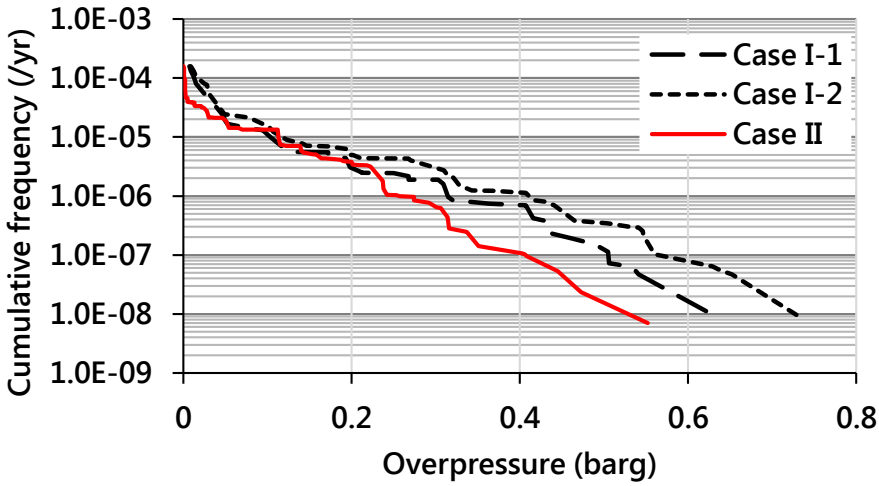

(a) S6-P-U

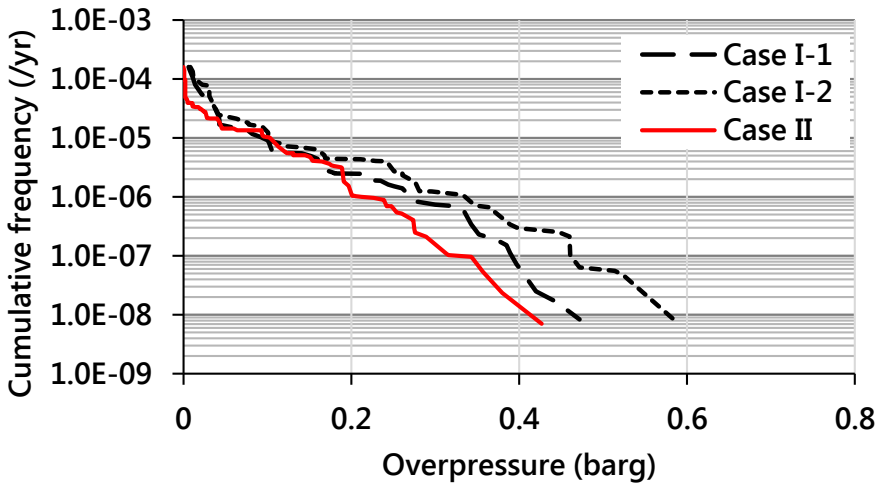

(b) S6-U-T

Fig. 30 Overpressure exceedance curves for deck spaces in S6 module[7]

[7] Since the explosion simulations are updated by adding initial turbulence, the results are different from the original version published in Jin and Jang (2018b).

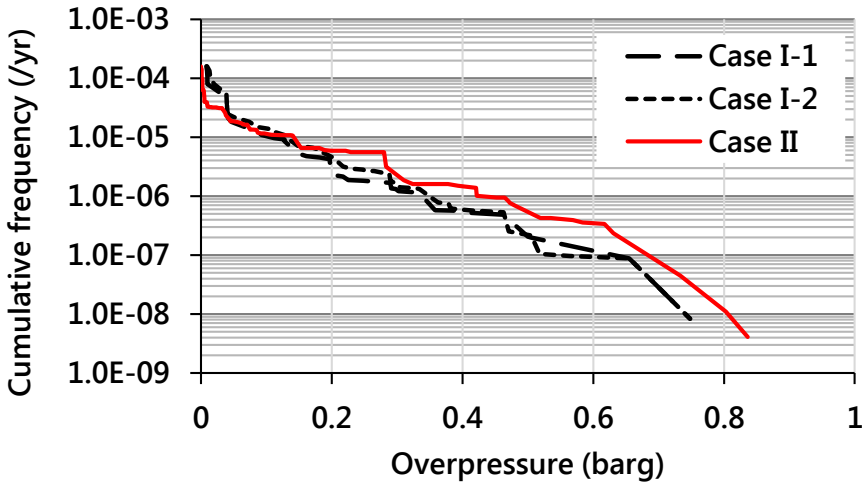
1.0E-03
1.0E-04
1.0E-05
1.0E-06
1.0E-07
1.0E-08
1.0E-09
Cumulative frequency (/yr)
0
0.2
0.4
0.6
0.8
1
Overpressure (barg)
Case I-1
Case I-2
Case II

(a) P6-P-U

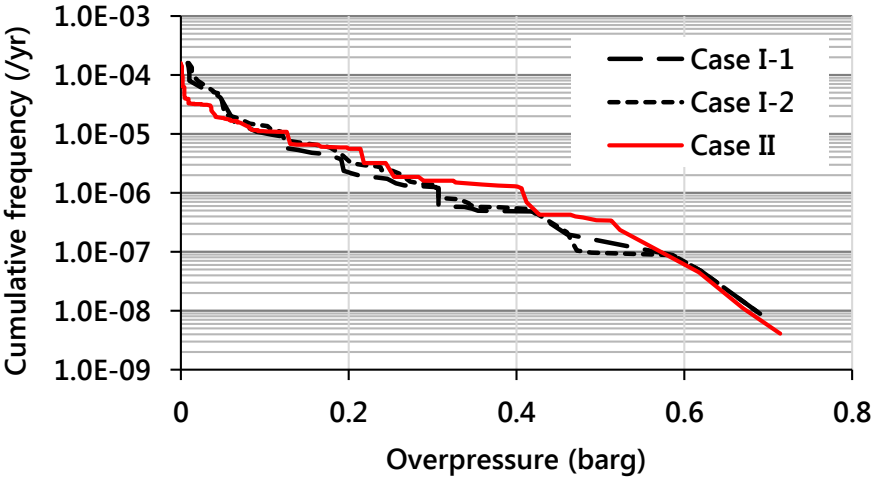
1.0E-03
1.0E-04
1.0E-05
1.0E-06
1.0E-07
1.0E-08
1.0E-09
Cumulative frequency (/yr)
0
0.2
0.4
0.6
0.8
Overpressure (barg)
Case I-1
Case I-2
Case II

(b) P6-U-M

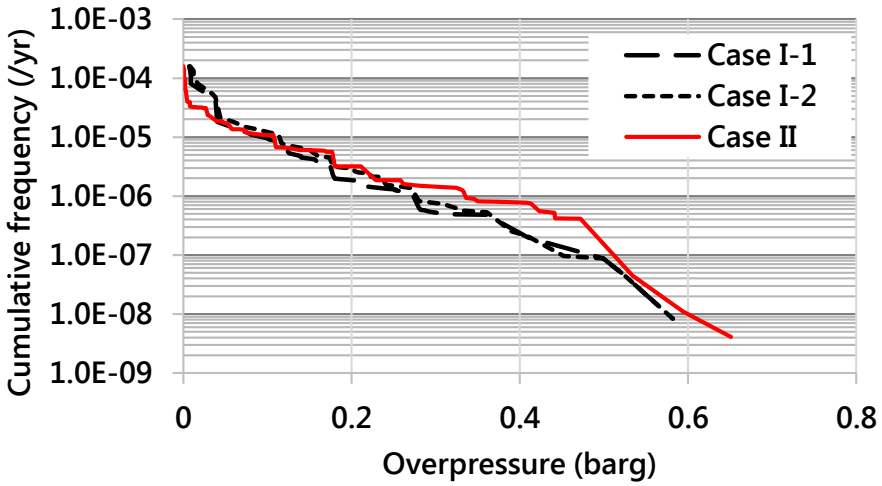

(c) P6-M-T

Fig. 31 Overpressure exceedance curves for deck spaces in P6 module[8]

In addition, when looking into the difference between the two cases for the targets in S6 and P6, the magnitude is also different from each other. For the targets in P6 module, the difference mainly is dominated by a low range of the overpressure and decreases when the overpressure grows up. This can be explained by the fact that the ESCs located in the back two corners produce low overpressure loads for the targets, and most of the large overpressure loads are provided by the ESCs located in the front two corners. Therefore, even if the ESCs are moved forward in Case I-2, the anticipated increase of the exceedance curve is observed only at the low overpressure ranges but not in the high ranges. On the other hand, the difference is apparent for the targets in S6 modules (i.e. "S6-P-U" and "S6-U-T" in

[8] Since the explosion simulations are updated by adding initial turbulence, the results are different from the original version published in Jin and Jang (2018b).

Fig. 30) and has an exceptional tendency, especially in the high overpressure ranges. Normally, the difference should not appear in the high overpressure ranges since the position 2 and position 4 remain unchanged in Case I-2. However, when compared to the targets in P6, the difference for the targets in S6 modules has a large value in the high overpressure ranges. This is because higher overpressure loads are exerted on the deck spaces when the gas clouds are placed in position 3 rather than position 4, and the reason may be accounted by the surrounding geometric conditions of the position 3 in Case I-2.

As well known, both flame speed and explosion pressure are highly dependent on geometric conditions within the cloud or geometries confining the cloud (Bjerketvedt et al., 1997). Generally, the fluid flow ahead of the flame front is turbulent, which is caused by the fluid interacting with surrounding obstacles such as process equipment, piping, structures etc. A highly congested geometric condition usually results in strong turbulence and thereby accelerates the flame speed. The turbulence in front of the flame can enhance the combustion by increasing flame surface area and diffusion of heat and mass. The increased flame speed then causes the explosion pressure to rise and expands the gas mixture, which in return strengthens the turbulence again. Consequently, the mechanism of flame acceleration due to the geometric conditions constitutes a strong positive feed-back loop (Bjerketvedt et al., 1997), and this is very disadvantageous in terms of the explosion consequences.

In the current case study, the geometric condition is investigated by the congestion ratio, which is generally defined as the volume fraction of the obstacles in a specified space. To see how the

congestion ratio varies with the path that the flame can propagate, the space is defined using a partially extendable half−cube shown in Fig. 32.

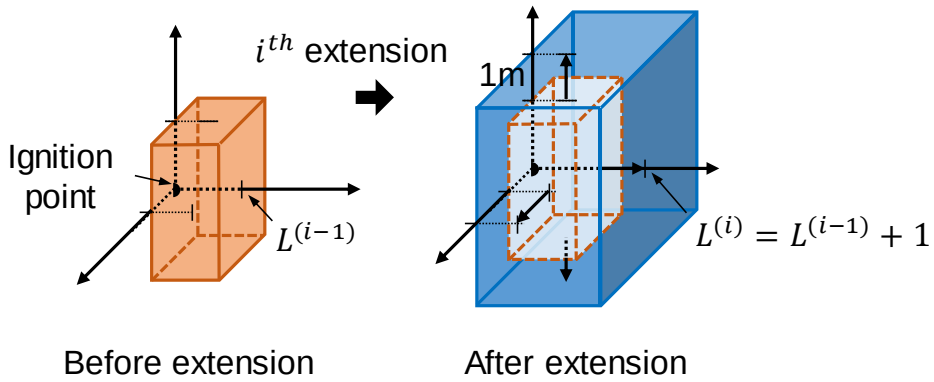

Fig. 32 Partially extendable half−cube

Starting from the ignition point, the half−cube is designed to only extend perpendicularly by advancing the unit length in each direction, and the congestion ratio is calculated for each extension until the half−cube reaches the firewall. When calculating the congestion ratio, the space should be considered only as a net incremental volume. For example, in Fig. 32, if V_{i-1}, V_i are defined as the volumes of the half−cube before and after the i^{th} extension, then the corresponding net incremental volume becomes $V_i - V_{i-1}$. The results of the entire calculation are plotted using the length L, which is the distance from the ignition point to the boundary of the half−cube. In the current case study, the congestion ratio is calculated for Case I−2, and the results are shown in Fig. 33. It is found that the congestion ratio surrounding the position 3 is obviously higher than the others. This result provides a clue to understand that when the ESCs are placed in position 3 the

pressure loads acting on the deck spaces in S6 module can be evaluated much higher than expected and sometimes higher than the position 4. This is why the maximum overpressure loads on "S6-P-U" and "S6-U-T are greater in Case I-2 than Case I-1.

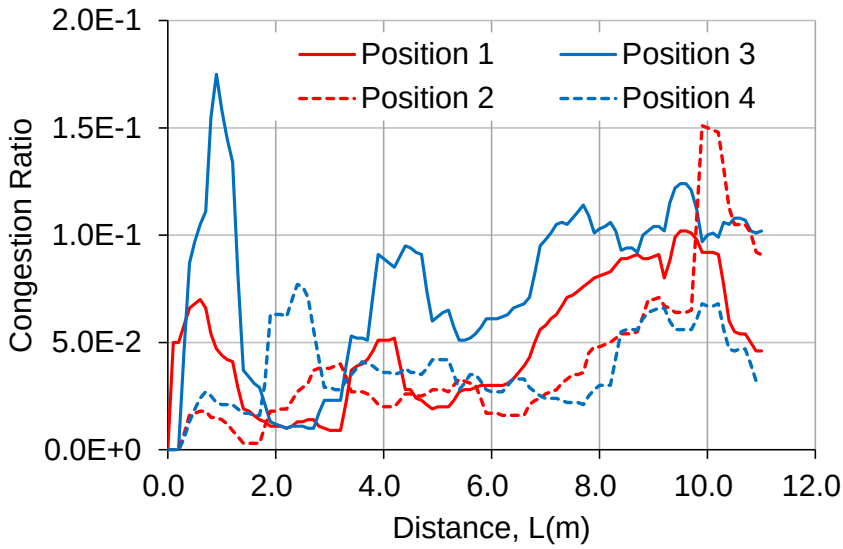

Fig. 33 Congestion ratios inside the clouds located in the four corners for Case I-2

4.4.2. Case study II: Difference in ERA results between the existing gas cloud frequency distribution and the MVFD

As described in the previous section, when using the existing gas cloud distribution to investigate the explosion scenarios, there are usually some size-position mismatched clouds that may misinterpret the results of the dispersion simulations. To verify this, the ERA results of Case II are presented in this section, and discussed with the previous two cases.

To evaluate the exceedance curves, the explosion scenarios should be investigated first, and in Case II the process is automatically completed by the MVFD. More specially, the explosion scenarios are readily obtained by extracting the joint categories that have an explosion frequency greater than zero. The whole investigated explosion scenarios for Case II are presented in Fig. 34. Compared with the Case I-1 and Case I-2, it is found that most of the large gas clouds in Case II are mainly distributed in the front corner of the port side and the size of the investigated cloud is generally small in the remaining areas. Therefore, it can be expected that the exceedance curves for the targets in P6 modules may be evaluated higher than the previous two cases, but the curves for the remaining targets may be evaluated rather lower. These anticipated results are justified in

Fig. 28 to Fig. 31. For each target of "P6-P-U, "P6-U-M" and "P6_M_T", the curves in Case II is higher than the other two curves within most overpressure ranges, but an opposite result is observed for the remaining targets. In particular, it is also observed that the gas clouds investigated by the existing distribution significantly misinterpret the results of the dispersion simulations for the targets

in S5 modules, resulting in a large difference between the Case II and the previous two cases.

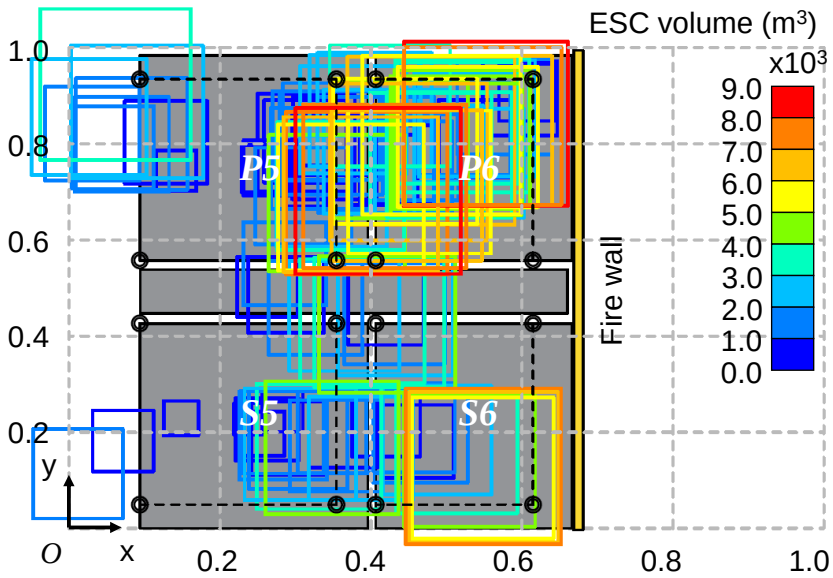

Fig. 34 Explosion scenarios investigated by the MVFD, Case II

4.5. Summary

Consequently, the case studies shown in this chapter demonstrate that the ERA results evaluated by the existing distribution can vary with the choice of the gas cloud position, which in return implies that the ERA results are largely dependent on engineering judgment. In addition, it is proven that there is a difference in the ERA results between the existing and proposed distributions, which can be explained by the size–position mismatched clouds shown in the exiting approach. In particular, relatively large differences can be observed within a certain overpressure range, which may affect the accuracy of the determined DALs.

Chapter 5. Shaped Equivalent Gas Cloud

5.1. Necessities

The shape of the gas cloud represents the boundary of fuel mixture that can affect the overall picture of overpressure in the explosion simulation. The shape of the gas cloud can determine the path of the flame propagation, which means that the distance and direction of the flame probation and the geometric condition that the flame may experience can vary depending on the shape.

In order to improve the accuracy of investigated explosion scenarios, the gas cloud position has been considered with the MVFD introduced in Chapter 4. However, even if the ESC is placed at the same position with the same volume, given a different shape, the resulting overpressure distribution can be significantly different depending on the distance and direction of the flame propagation. For example, as illustrated in Fig. 35 the overpressure distribution is determined by the aspect ratio of the rectangular that represents the ESC. When aspect ratio is small, namely, close to a cubic shape in (a), the overpressure distribution shows a radial shape because the flame propagation distance is almost similar in all directions. Whereas, if the aspect ratio is large, the flame mainly propagates along the longitudinal direction, and large overpressures are generated at ends of the ESC in the longitudinal direction. The reason for having a relatively large overpressure may be explained by the longer flame propagation distance, which may provide more turbulence to increase the overpressure for (b) and (c). In addition, depending on the orientation in the longitudinal direction, the difference in overpressure distribution can be observed between (b)

and (c).

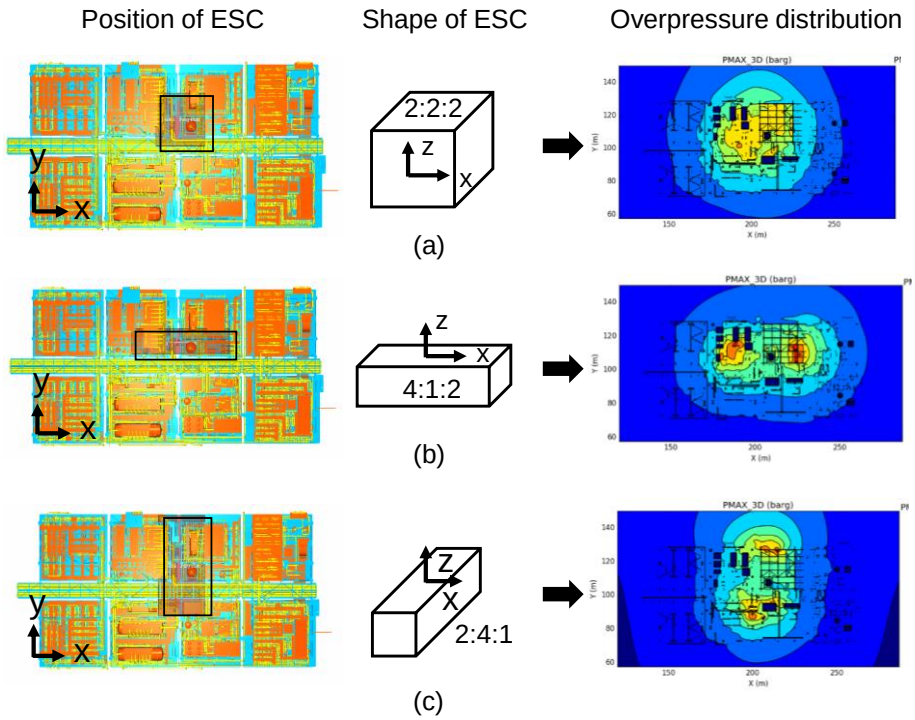

Fig. 35 Overpressure distributions with different ESC shapes

On the other hand, geometric conditions inside the cloud can also affect the overpressure distribution. As the flames propagate along different paths, they can experience different geometric conditions and the resulting turbulences can be different as well. As discussed in Chapter 4, the fluid flow ahead of the flame front is turbulent, which is caused by surrounding geometric condition. The turbulence in front of the flame is an importance factor that allows the flame to sustainably propagate to the boundary of the fuel mixture as it can enhance the combustion by increasing the flame surface area and diffusion of heat and mass (Bjerketvedt et al., 1997). As a result, the different flame propagation paths consequently lead to different

overpressure distributions. For example in Fig. 35, the magnitude of overpressure at the end of the ESC is different between (b) and (c). This indicates that that the turbulence generated in the two cases is different due to different geometric within the ESC. In summary, it can be said that the shape of the gas cloud determines the flame propagation path, which is an important aspect for obtaining an accurate overpressure distribution.

However, since there has been little previous research or regulation on how to determine the shape of the ESC, the shape used to be conservatively determined by engineering judgment and experience. Therefore, some limitations similar to that of the gas cloud position are raised again. One of them is that the determined shape may not adequately represent the actual cloud shapes, which can lead to a significantly different overpressure distribution. The other is that there is a reliability issue because the ERA results can vary from engineer to engineer. In consideration of this, the work in the current chapter is to find a way to determine the shape of the gas cloud for the explosion scenarios, which are investigated by the MVFD introduced in Chapter 4. The main objective is to improve the accuracy of the investigated explosion scenarios.

The size and position of the gas cloud can be used to derive the MVFD because both of them are scalar values. On the contrary, the shape of gas cloud is a kind of field data that cannot be measured with a scalar value, and thus it cannot be reflected into the MVFD. In the current study, the concept of shaped equivalent gas cloud is proposed to account for the shape of the gas cloud in the investigated explosion scenarios. The overall ERA procedure using the shaped equivalent gas cloud is illustrated in Fig. 36. As explained in the previous chapter, each investigated explosion

scenario corresponds to a joint category of the MVFD with an explosion frequency greater than zero. As presented in Fig. 36, for each joint category, the shaped equivalent gas cloud is determined by considering the shapes of the actual gas clouds belonging to it. In the gas dispersion simulation results, the actual gas clouds are generally represented by a number of CVs with different mass fractions. The shaped equivalent gas cloud can be determined by taking into account the CVs that all actual gas clouds occupy in common. To do this, the actual gas clouds must overlap each other to create a common area. Without the common area, there is great difficulty in determining the shaped equivalent gas cloud.

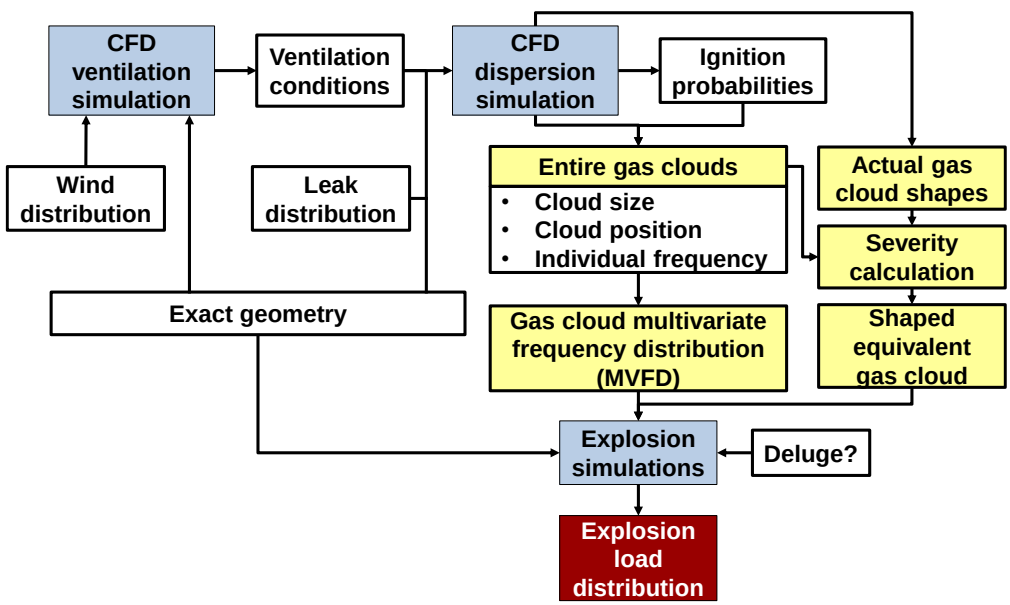

Fig. 36 ERA procedure with shaped equivalent gas cloud

Fortunately, such concerns are implicitly solved by the MVFD introduced in Chapter 4. More specifically, the actual gas clouds in a joint category are likely to overlap with each other because they

have similar positions and sizes. For example, if a joint category is selected as shown in Fig. 37, the likelihood distribution of actual gas clouds cannot be (a), but is more likely to be (b) shown in Fig. 38. In case (a), each actual gas cloud comes from different cloud size categories and hence the case cannot correspond to the MVFD. However, in case (b), all gas clouds come from the same cloud size category and are close together to produce a common area. This indicates that the MVFD provides a prerequisite for determining the shaped equivalent gas cloud.

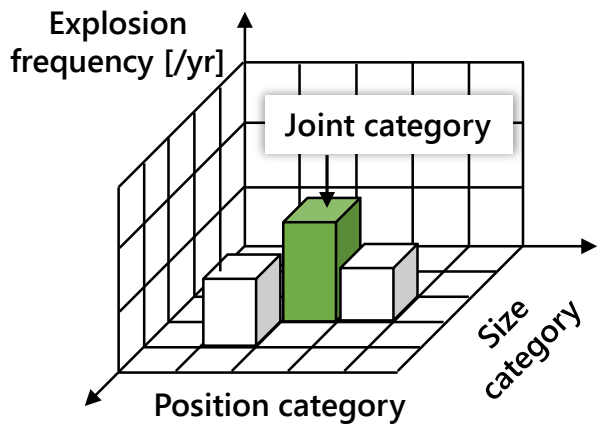

Fig. 37 Example of joint category in MVFD

The equivalent shape cannot be determined simply by identifying a number of common CVs, but rather by taking into consideration various aspects. These aspects include the order of selecting the common CVs, the number of CVs that must be selected, and the way to specify mass fractions (or fuel concentration) for the selected CVs. The following sections are used to illustrate how such aspects are considered in this study and a general methodology for determining the shaped equivalent gas cloud is

presented consequently.

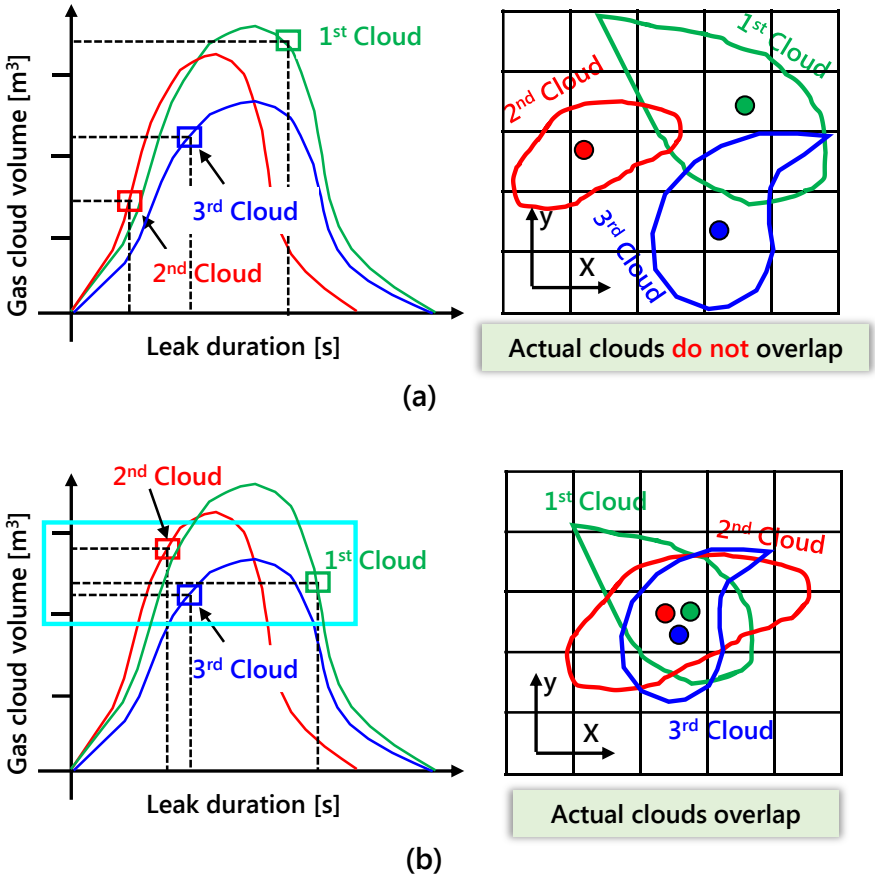

Fig. 38 Actual gas clouds in a joint category

5.2. Conversion of field data

Before determining the shaped equivalent gas cloud, it is necessary to reflect the actual clouds in the same grid resolution. In most cases, however, local grid refinement is necessary in gas dispersion simulations as shown in Fig. 39. The purpose of the grid refinement is to reduce computational costs and to consider a small grid that represents the size of leak hole (Gexcon, 2015).

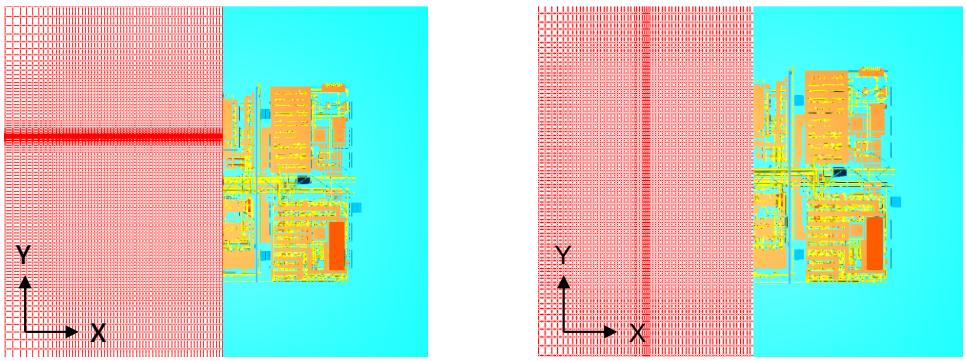

(a) Refinement along x direction (b) Refinement along y direction

Fig. 39 Example of grid refinement

In general, FLACS software (Gexcon, 2015) has the ability to convert field data from one grid to another via a dump file. The dump file is a type of restart file designed to perform explosion simulations by loading the field data of gas dispersion simulations. Since the required grid resolution as well as the boundary condition are different between the dispersion and explosion simulations, the dump files are required to transfer the field data from the dispersion simulation to the explosion simulation (Gexcon, 2015). A dump file saved at a specific grid resolution can be converted to another new dump file at the grid resolution that the user specifies. In order to determine the shape of the gas cloud, it is necessary to access the field data and modify it. However, the dump files are saved only in binary format in FLACS and cannot be accessed externally by the users. Therefore, in the present research, the field data representing the actual gas clouds has to be manually exported from original gas dispersion simulation results (i.e. r3file in FLACS (Gexcon, 2015)). An external field data converting function has been developed to convert all collected filed data to the

same reference grid. Details on how the filed data is converted are presented in Fig. 40 below. When the old and the new grid are staggered, the CV of the new grid, CV_n can be divided into several parts and each part indicates the intersection with the old CV, CV_m. For each intersection, the amount of contained fuel is calculated according to the data stored in CV_m, and summed together to predict the amount of fuel contained in CV_n. Using the same approach, the remaining properties such as the volume and porosity of the new CV can be calculated, which are shown at Eq. (5.3) and Eq. (5.4). The term $f_{n,m}$ shown in Eq. (5.2) represents to the volume fraction of CV_m contributing to the CV_n, which indicates the intersection between the old the new CVs. The final fuel mole fraction in new CV can be determined using Eq. (5.1).

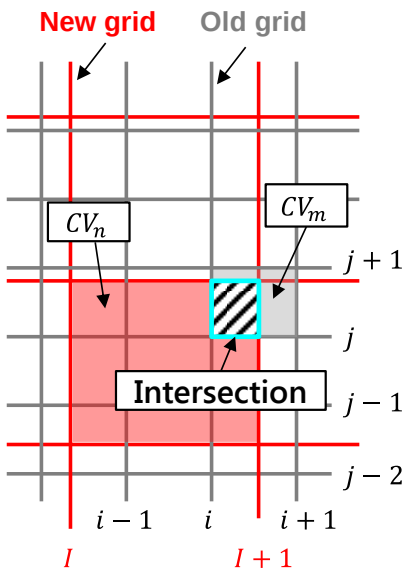

Fig. 40 Conversion of grid

$$MoleF_n = \frac{\sum_{for\ all\ m} f_{n,m} \cdot V_{cv,m} \cdot MoleF_m \cdot PORV_m}{\sum_{for\ all\ m} f_{n,m} \cdot V_{cv,m} \cdot PORV_m} \tag{5.1}$$

where, $V_{cv,m}$ stands for the volume and $PORV_m$ stands for the porosity of old CV, CV_m. $MoleF_m$ is the data stored in CV_m, indicating the mole fraction fuel in the CV_m.

$$f_{n,m} = \frac{\big(X(I+1) - x(i)\big) \cdot \big(Y(J+1) - y(j)\big)}{\big(x(i+1) - x(i)\big) \cdot \big(y(j+1) - y(j)\big)} \tag{5.2}$$

where, (X, Y) and (x, y) refer to the coordinates of the old and the new grid, respectively, and each coordinate is a function of coordinate index (I, J for new grid and i, j for old grid).

$$PORV_n = \frac{\sum_{for\ all\ m} f_{n,m} \cdot V_{cv,m} \cdot PORV_m}{\sum_{for\ all\ m} f_{n,m} \cdot V_{cv,m}} \tag{5.3}$$

$$V_{cv,n} = \sum_m f_{n,m} \cdot V_{cv,m} \tag{5.4}$$

where, $V_{cv,n}$ stands for the volume and $PORV_n$ stands for the porosity of the new CV, CV_n.

5.3. Severity calculation

In order to determine the shaped equivalent gas cloud, it is necessary to consider the order of selecting the common CVs. Some of these CVs can have the same fuel mass fraction and in that case it is difficult to determine which one should be selected first. In the present study, the priority is determined by introducing the severity as shown in Fig. 36. Following Eq. (5.5)−(5.6) represents the definition of the severity, which is also calculated using the concept of ESC as with the gas cloud position introduced in Chapter 4.

$$S_{i,j} = V_{cv,i}^{es} \cdot f_{ign,j} \tag{5.5}$$

$$V_{cv,i}^{es} = V_{cv,i} \cdot PORV \cdot F_{ESC}(MassF_i) \tag{5.6}$$

$$F_{ESC}(MassF_i) = \frac{[V_e(MassF_i) - 1] \cdot \mathrm{ERfac}(MassF_i)}{[V_e(MassF_{max}) - 1] \cdot \mathrm{ERfac}(MassF_{max})} \tag{5.7}$$

where, $S_{i,j}$ stands for the severity of i^{th} CV at j^{th} actual cloud illustrated Fig. 41 in and $V_{cv,i}^{es}$ indicates the equivalent stoichiometric volume of i^{th} CV. $f_{ign,j}$ refers to the individual frequency of the j^{th} actual cloud introduced in Chapter 3. The weighting factor F_{ESC} is dependent on the fuel concentration, which can be measured both by the ER (used in Fig. 18) or mass fraction, $MassF$. The reason for using the mass fraction instead of the ER is because the shaped equivalent gas cloud needs to be represented by the mass fraction. More details related to this are described in Section 5.4. In Eq. (5.7) the $MassF_{max}$ refers to the mass fraction that gives the maximum

value of the term, $(V_e - 1) \cdot \mathrm{ERfac}$. When $MassF_i = MassF_{max}$, the F_{ESC} is equal to 1.0, which is the maximum value.

According to Eq. (5.5), the severity of a single CV is defined as the product of its fuel mass fraction and the individual frequency of the actual gas cloud that provides the mass fraction. The $MassF_i$ can determine the equivalent stoichiometric volume of the CV, $V_{cv,i}^{es}$, which is directly related to the overpressure caused by the actual gas cloud. Therefore, even if some of the common CVs have the same fuel mass fraction for different actual clouds, they can be further differentiated by the severity due to different individual frequency.

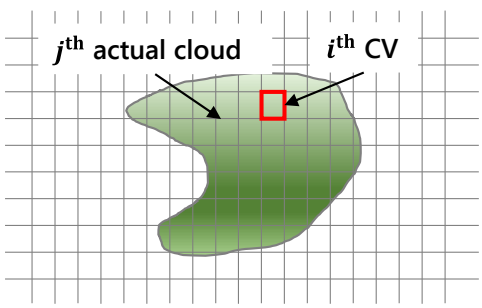

Fig. 41 A single CV in actual gas cloud

5.4. Methodology

5.4.1. Overall procedure

A joint category may contain many actual gas clouds shown in gas dispersion simulation results. Each actual gas cloud is represented by a number of CVs with different mass fractions and has its own individual frequency. Determining the shaped equivalent gas cloud means selecting a certain number of CVs using the data of actual gas clouds, which requires three aspects to be considered. One is the sequence in which the CVs are selected, the other is the number of CVs that must be selected, and the last is how to specify the mass fraction of the selected CVs.

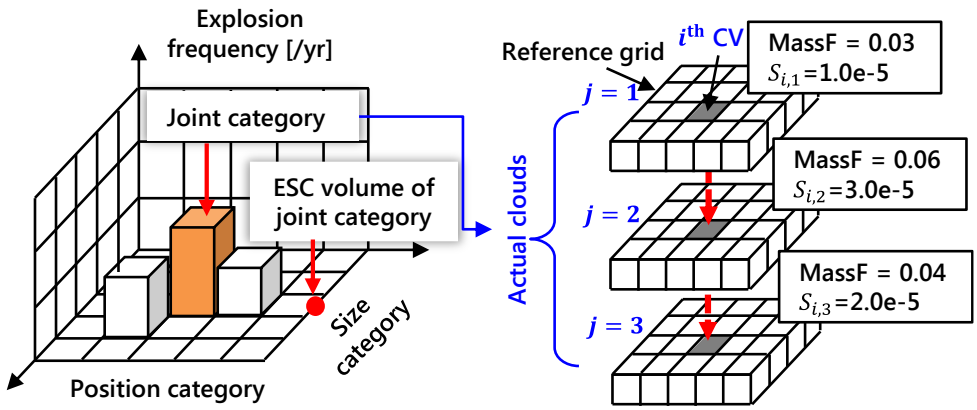

Fig. 42 Example of multiple sets of severity and mass fraction for a single CV

When considering the actual gas clouds, a CV can have multiple sets of mass fraction and individual frequency, each from an actual gas cloud. An example is illustrated in Fig. 42 where three actual gas clouds are presented, and the i^{th} CV in the figure has three

sets of mass fraction and severity.

In order to select the CVs for the shaped equivalent gas cloud, all single CVs must be uniquely determined. More specifically, one representative set of mass fraction and severity out of the multiple sets must be determined. The sequence of CV selection or the number of CVs that need to be selected is then determined by the representative set of the mass fraction and severity. In the present study, two methods are proposed to determine the representative set of mass fraction and severity and each one is described in the following sections.

Assume that all single CVs are assigned with the represent set of mass fraction and severity, then the shaped equivalent gas cloud can be determined according to the procedure presented in Fig. 43. The sequence of CV selection is determined by the assigned severity in descending order. The total number of CVs to be selected is determined by the criterion that the total equivalent stoichiometric volume of the selected CVs is equal to the ESC volume of the joint category (or the represent gas cloud volume of the joint category) as shown in Fig. 42. The equivalent stoichiometric volume (ESV) can be calculated using the Eq. (5.5), but the mass fraction should be taken as the representative value.

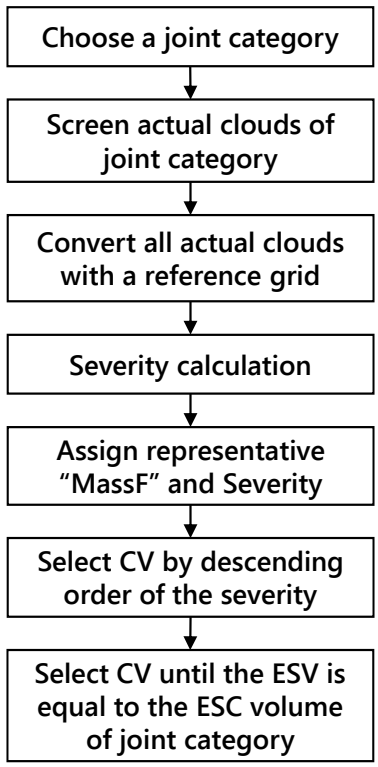

Fig. 43 Overall procedure of determining equivalent gas cloud shape

5.4.2. Determination of mass fraction and severity

Risk is defined as the product of consequence and frequency. In ERA, the consequence usually refers to overpressure caused by VCE. According to the definition of severity, it is not difficult to recognize that the severity is comparable to risk because the equivalent stoichiometric volume of the CV, $V_{cv,i}^{es}$ shown in Eq. (5.5) is directly related to the overpressure. With this in mind, the representative severity of a single CV can be determined by the maximum or cumulative value of the multiple severities from actual clouds.

An example is presented in Fig. 44, where option 1 indicates the case of considering the maximum severity and option 2 refers to the cumulative value. Three actual clouds ($j = 1, 2, 3$) are presented in the figure, and the maximum severity of the i^{th} CV is given by the second ($j = 2$) cloud, i.e. $S_{i,2} = 3.0e-5$, and the cumulative value is $6.0e-5$.

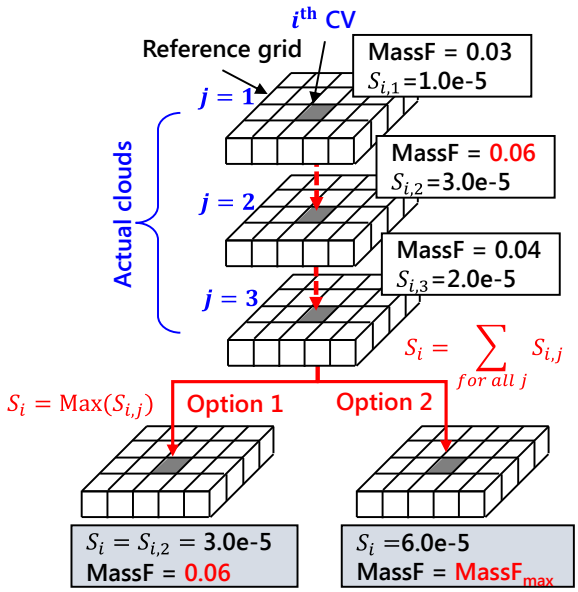

Fig. 44 Determination of representative severity and mass fraction

Taking into account the fact that the CVs are selected in descending order of severity as described in Fig. 43, the physical meaning of choosing the representative severity as the maximum or cumulative value implies that the shaped equivalent gas cloud is determined using the CVs with high risks.

When a certain CV is selected during the process of determining the shaped equivalent gas cloud, a representative mass fraction also needs to be specified. The way to determine the mass fraction is

subjected to the way to determine the severity. In the case of considering the maximum severity, the mass fraction can readily be determined by the value corresponds to the maximum severity. For example, using the option 1 in Fig. 44, the determined mass fraction of i^{th} CV is 0.06, which is equivalent to the second actual cloud. On the other hand, if the representative severity is considered by the cumulative value, it is generally difficult to determine which of the multiple mass fractions from actual clouds should be used. In such a case, the mass fraction is determined by a specific value, i.e. the $MassF_{max}$ in Fig. 44 and Fig. 45, which gives the $F_{ESC} = 1.0$ in Eq. (5.7).

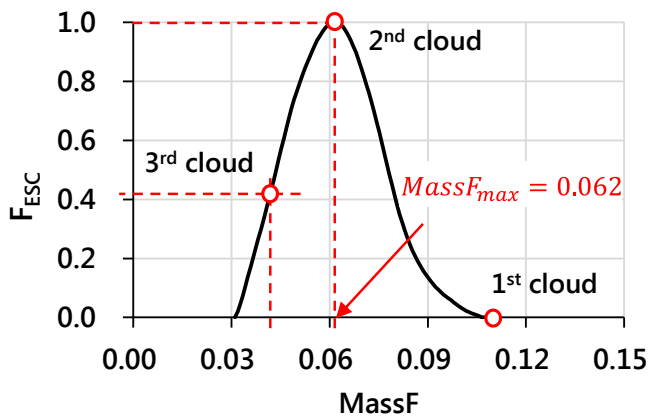

Fig. 45 Example of $MassF_{max}$

Depending on how the severity and mass fraction are determined, the overall procedure shown in Fig. 43 can be further divided into two parts as presented in Fig. 46.

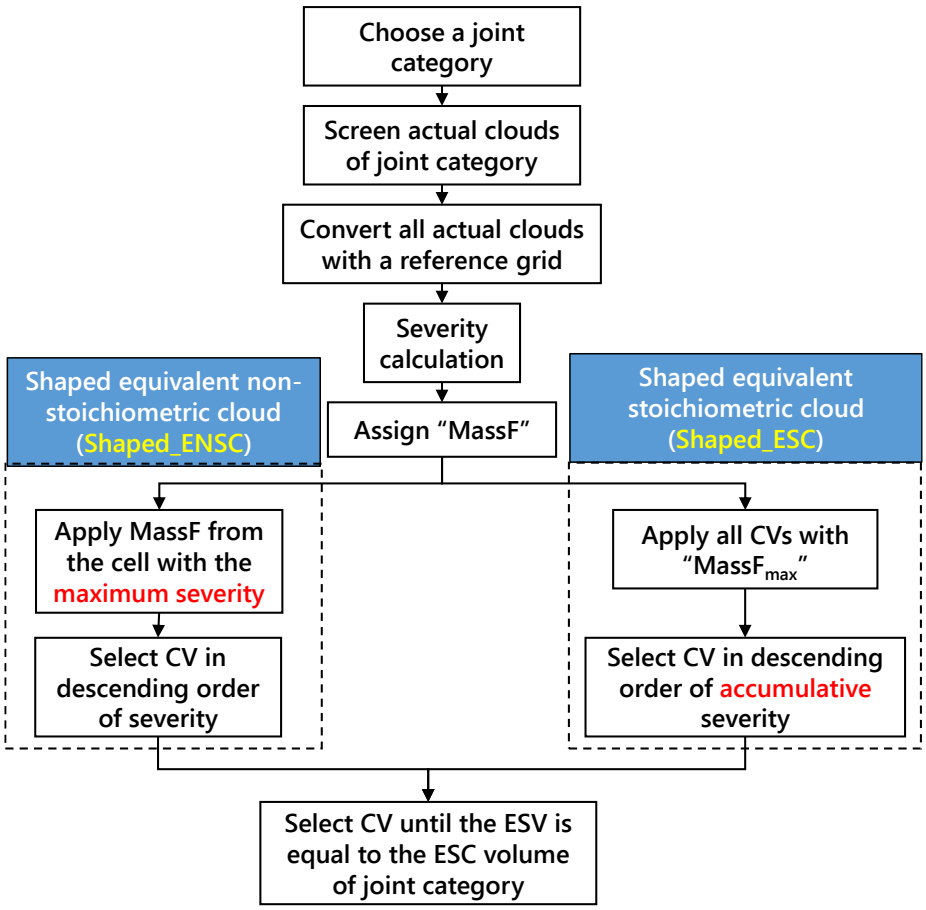

Fig. 46 Overall procedure for "Shaped_ENSC" & "Shaped_ESC"

In consequence, two types of shaped equivalent gas cloud can be obtained through the procedure. "Shaped_ENSC" refers to the case of considering the maximum severity and the corresponding mass fraction. The name is short for shaped equivalent non-stoichiometric cloud, which is named after the non-stoichiometric mass fraction distribution contained by the cloud. On the other hand, "Shaped_ESC" corresponds to the case where the cumulative severity is used to determine the sequence of CV selection and the mass fraction is given by $MassF_{max}$ for the selected CVs. The name stands for the shaped equivalent stoichiometric cloud, indicating

that mass fraction within the cloud is close to stoichiometric conditions. Examples of both types are illustrated in following Fig. 47 and Fig. 49.

Assume that the joint category has three actual clouds shown in both Fig. 47 and Fig. 49, and the ESC volume is 11.4 m^3. Only one layer of CVs is taken into consideration in the entire CFD calculation domain, and the process of determining the representative severity and mass fraction is presented in the figures, respectively. For example, for the i^{th} CV, three sets of mass fraction and severity can be available as listed in Table 5, each from the actual cloud shown in Fig. 45. The mass fraction determines the weighting factor used to calculate the ESV.

Table 5 Mass fraction and severity for i^{th} CV

Cloud No.	$MassF$ [kg/kg]	PORV.	Volume of CV [m^3]	F_{ESC}	Individual frequency [/yr]	Severity
1	0.110	1.0	1.0	0.0	3.10e−5	0.0
2	0.062	1.0	1.0	1.00	2.10e−5	2.10e−5
3	0.041	1.0	1.0	0.40	1.10e−5	4.40e−5

As illustrated in Fig. 47, in the case of “Shaped_ENSC”, the representative severity is determined by the maximum value, i.e., 4.40e−5, and the mass fraction is assigned by 0.041, which is from the 3rd actual cloud in Table 5. On the other hand, when considering the “Shaped_ESC” in Fig. 49 , the representative severity become the cumulative value, i.e., 6.50e−5, and the mass fraction is to be assigned by $MassF_{max}$ = 0.062 in Fig. 50.

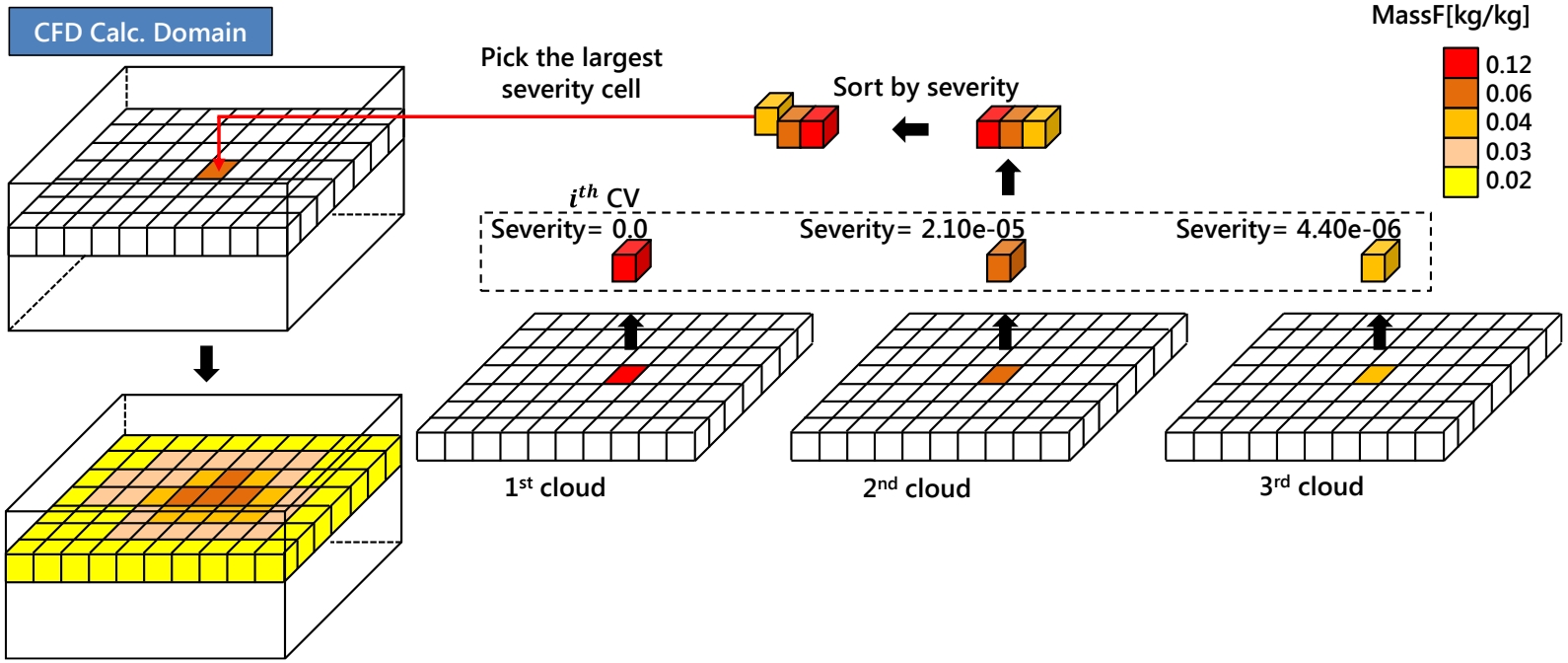

Fig. 47 Determination of representative severity and mass fraction for “Shaped_ENSC”

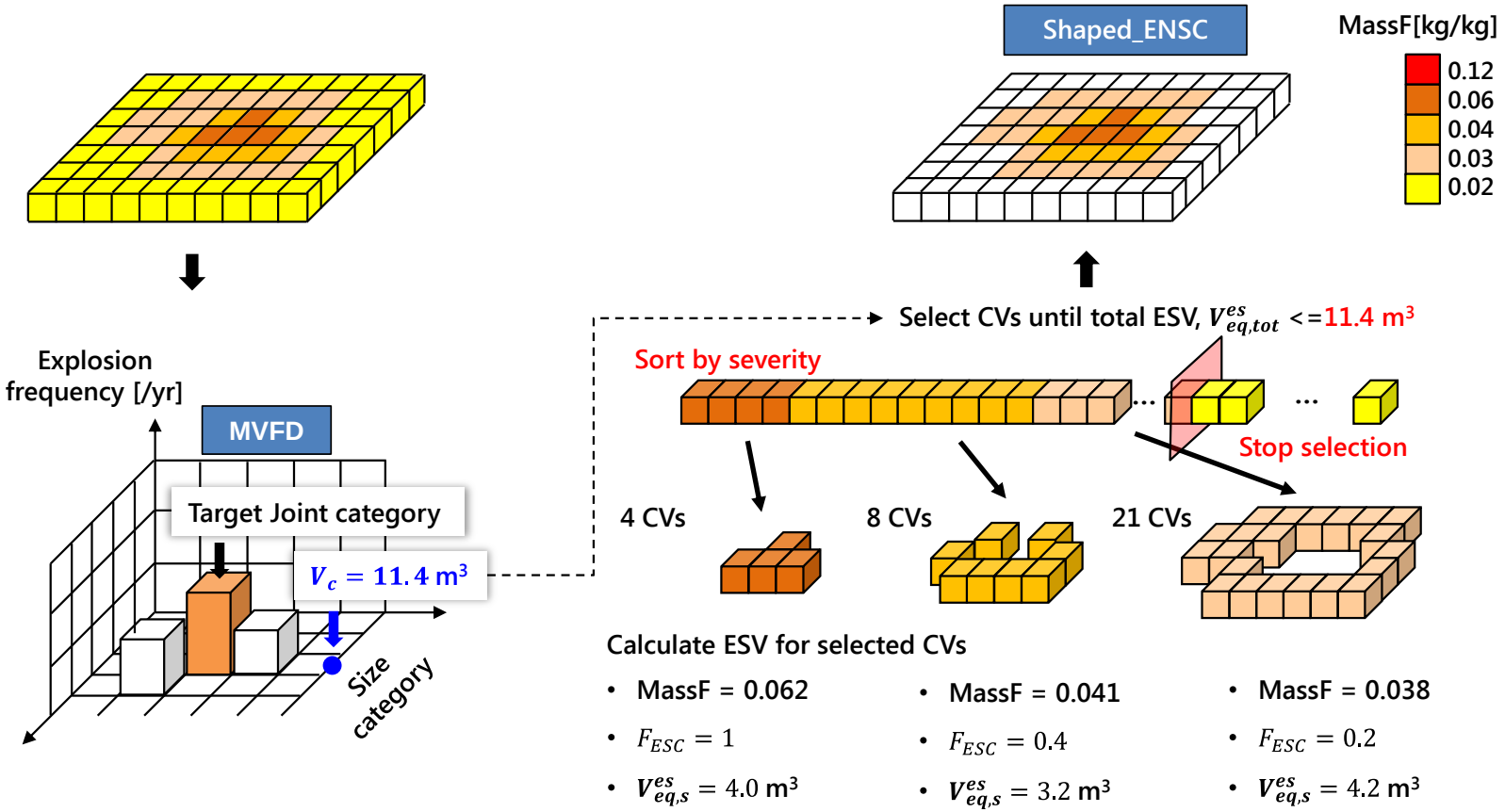

Fig. 48 Selection of CVs for "Shaped_ENSC"

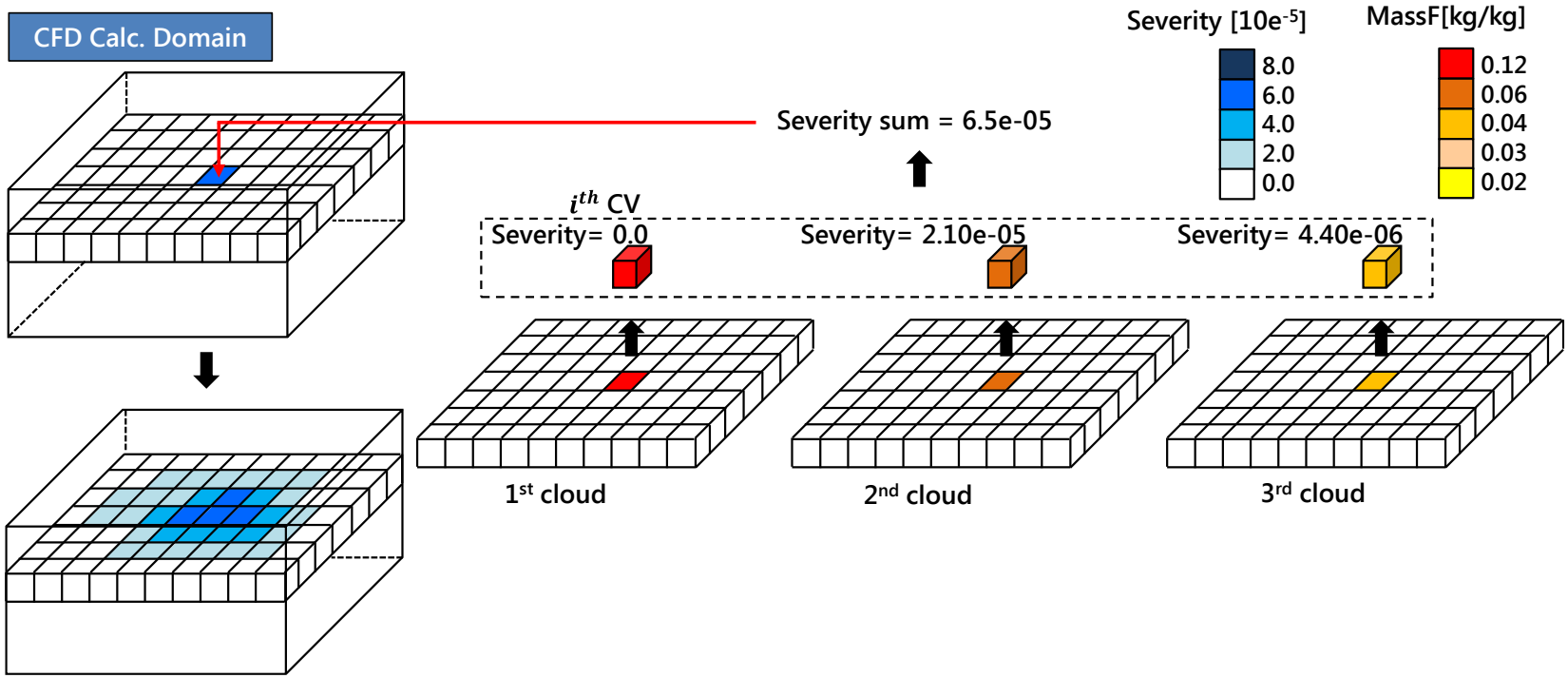

Fig. 49 Determination of representative severity and mass fraction for "Shaped_ESC"

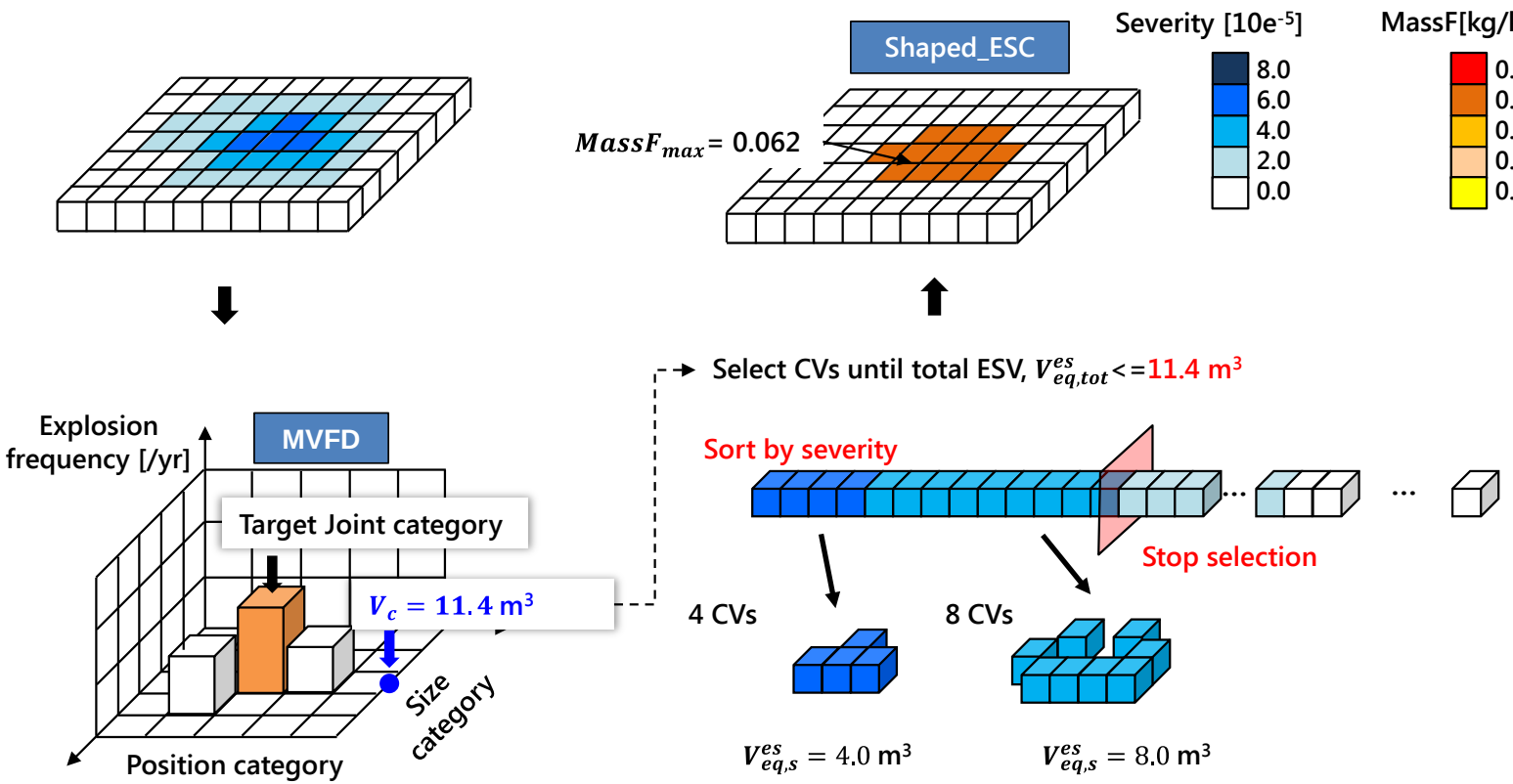

Fig. 50 Selection of CVs for “Shaped_ENSC”

Once all CVs have been redefined with the representative set of the severity and mass fraction, the CV selection is then proceeded to create the shaped equivalent gas cloud. The priority of CV selection is determined by the assigned representative severity. For example, as demonstrated in both Fig. 48 and Fig. 50, the CVs from the demo layer are sorted by the assigned severities, and selected one by one until the total ESV of the selected CVs is equal to the ESC volume (i.e. V_c = 11.4 m^3) of the target joint category. In the case of "Shaped_ENSC", the assigned mass fractions do not correspond to the condition of F_{ESC} =1.0 (or $MassF = MassF_{max}$). Therefore, in order to check whether the total equivalent stoichiometric volume of the selected CVs (i.e. $V_{eq,tot}^{es}$ in Fig. 48 and Fig. 50) is approaching the ESC volume of the target joint category, the $V_{eq,tot}^{es}$ must be recursively calculated for the currently selected CVs. For example, in Fig. 48, a total of 33 CVs are selected, including three different mass fractions. The total selected volume is 33 m^3 assuming that the porosity values of all the selected CVs are 1.0 and that the grid size of reference grid is 1m. When calculating the equivalent stoichiometric volume for the 33 selected CVs, the value is 11.4 m^3, which is the same as the ESC volume of the joint category and hence the final "Shaped_ENSC" only consists of these 33 CVs as shown in Fig. 48.

On the contrary, the mass fraction in "Shaped_ESC" is only considered with the $MassF_{max}$, which means that the total equivalent stoichiometric volume of the selected CVs is the same as the total volume of the CVs. For example, in Fig. 50, the CV selection is stopped when the total volume reaches 12 m^3, which is close to the ESC volume of the target joint category.

5.4.3. Method of input proposed gas cloud to explosion simulation

In FLACS, since the wind boundary condition cannot be applicable in explosion simulations, the best way to combine the dispersion and the explosion simulation is to use a dump file (Gexcon, 2015). An explosion simulation can be started with the dump file which contains a 'snapshot' of the dispersion simulation at the specified time instant. However, since the dump file cannot be edited externally, it cannot be used to enter the generated equivalent gas cloud into the explosion simulation. As an alternative, in the current study, a custom cloud file (Gexcon, 2015) is used to import the generated gas cloud when performing the explosion simulation. The custom cloud file is a kind of text file in which the gas cloud is defined by a number of scatter points (i.e. a combination of 3D coordinates and mass fraction). When a shaped equivalent gas cloud is determined, a custom cloud file can be created by listing the center coordinates and the mass fraction of the selected CVs.

The custom cloud file is a convenient tool that allows the users to input any gas cloud they want to the explosion simulation, but there are some limitations to the current study. The shape of the gas cloud represented by the shaped equivalent gas cloud can be either concave or convex, but if the shape is concave, it cannot be input correctly into the explosion simulation. An example is shown in Fig. 51. The shape of the input gas cloud in this example is concave but turns into a convex shape in the simulation. This is because the core simulator of FLACS recognizes only the convex shape and therefore even if the input gas cloud is concave, it is forcibly recognized as convex. To solve this problem, the shaped equivalent

gas cloud is entered into the explosion simulation with a boundary rectangular box as illustrated in Fig. 51. The boundary box is created according to the lower and upper bounds of the input cloud in 3D space. By setting the mass fraction of the non-cloud area (i.e. the remaining space in the boundary box, excluding the input cloud.) to zero, it is possible to expect that the user-desired gas cloud can be correctly input to the simulation.

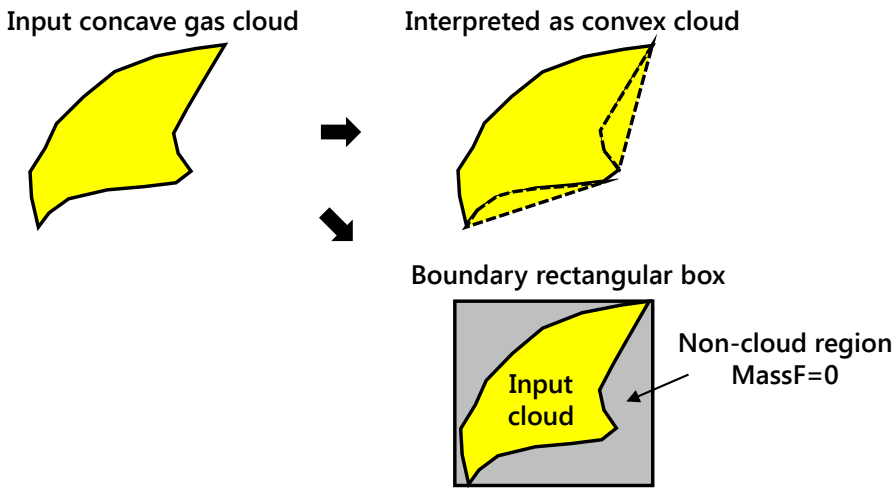

Fig. 51 Boundary rectangular box with input cloud

Another major problem of using the custom cloud file is the interpolation of mass fraction field data employed by the FLACs core simulator. Since the gas cloud is defined by a number of scatter points, the mass fraction field data becomes discontinuous when imported into the simulation. Therefore, an automatic interpolation function is basically embedded in the core simulator to smooth the discontinuous mass fraction field data. When using the boundary rectangular box, the degree of interpolation may be greater than when it is not used. This can be explained by a large gradient of mass fraction between the cloud and non-cloud regions.

As a result, although the boundary box is designed to overcome the limitations of using the custom cloud file, but it still cannot afford to correctly input the gas cloud into the simulation.

In order to reduce the degree of interpolation and also increase the accuracy of importing the input gas cloud to the explosion simulation, an improved method of using the boundary box has been proposed. Details of the method are illustrated in Fig. 52.

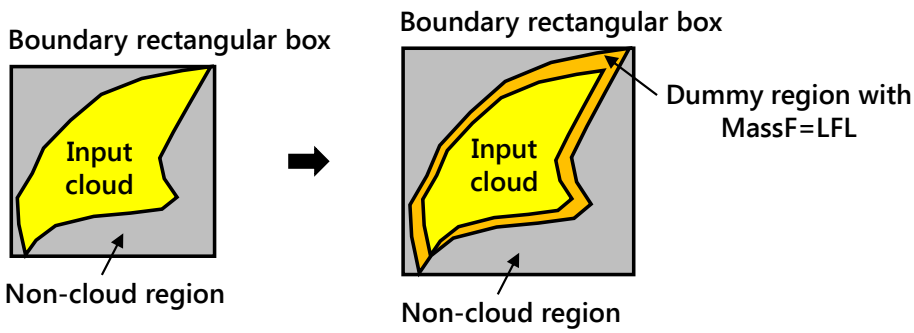

Fig. 52 Improved method with custom cloud file

In comparison with Fig. 51, a dummy region is added to the boundary of the input cloud to reduce the gradient of mass fraction between the cloud and non-cloud regions. The dummy region can be represented by multiple layers of dummy CVs in 3D calculation domain or by multiple scatter points around the region of input cloud in the custom cloud file. The mass fraction of the dummy region is given by LFL so that the dummy region does not contribute to the equivalent stoichiometric volume. Two effects may be expected when using the dummy region. One is to prevent dilution of the gas cloud during the explosion and the other to weaken the interpolation effect. Both effects may result in slightly overestimating the explosion consequence, which is beneficial in terms of risk. The remaining problem for using the dummy region is

how to determine its size. The answer can be found in the difference in fuel mass between the actual cloud and the shaped equivalent cloud. In general, considering the same equivalent stoichiometric volume, the volume of actual cloud is much larger than the volume of ESC. The reason can be found in the mass fraction of the actual cloud. In general, the mass fraction of the actual cloud is inhomogeneous and is widely distributed around the $MassF_{max}$ shown in Fig. 53. Therefore, the corresponding F_{ESC} value is generally lower than 1.0 and more volumes are needed to compensate for the same amount of ESC. In other words, if the mass fraction in a cloud is more widely distributed around the $MassF_{max}$, more volume is required in order to generate the same volume of ESC.

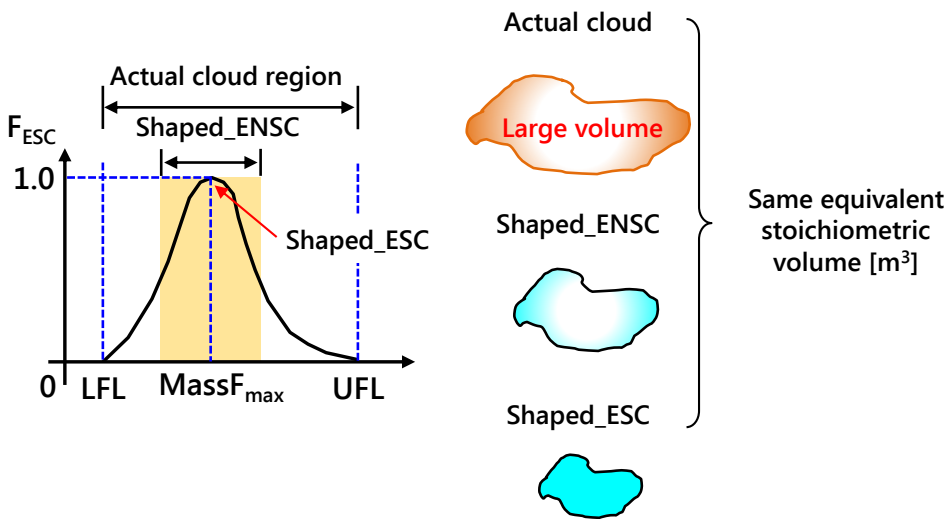

Fig. 53 Comparison of volume between actual gas cloud and shaped equivalent gas cloud

In a similar manner, the volume of “Shape_ENSC” is also smaller than the actual cloud when considering the same equivalent stoichiometric volume because mass fraction of the “Shaped_ENSC” is also less dispersed than the actual cloud.

Recalling the process of determining the “Shaped_ENSC”, the CV with the highest severity is considered preferentially and therefore the mass fraction can be biased towards the $MassF_{max}$ and less dispersed than the actual cloud. Consequently, with a relatively large volume, the fuel mass of the actual gas cloud is always greater than the shaped equivalent gas cloud. An example is also presented in Fig. 54. Considering the 33 CVs with different mass fractions, the equivalent stoichiometric volume and the fuel mass of the actual cloud is 11.4m^3 and 1.62kg, respectively. On the other hand, for the ESC, the fuel mass corresponds to the same equivalent stoichiometric volume is 0.81 kg, which is half of the actual cloud.

The difference in fuel mass between the actual gas cloud and the shaped equivalent gas cloud can be used to determine the size of dummy region. The mass fraction in dummy region is defined by LFL, and therefore the number of dummy CVs for the difference in fuel mass can be calculated. Beyond that, the dummy CVs must be identified in 3D space taking into account the region of the input cloud. More specifically, these dummy CVs must be identified among the CVs that are not occupied by the input gas cloud. In addition, in order to prevent the formation of voids in the gas cloud, the dummy CVs must be clustered together and also be bordered by the input cloud. More information on how to determine the dummy region in the 3D calculation domain is introduced in the next section.

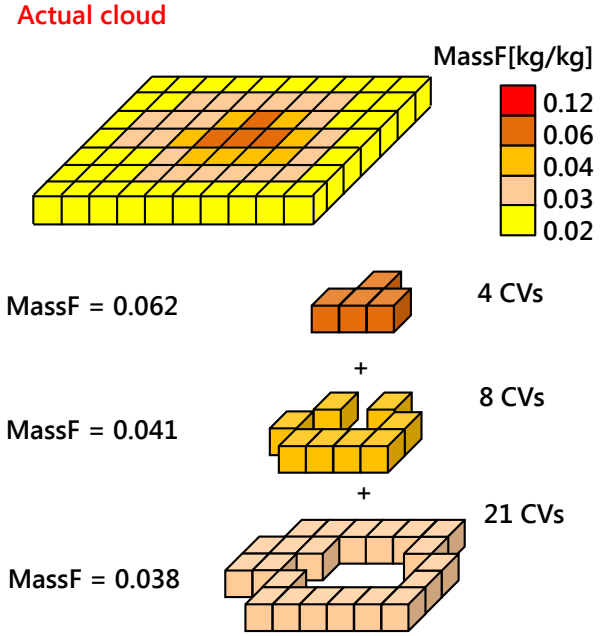

Fuel mass for actual cloud

• $MassF$ = 0.062	• $MassF$ = 0.041	• $MassF$ = 0.038
• $\rho = 1.171$ [kg/m³]	• $\rho = 1.175$ [kg/m³]	• $\rho = 1.176$ [kg/m³]
• $F_{ESC} = 1$	• $F_{ESC} = 0.4$	• $F_{ESC} = 0.2$
• $V_{eq,s}^{es} = 4.0$ m³	• $V_{eq,s}^{es} = 3.2$ m³	• $V_{eq,s}^{es} = 4.2$ m³
• $m_{eq,s}$ = 0.29 [kg]	• $m_{eq,s}$ = 0.39 [kg]	• $m_{eq,s}$ = 0.94 [kg]

$V_{eq,tot}^{es}$ = 11.4 m³ and $m_{eq,tot}$ = 1.62 [kg]

Fuel mass for ESC(=11.4 m³)

- $MassF$ = 0.062
- ρ = 1.171 [kg/m³]
- V_c = 11.2 m³
- $m_c = 11.2 \times 1.171 \times 0.062 = 0.81$[kg]

Fig. 54 Example of diffence in fuel mass [kg]

5.4.4. Algorithm for shaped equivalent gas cloud.

In previous section, the methodology for generating the shaped equivalent gas cloud has been discussed in a qualitative way. The entire procedure of the methodology is relatively complex and requires a self-developed code to automate it. The purpose of this section is intended to introduce the algorithms used in the self-developed code, and some of the following descriptions may overlap with the previous sections.

The entire process of creating a shaped equivalent gas cloud can be divided into three stages, each of which is demonstrated in Fig. 55 to Fig. 57. The 1st stage is the main part used to determine the cloud region of the shaped equivalent gas cloud, and the other two stages are only responsible for determining the dummy region. Assume that the total number of CVs in reference grid is n and the number of actual clouds in the target joint category is m in Fig. 55. The severity is recursively calculated for each CV in actual cloud. The representative set of severity and mass fraction is then assigned to each CV, depending on the type of the shaped equivalent gas cloud (i.e. “Shaped_ENSC” or “Shaped_ESC”). After that, the CVs are sorted in descending order according to the assigned severity and to be selected one by one to generate the shaped equivalent gas cloud.

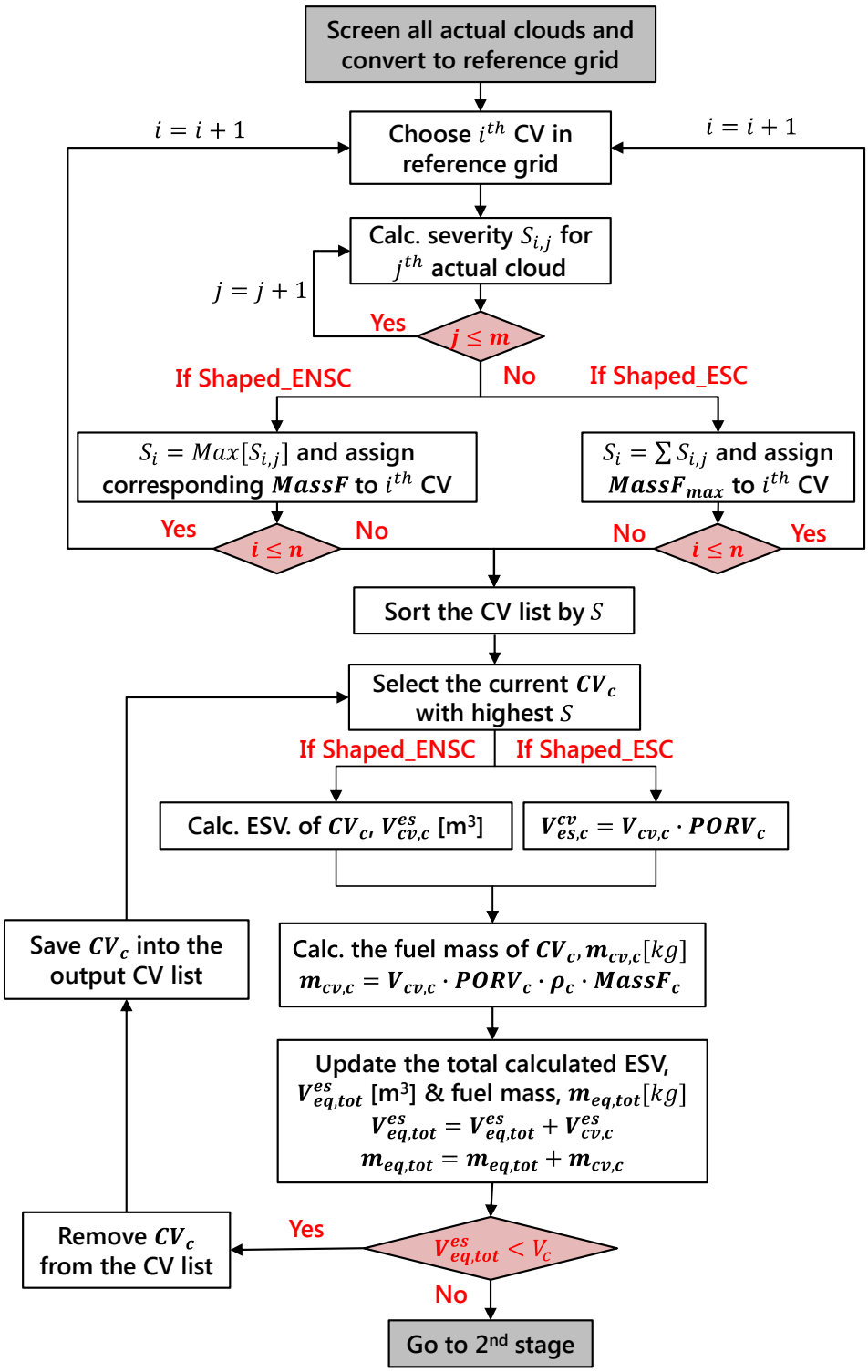

Fig. 55 Algorithm for shaped equivalent gas cloud, 1st stage

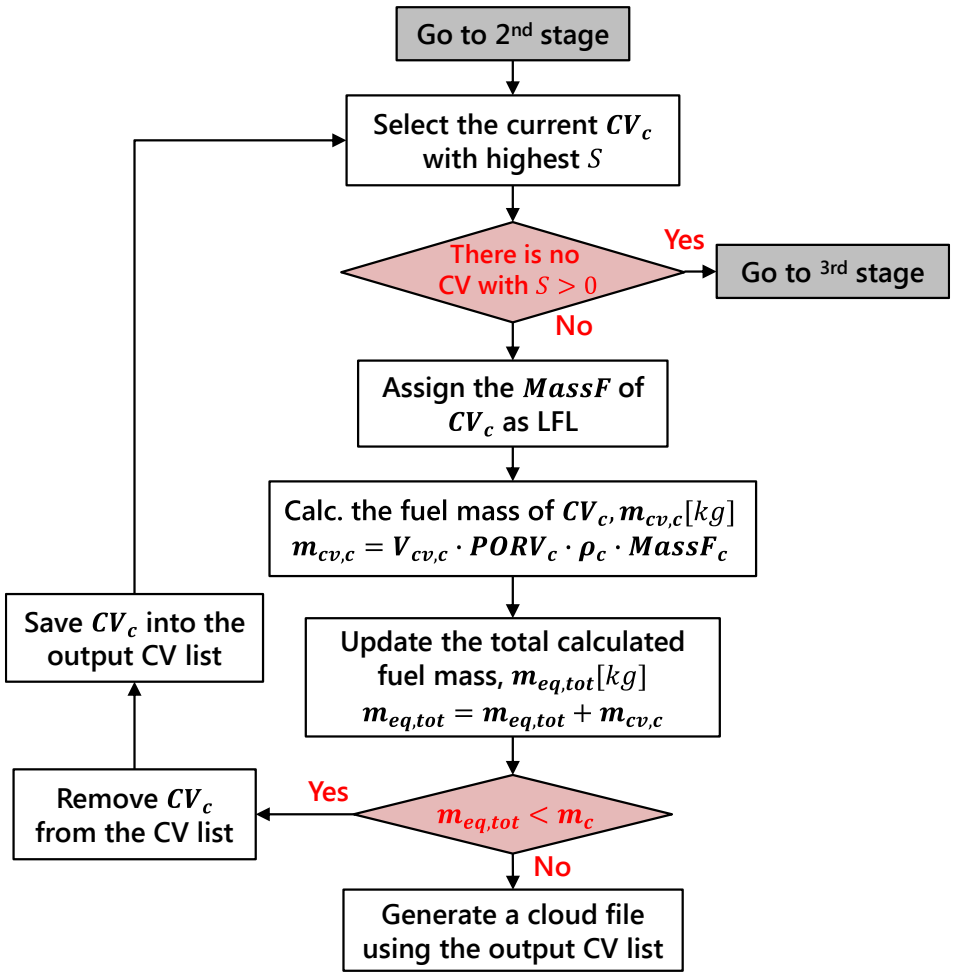

Fig. 56 Algorithm for shaped equivalent gas cloud, 2nd stage

The CV selection should also be proceeded in a recursive manner. That is, only one CV can be selected at a time, and the total equivalent stoichiometric volume, $V_{eq,tot}^{es}$ and mass fuel, $m_{eq,tot}$ of all the CVs selected up to the previous step (or the CVs in output CV list) should be updated considering the CV selected at current step, CV_c. When the total equivalent stoichiometric volume reaches the volume ESC of the target joint category, V_c, the selection of CV is stopped and the algorithm moves to the 2nd stage.

Both of the second and the third stages are designed to determine the dummy region but the difference between them is the criterion used to determine the priority of the CV selection.

The CVs at the 2nd stage are continuously selected in descending order of the severity as shown in Fig. 56. Given that the final determined dummy region must be bordered by the gas cloud region, using the same criterion as at the 1st stage can ensure that the selected dummy CVs are close to the gas cloud region. However, after selecting a certain number of CVs, the severity can no longer be used to determine the priority of the CV selection because the severity of the remaining CVs is zero. Correspondingly, a condition is added to the second stage as illustrated in Fig. 56. If the severity of currently selected CV is not zero, the mass fraction is assigned by LFL and the remaining process is the same as the 1st stage. Otherwise, the algorithm then moves to the 3rd stage.

At the 3rd stage, a new criterion must be defined to further determine the priority of the CV selection. The severity of all unselected CVs is zero due to $f_{ESC} = 0.0$ (i.e. the mass fractions of all unselected CVs are lower than the LFL), and therefore all the CVs have the same priority in terms of severity. Considering the continuity between the gas cloud region and the dummy region, the dummy CV at this stage is designed to be selected one by one to fill the boundary of the already selected output CV list in 3D space. The priority is determined by the variable r shown in Fig. 58, which is the distance from each CV in the boundary CV list to the center of the output CV list in 3D space.

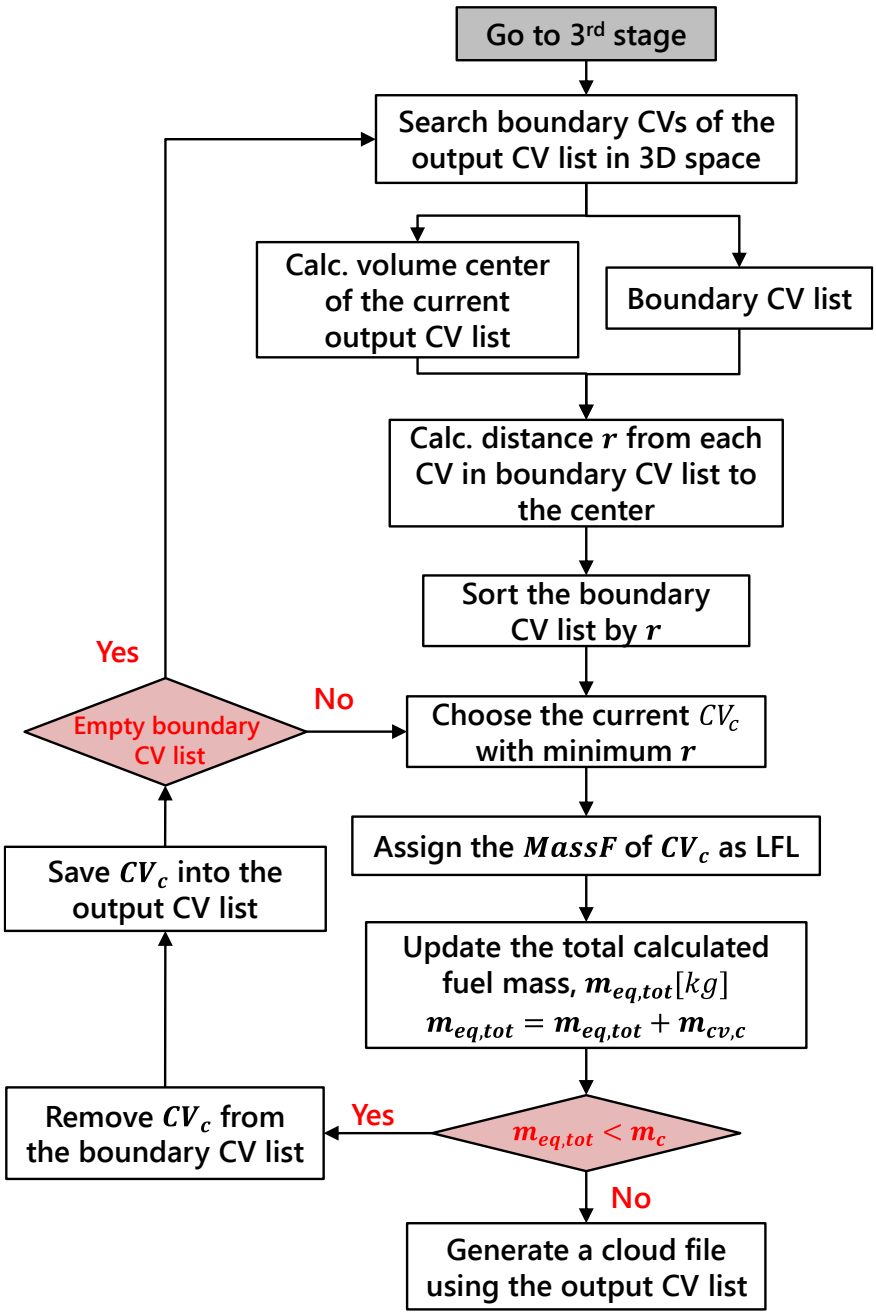

Fig. 57 Algorithm for shaped equivalent gas cloud, 3rd stage.

As illustrated in Fig. 57, the 3rd stage is started with searching the boundary CVs of the output CV list in 3D space, and then the distance r is calculated for each CV in the boundary CV list. The new criterion is used to choose the current CV in descending order of r, and the remaining procedure is the same as the 2nd stage. When all the CVs in the boundary CV list are used up but the total fuel mass for the selected CVs is still less than the mass of the target joint category, a new boundary CV list is then searched again for the current output CV list. The new boundary CV list is searched considering the newly added dummy CVs from the previous boundary CV list, and thus the procedure is also recursive.

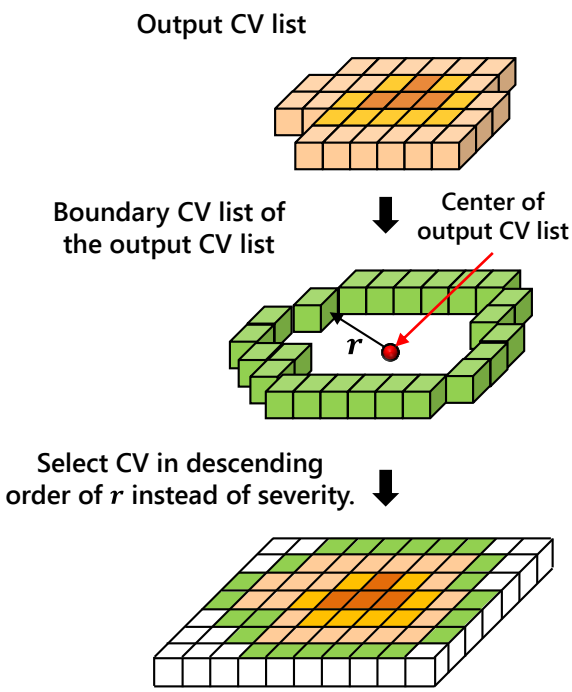

Fig. 58 Selection of dummy CVs at the 3rd stage

5.5. Validation

This section is intended to demonstrate the validity of the proposed gas cloud. The shaped equivalent gas is designed to represent the actual clouds, but it is still questionable whether it is comparable to the actual clouds. Two types of validation are performed for this. One is to compare the overpressure distributions caused by both the equivalent and actual gas clouds. The other one is to check whether the proposed gas cloud can create an exceedance curve of overpressure similar to that caused by the actual clouds. Both validations are described in the following sections, respectively.

5.5.1. Validation of overpressure

Overpressure is a major consequence of the explosion accident, and thus it is necessary to investigate whether the shaped equivalent gas cloud can cause overpressure similar to the actual clouds. Since the proposed gas cloud is a combination of several actual clouds, the difference from the actual clouds are inevitable. In other words, it is meaningless to compare the proposed gas cloud with the actual cloud one by one. To carry out the validation, a new type of dedicated error is employed in the present study. The new error is measured by introducing the equivalent overpressure defined in the Eq. (5.10). Considering that the proposed gas cloud is determined using the severity that is analogous to the risk, the equivalent overpressure can be calculated according to the conditions under which the equivalent gas cloud and the actual gas clouds have the same risk.

As illustrated in Fig. 59, the equivalent overpressure is calculated for every single CV with the reference grid using following Eq. (5.8)−(5.10). The calculation is performed with the overpressures caused by each actual cloud and the corresponding individual frequency defined in Chapter 3.

$$P_{eq,i} \cdot f_{exp,JC} - \sum_{for\ all\ j} P_{i,j}^{ac} \cdot f_{ign,j} = 0 \tag{5.8}$$

$$f_{exp,JC} = \sum_{for\ all\ j} f_{ign,j} \tag{5.9}$$

$$P_{eq,i} = \sum_{for\ all\ j} \frac{P_{i,j}^{ac} \cdot f_{ign,j}}{f_{exp,JC}} \tag{5.10}$$

where $P_{eq,i}$ refers to the equivalent overpressure of i^{th} CV with the reference grid and $P_{i,j}^{ac}$ is the actual overpressure of i^{th} CV caused by the j^{th} actual cloud. $f_{exp,JC}$ and $f_{ign,j}$ represents the explosion frequency of the joint category and the individual frequency of the j^{th} actual cloud, respectively. The sum of all individual frequencies is equal to the explosion frequency of the joint category according to Eq. (4.14). The new error is then calculated by using the overpressure caused by the shaped equivalent gas cloud, i.e. $\hat{P}_{eq,i}$ and the equivalent overpressure $P_{eq,i}$ calculated by Eq. (5.11).

$$E_i = \frac{\hat{P}_{eq,i} - P_{eq,i}}{P_{eq,i}} \tag{5.11}$$

where E_i refers to the error of i^{th} CV with the reference grid.

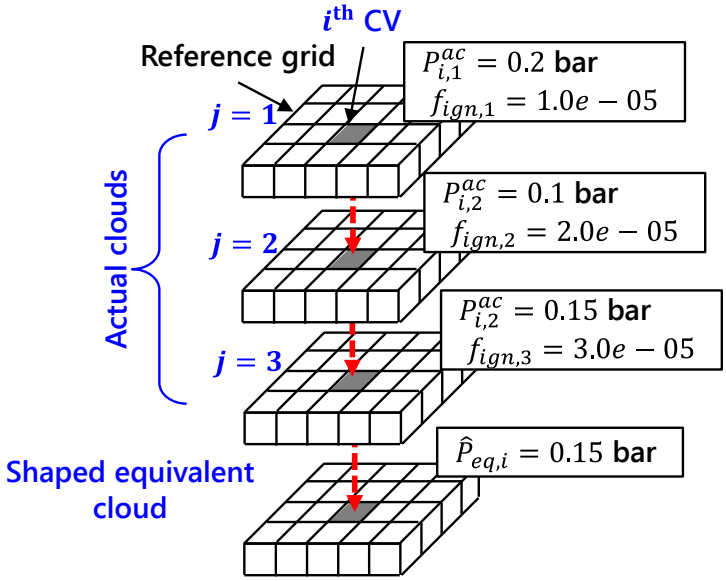

$$P_{eq,i} = \frac{(0.2\times1.0+0.1\times2.0+0.15\times3.0)}{(1.0+2.0+3.0)} = 0.142 \text{ bar}$$

$$E_i = \frac{0.15 - 0.142}{0.142} = 5.88\%$$

Fig. 59 Example of calculating overpressure error

In order to calculate the equivalent overpressure corresponding to a joint category, the explosion simulation should be performed for each actual cloud to get the $P_{i,j}^{ac}$ shown in Eq. (5.3). In general, however, the number of actual clouds in a joint category is enormous, especially for small ESC volumes. Therefore only two joint categories are examined and the actual gas clouds for the two test joint categories are listed in following Table 6 and Table 7, respectively. Both joint categories have been chosen to increase the confidence in validation with the actual clouds coming from various leak scenarios, including different leak location, rate and direction.

Table 6 Actual gas clouds for test joint category I

Leak scenario No.	Time	Individual Frequency
150075	397	3.89E−09
150075	398	3.70E−09
150075	399	3.52E−09
150075	400	2.96E−09
150075	401	2.96E−09
150075	402	2.59E−09
150075	403	2.41E−09
150075	404	2.22E−09
150075	405	1.94E−09
250073	388	8.40E−09
250073	389	9.27E−09

Table 7 Actual gas clouds for test joint category II

Leak scenario No.	Time	Individual Frequency
150061	405	4.88E−10
150061	406	4.88E−10
150061	407	4.88E−10
150061	408	4.88E−10
150061	409	4.88E−10
150061	410	4.88E−10
150061	411	4.88E−10
150071	415	9.26E−11
150071	416	9.26E−11
150071	417	9.26E−11
150071	418	9.26E−11

The leak scenario number refers to the job number of the gas dispersion simulation applied in FLACS (Gexcon, 2015). The first number indicates the segment (or leak position) involved in the leak scenario (i.e. 1 for the 1st segment and 2 for the 2nd segment shown in Fig. 22). In addition, the last number and the penultimate number indicates the leak direction and initial leak rate, respectively. Given the meaning of these numbers, the actual clouds in test joint category I come from the two scenarios with two different segments and two different leak directions. In the same way, the actual clouds in test joint category II originate from two leak scenarios, both of which are investigated by the same segment and the leak direction. The difference however is that they represent different initial leak rates.

Those actual clouds are also presented in Fig. 60 and Fig. 61, and compared with three different equivalent gas clouds graphically. Each gas cloud shown in the figures is represented using the mass fraction distribution. The “Cubic_ESC” indicates the equivalent gas cloud whose size and position are determined by MVFD automatically. Such clouds are the same as the clouds shown in Fig. 34. The “Shaped_ENSC” and “Shaped_ESC” refer to the shaped equivalent gas clouds proposed by the present study.

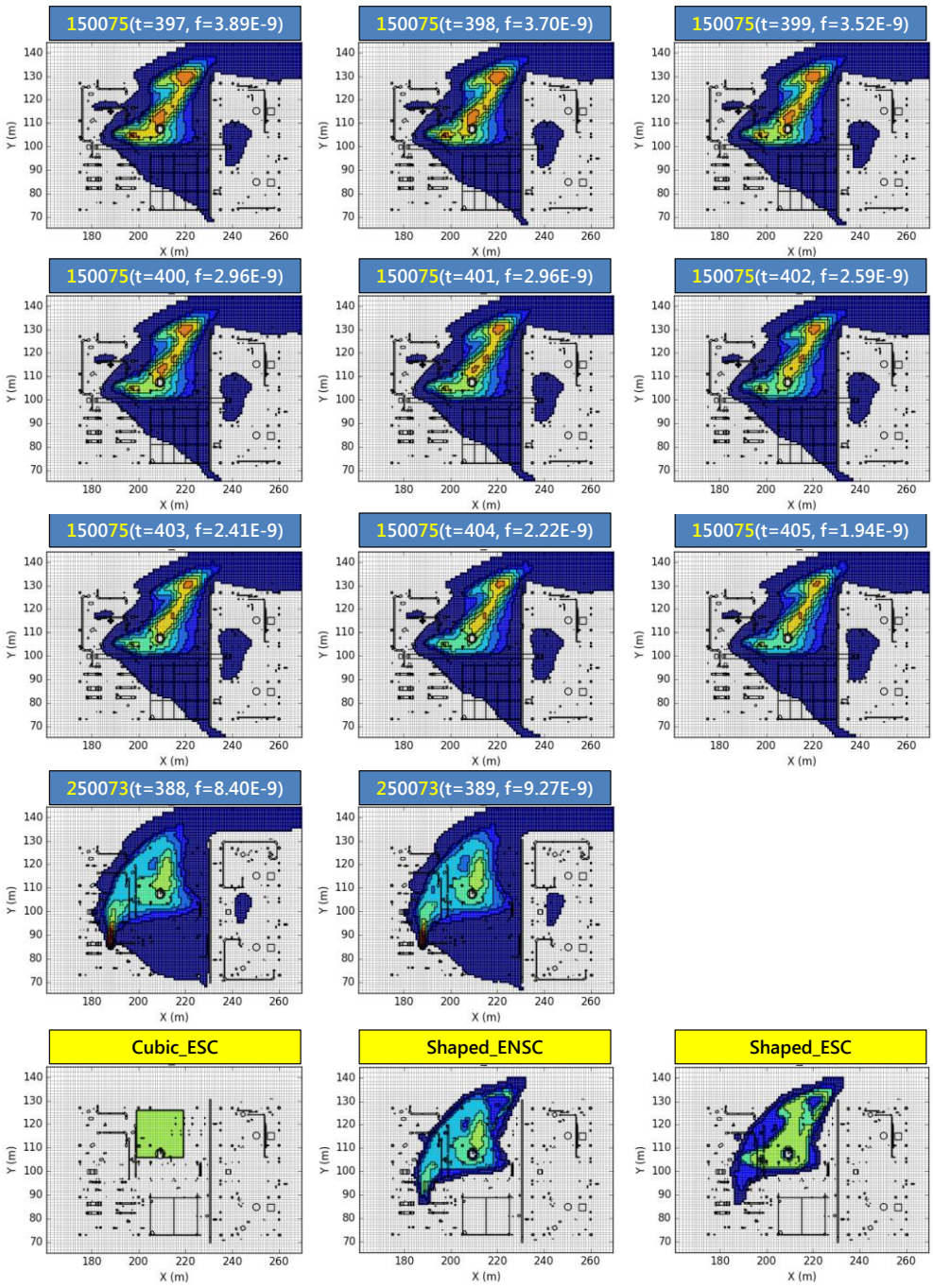

Fig. 60 Actual gas clouds and equivalent gas clouds for test joint category I

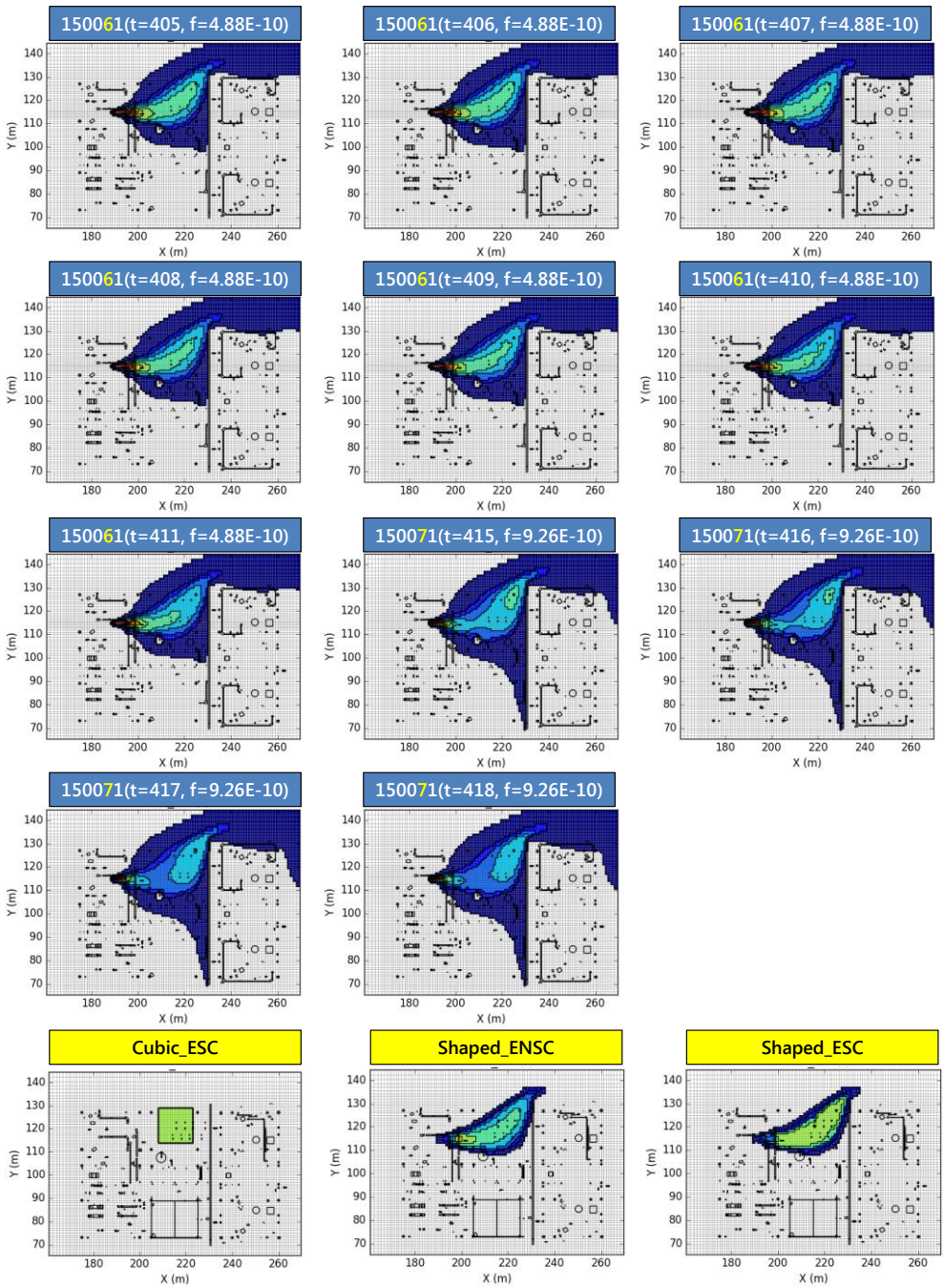

Fig. 61 Actual gas clouds and equivalent gas clouds for test joint category II

The validation results are presented in Fig. 62 to Fig. 65. The error can be calculated for the entire 3D calculation domain using the Eq. (5.4). For convenience, however, the error is only plotted in a 2D plan view of certain elevations and cross sections. Fig. 62 and Fig. 63 show the errors in X−Y plane (elevation), and Fig. 64 and Fig. 65 show the errors in X−Z plane (cross section). For test join category I, the errors caused by “Shaped_ESC” and “Cubic_ESC” are generally similar, but both are higher than the “Shaped_ENSC”. Whereas, for test joint category II, the error caused by the “Shaped_ESC” is the largest and the remainder is similar to the test joint category I. The reason why the “Shaped_ESC” gives the largest error can be explained by the fact that its fuel mass difference with the actual clouds is larger than the “Shaped_ENSC”. Usually, the difference in fuel mass is compensated by adding the dummy CVs, which means that more dummy CVs are needed for the “Shaped_ESC”. The average error for each case is also presented in Table 8 and Table 9, and similar results can be observed for the “Shaped_ESC”. Consequently, the results explain that the “Shaped_ESC” is less reasonable than the “Shaped_ENSC”.

On the other hand, when compared to the “Shaped_ENSC”, the overpressure caused by the “Cubic_ESC” is significantly overestimated or underestimated in certain positions, and this aspect can be problematic when evaluating the exceedance curve for specific targets. The reason can be explained by the improper consideration of the shape of the gas cloud, which is described in more detail in the following section.

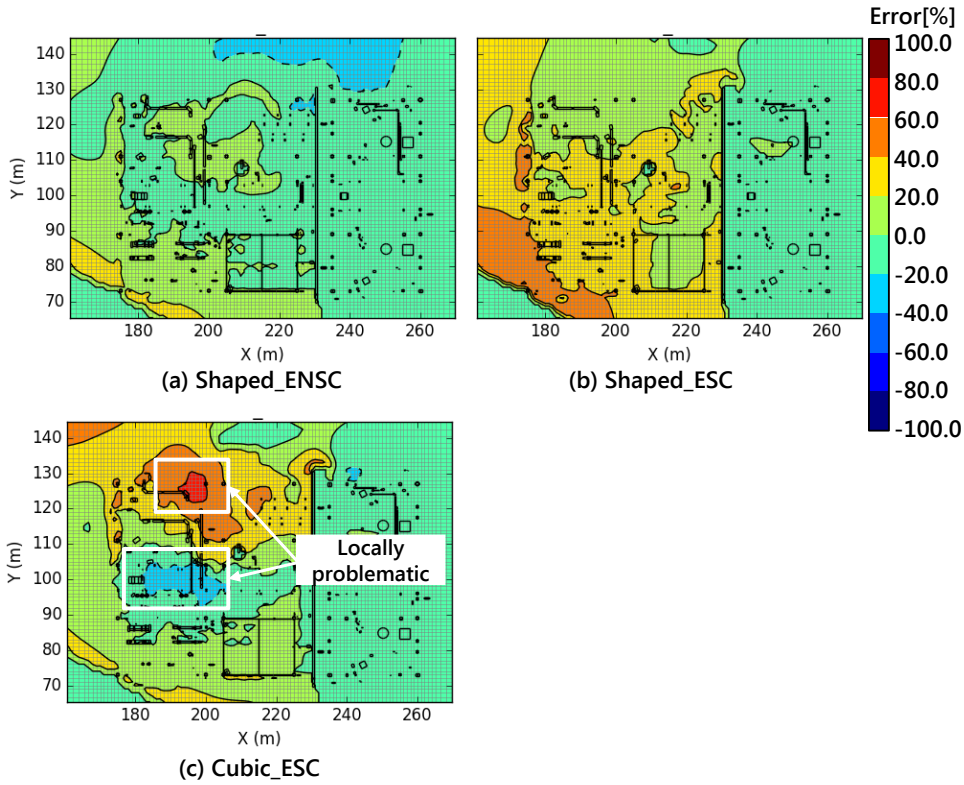

Fig. 62 Error plot of overpressure in X−Y plane for test joint category I

Table 8 Overall errors for test joint category I.

Equivalent Clouds Cloud Type	Error
Shaped_ENSC	+11.896
Shaped_ESC	+24.532
Cubic ESC	+24.843

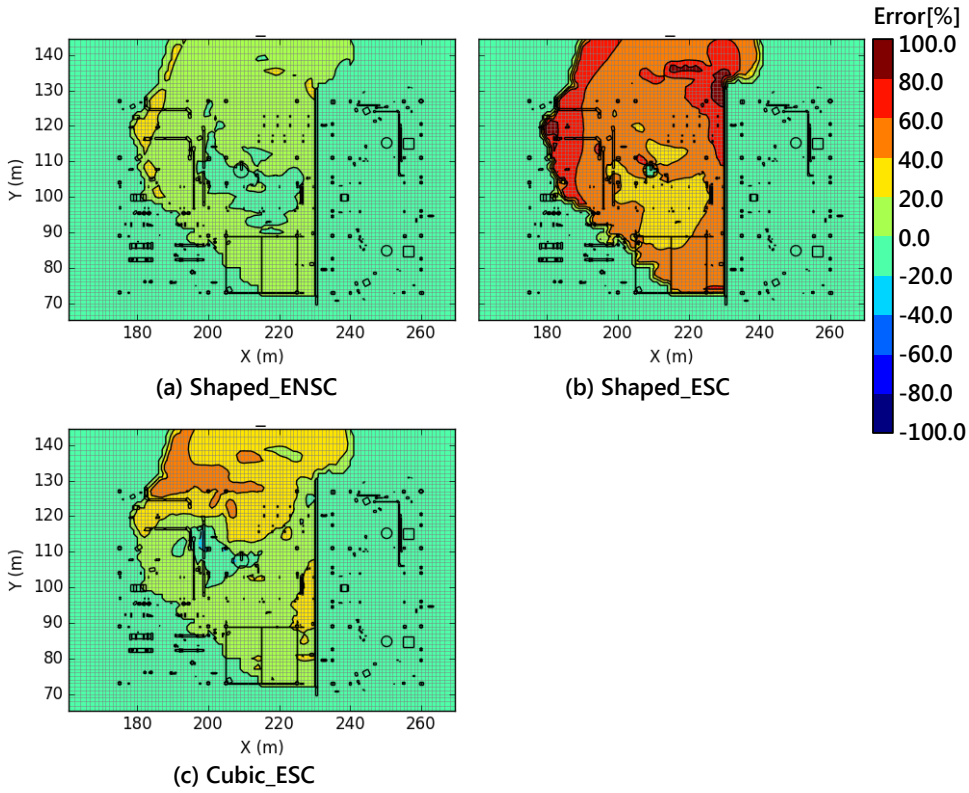

Fig. 63 Error plot of overpressure plot in X−Y plane for test joint category II

Table 9 Overall errors for No.97 joint category II.

Equivalent Clouds Cloud Type	Error
Shaped_ENSC	+7.620
Shaped_ESC	+52.867
Cubic ESC	+28.923

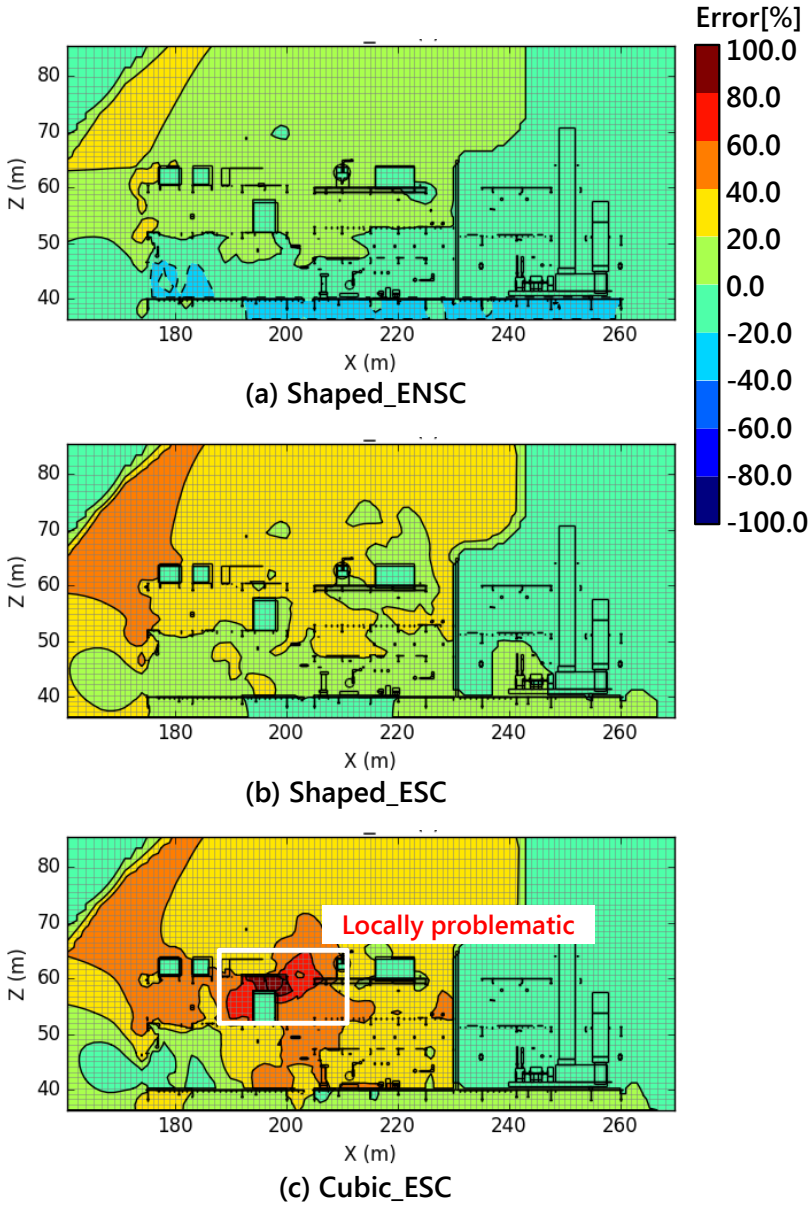

Fig. 64 Error plot of overpressure in X−Z plane for jest joint category I

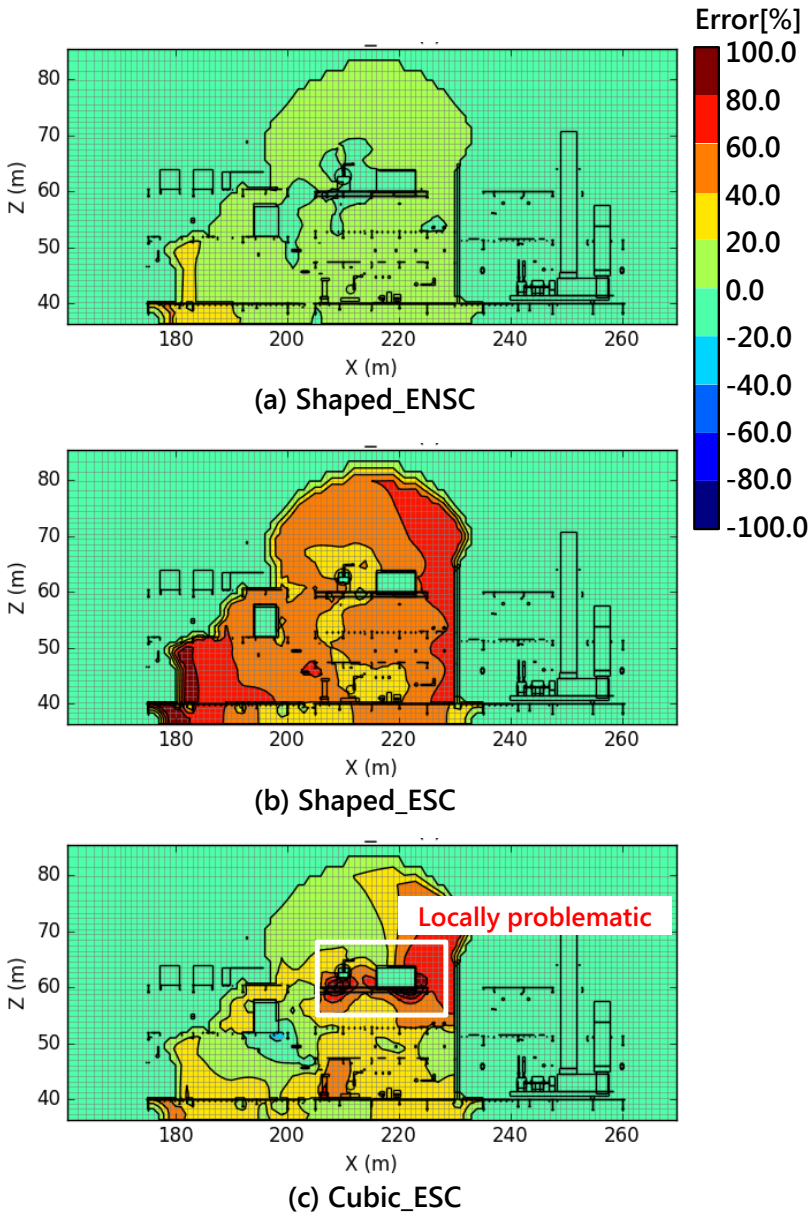

Fig. 65 Error plot of overpressure plot in X−Z plane for jest joint category II

5.5.2. Validation of exceedance curve

In general, the design accident loads (DALs) is determined by overpressure exceedance curve, and thus it is necessary to investigate whether the exceedance curve evaluated by the proposed gas cloud is comparable to that evaluated by the actual clouds. In the MVFD derived in Chapter 4, the total number of joint categories with an explosion frequency greater than zero is 105. This means that the exceedance curves described in Chapter 4 are evaluated with 105 explosion scenarios. However, since the number of the actual clouds corresponding to the 105 explosion scenarios is substantial, it is quite costly to perform the validation using the entire actual clouds. To reduce the computing costs, only eight joint categories are taken into account in the present study. The eight joint categories are listed in Table 10, each representing a different gas cloud size category.

Table 10 Joint categories for verification

Explosion Scenario No.	Joint category ESC volume [m^3]
95	1000-2000
96	2000-3000
97	3000-4000
98	4000-5000
99	5000-6000
100	6000-7000
101	7000-8000
102	8000-9000

In addition, these joint categories are identified by the same gas cloud position shown in Fig. 68 with the range of $X \in (0.6, 0.8)$, $Y \in (0.8, 1.0)$ and $Z \in (0.4, 0.6)$. The MVFD derived in Chapter 4 is presented in Fig. 66 and Fig. 67, and each joint category is also identified in the MVFD. The total number of the actual clouds corresponding to the eight joint categories is 106. Typically, the actual clouds in No. 95 and No. 99 joint categories are listed in Table 11 and Table 12, respectively.

Table 11 Actual clouds in No. 95 joint category

No.	Leak scenario No.	Time	Individual frequency
1	150061	420	2.44E−10
2	150061	421	2.44E−10
3	150061	422	2.44E−10
4	150061	423	2.44E−10
5	150061	424	2.44E−10
6	150061	425	2.44E−10
7	150061	426	2.44E−10
8	150071	423	9.26E−11
9	150071	424	9.26E−11
10	150071	425	9.26E−11
11	150071	426	9.26E−11

Table 12 Actual clouds in No. 99 joint category

No.	Leak scenario No.	Time	Individual frequency
1	150061	380	1.98E-08
2	150061	381	1.44E-08
3	150061	382	1.22E-08
4	150061	383	1.00E-08
5	150061	384	6.34E-09
6	150061	385	6.34E-09
7	150061	386	3.42E-09
8	150061	387	2.20E-09
9	150061	388	2.20E-09
10	150061	389	1.22E-09
11	150061	390	1.22E-09
12	150061	391	7.32E-10
13	150061	392	7.32E-10
14	150061	393	7.32E-10
15	150061	394	7.32E-10
16	150061	395	7.32E-10
17	150061	396	7.32E-10
18	150061	397	4.88E-10
19	150071	372	3.51E-08
20	150071	373	2.56E-08
21	150071	374	1.92E-08
22	150071	375	1.60E-08
23	150071	376	1.10E-08
24	150071	410	1.85E-10
25	150071	411	1.85E-10
26	150071	412	1.85E-10

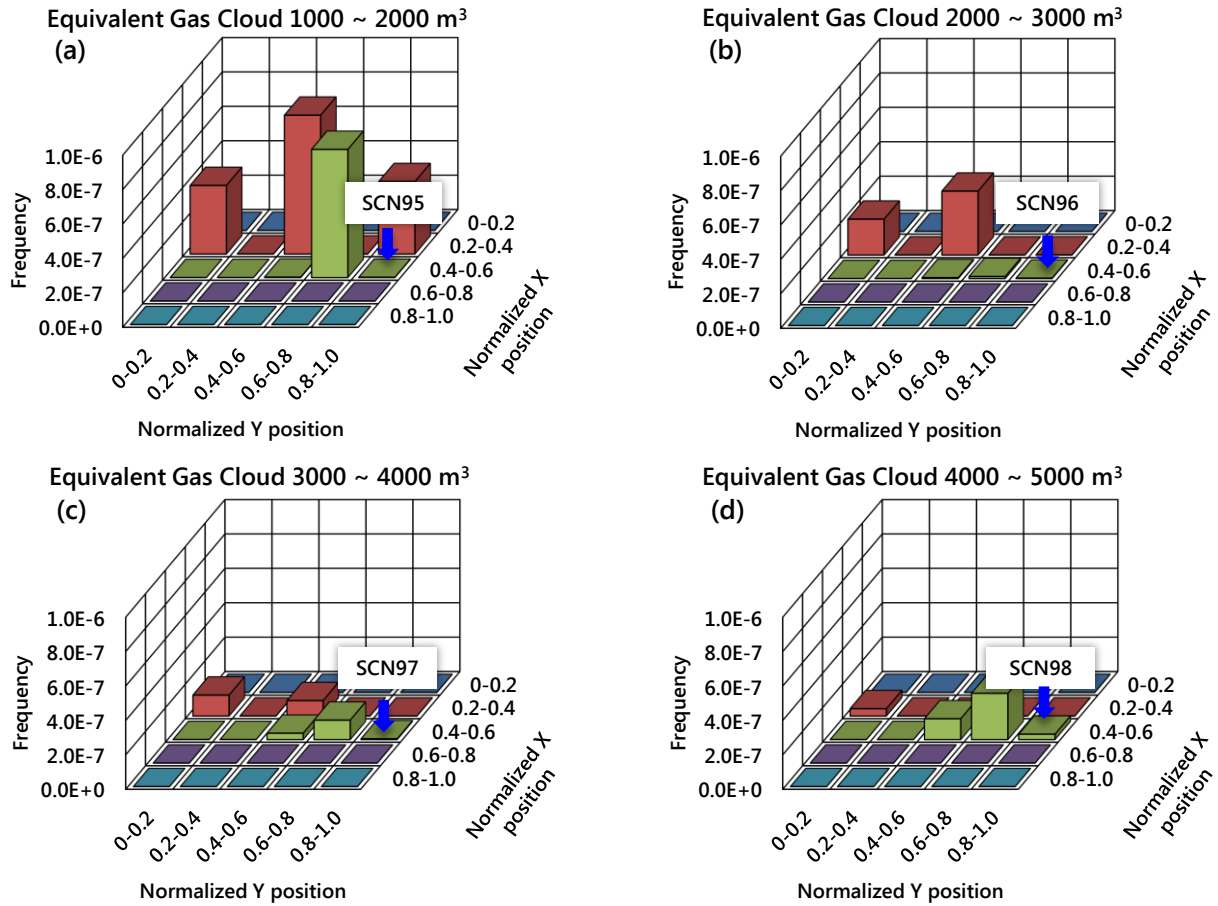

Fig. 66 Joint categories used in validation (No.95−No.98)

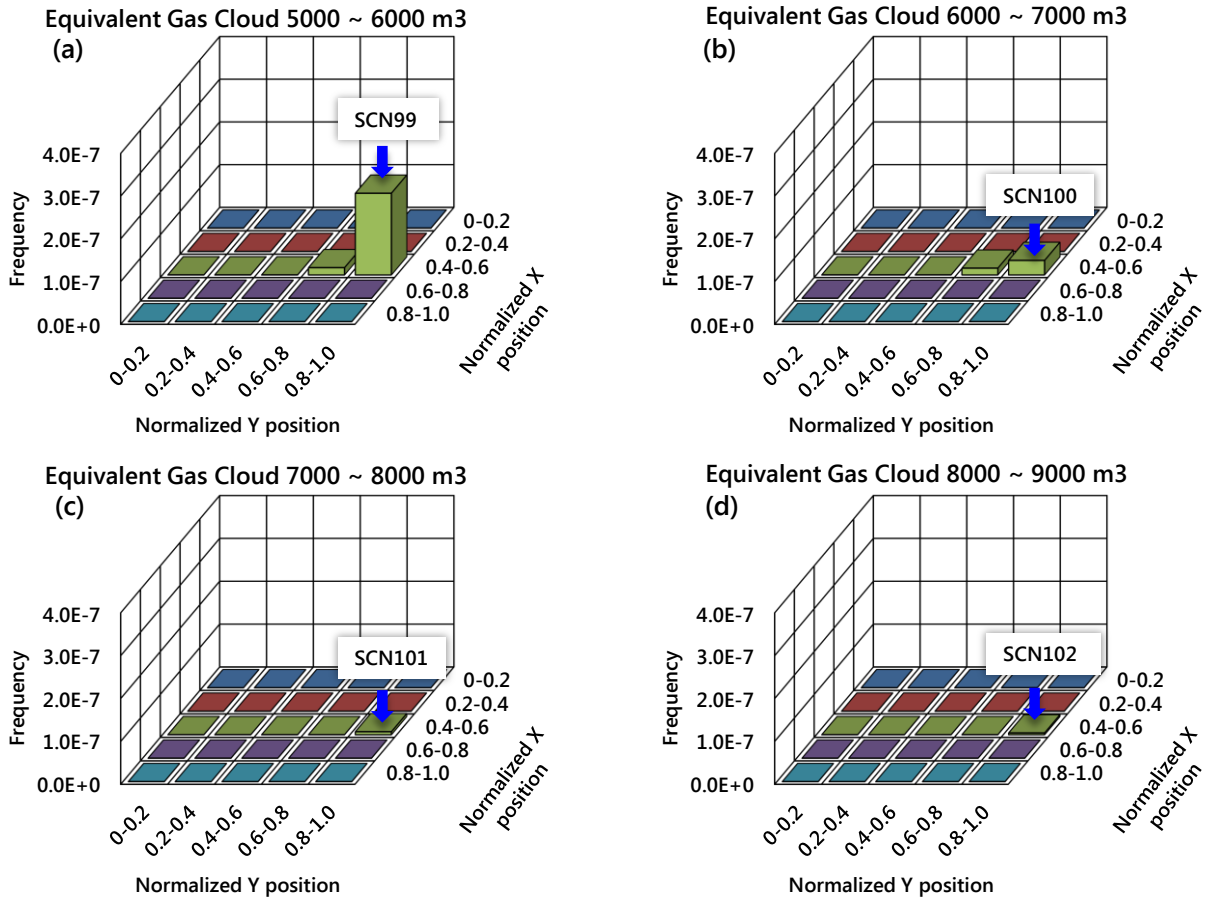

Fig. 67 Joint categories used in validation (No.99−No.102)

The targets for evaluating the exceedance curves keep in consistence with the targets shown in Fig. 26. Furthermore, two specific positions shown in Fig. 68 are additionally considered based on the results of previous validation, where the overpressure error caused by the “Cubic_ESC” is considerably large.

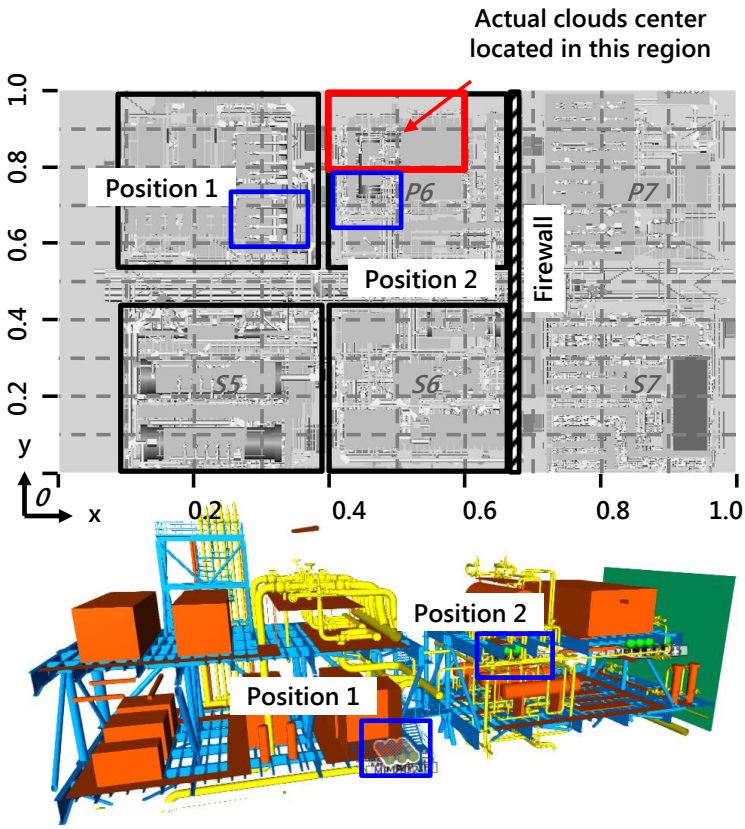

Fig. 68 Two target positions for evaluating exceedance curve.

The results of the evaluated exceedance curves are presented in Fig. 69 to Fig. 72. Generally, the curves evaluated by the “Shaped_ENSC” are more similar to the curves evaluated by the actual clouds than the “Cubic_ESC”. Moreover, when looking into the difference between the actual clouds and the “Shaped_ESC”, the

curves evaluated by the “Cubic_ESC” tend to be overestimated in the S6 and P6 modules but underestimated in the S5 & P5 modules.

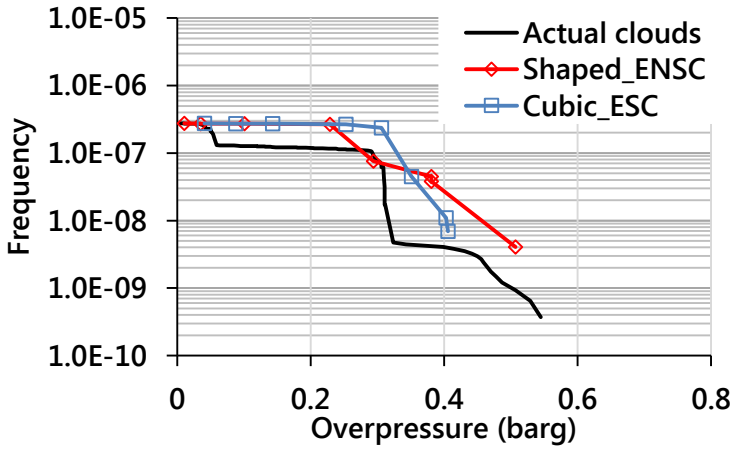

(a) S6-P-U

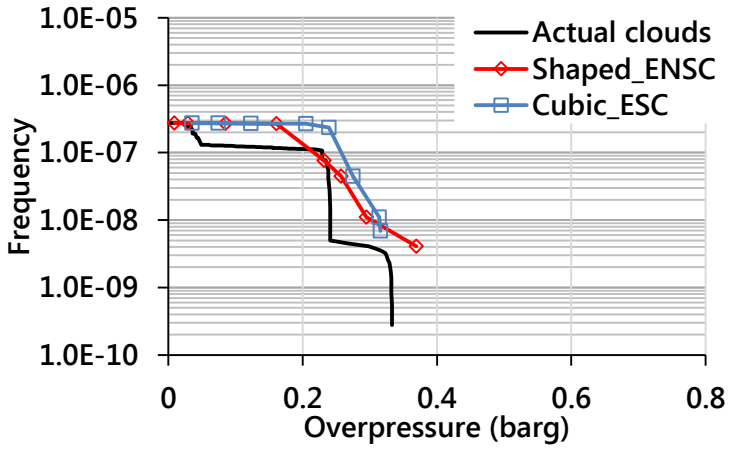

(b) S6-U-T

Fig. 69 Overpressure exceedance curves of S6 module for verification

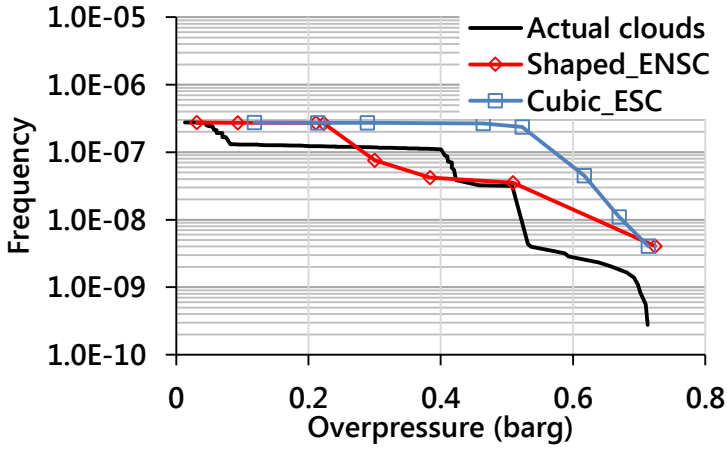

(a) P6-U-M

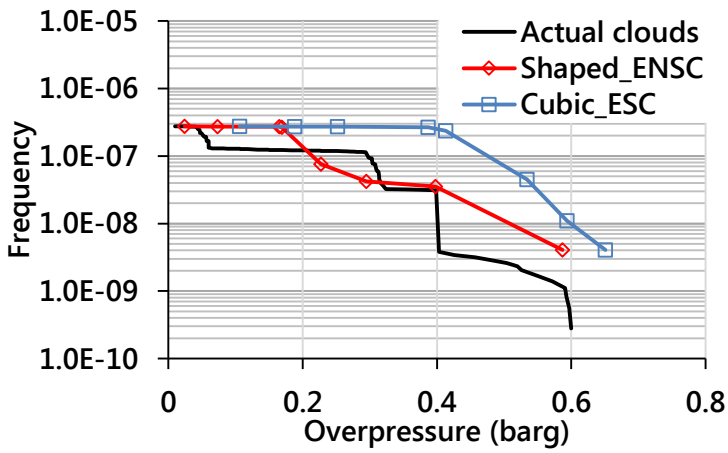

(b) P6-M-T

Fig. 70 Overpressure exceedance curves of P6 module for verification

The difference between the “Shaped_ENSC” and the “Cubic_ESC” can be explained by the aspect that the “Cubic_ESC” dose not correctly account for the shape of the gas cloud. As discussed in the previous section, the shape of gas cloud can determine the path of the flame probation and the meaning of the path has two aspects, including the direction and distance of the flame propagation. When the shape of gas cloud is determined by the “Cubic_ESC”, the the

flame propagation distance may be different from that caused by the "Shaped_ENSC" or the actual clouds and therefore a large difference in resulting overpressure can be expected. Typically, more details have been discussed with the two specific positions shown in Fig. 68.

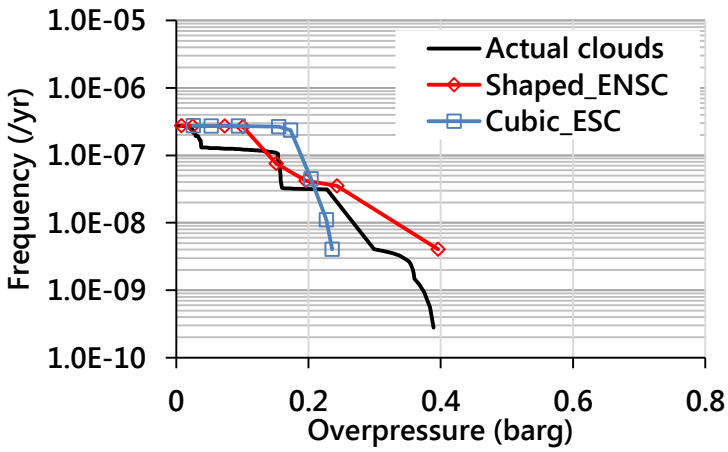

(a) S5-P-U

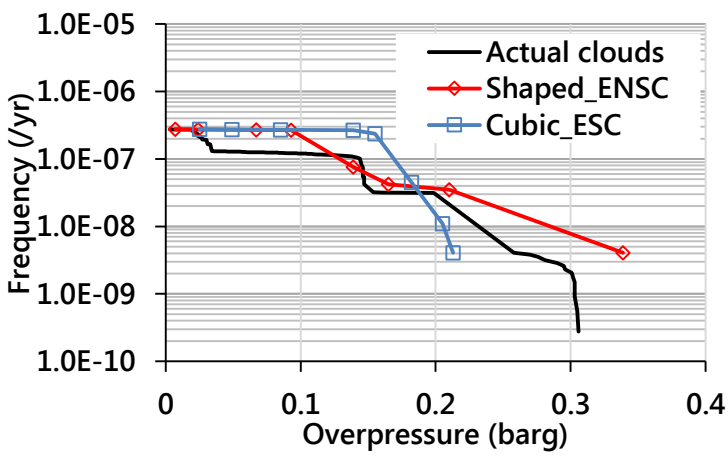

(b) S5-U-T

Fig. 71 Overpressure exceedance curves of S5 module for verification

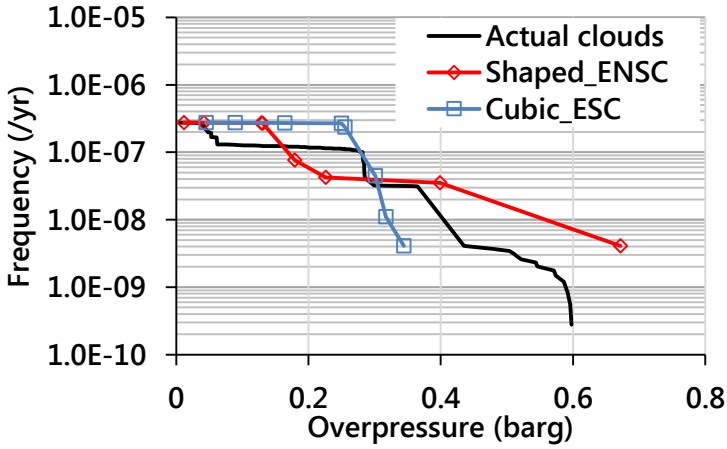

(a) P5-P-U

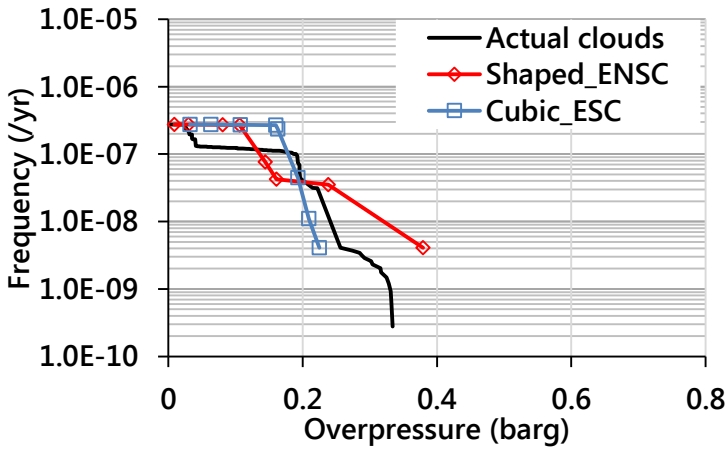

(b) P5-U-T

Fig. 72 Overpressure exceedance curves of P5 module for verification

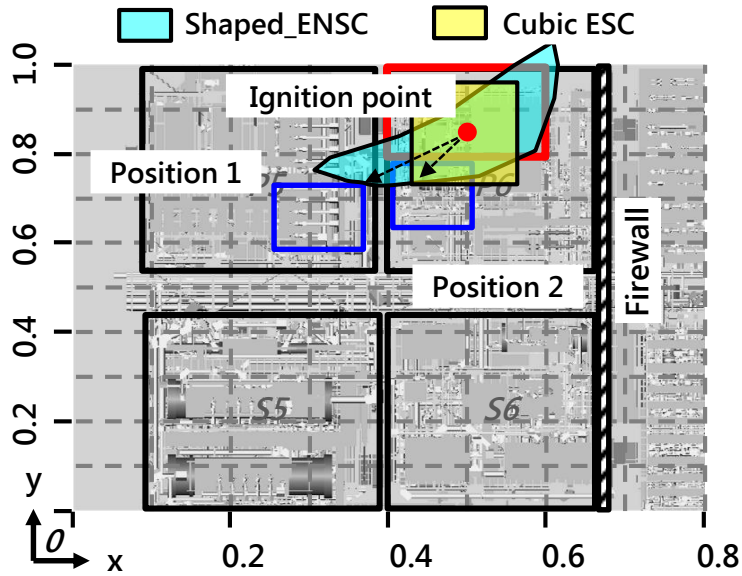

Fig. 73 Difference in flame propagation distance.

From the perspective of the position 1, the “Shaped_ENSC” approaches closer to the position 1 than the “Cubic_ESC” due to its long span of the gas cloud. In other words, this means that in the case of the “Shaped_ENSC”, the flame can propagate up to the position 1, but in the case of the “Cubic_ESC” it can be stopped midway. Therefore, the flame distance caused by the “Cubic_ESC” is shorter than other cases, and consequently the overpressure can be underestimated. For example, in Fig. 74 the maximum overpressure caused by the “Cubic_ESC” is about 0.4 barg, which is relatively lower than the values correspond to the “Actual clouds” or the “Shaped_ENSC”.

On the contrary, in the case of the position 2, little difference is observed in flame propagation distance between the “Shaped_ENSC” and the “Cubic_ESC”, but the difference in maximum overpressure is still evident. In this case, the reason may be explained by the amount of gas cloud rather than the distance of the flame

propagation. In Fig. 73, it can be observed that the total volume of the “Cubic_ESC” is more nearly concentrated to the position 2 than the “Shaped_ENSC”. This implies that in the case of the “Cubic_ESC” a larger amount of gas cloud may contribute to the overpressure buildup at the position 2 and thus the resulting overpressure is generally higher than other cases. For example, in Fig. 75 the maximum overpressure in the case of the “Cubic_ESC” is about 0.8 barg, which is higher than the values correspond to the “Actual clouds” or the “Shaped_ENSC”.

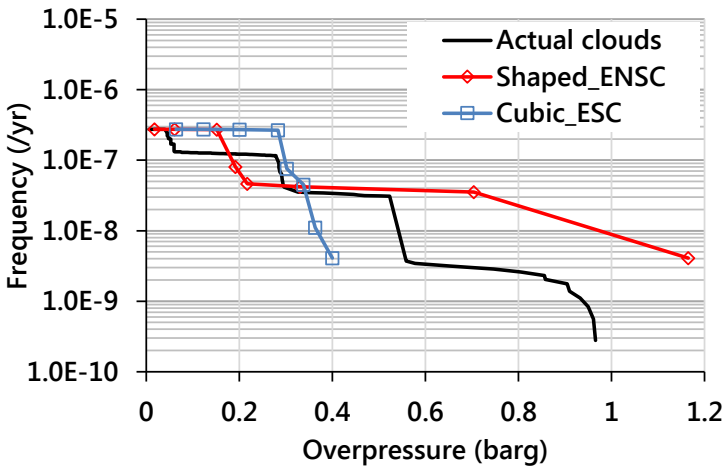

Fig. 74 Exceedance curves of position 1

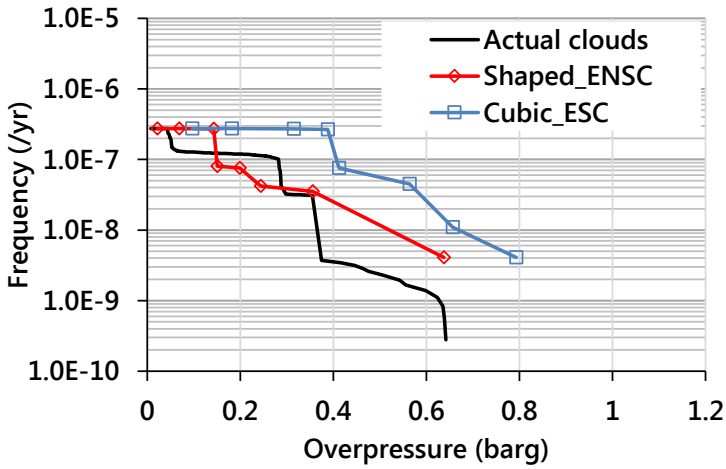

Fig. 75 Exceedance curves of position 2

In summary, when using the "Cubic_ESC" to evaluate the overpressure exceedance curve, the result can be different from that evaluated by the "actual clouds", and the reason is due to misjudgment of the gas cloud shape. On the other hand, when using the "Shaped_ENSC", the resulting overpressure exceedance curve is generally in a good agreement with that evaluated by the "actual clouds". Such results are inevitable because the proposed gas cloud is determined by considering the shapes of the actual clouds.

5.6. Case study

In the present study, case studies are conducted to demonstrate the importance of considering the shape of the gas cloud. Four cases are taken into consideration as listed in Table 13 and the first three cases have already been discussed in Chapter 4. The targets for evaluating the exceedance curves keep in consistence with the targets shown in Chapter 4. The results of case studies are presented in Fig. 76 to Fig. 79.

Table 13 Input cases applied to case studies

No.	Case Name	Gas cloud frequency distribution	Gas cloud position	Gas cloud shape
1	Exisiting_Cubic_ESC_1 (Case I-1 in Part II)	Ignited gas cloud frequency distribution	4 corners and 1 center	Cubic_ESC
2	Exisiting_Cubic_ESC_2 (Case I-2 in Part II)	Ignited gas cloud frequency distribution	4 corners and 1 center (Downwind)	Cubic_ESC
3	MVFD_Cubic_ESC (Case II in Part II)	MVFD	Automatically determined	Cubic_ESC
4	MVFD_Shaped_ENSC	MVFD	Automatically determined	Shaped_ENSC

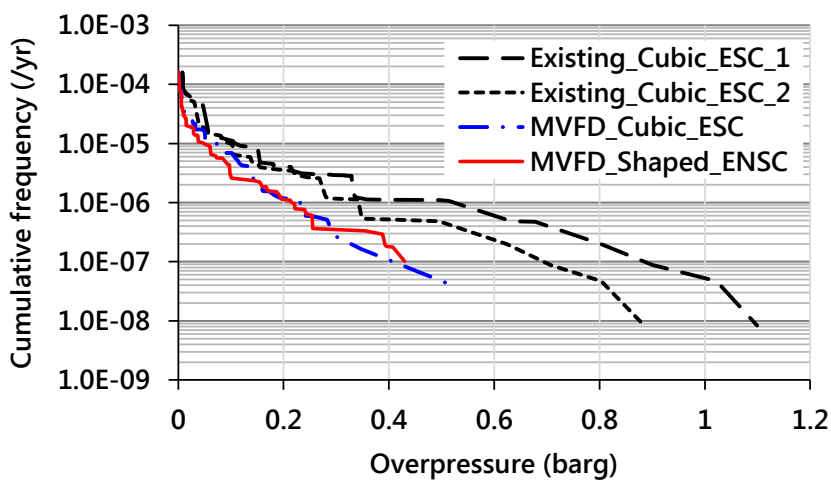

(a) S5-P-U

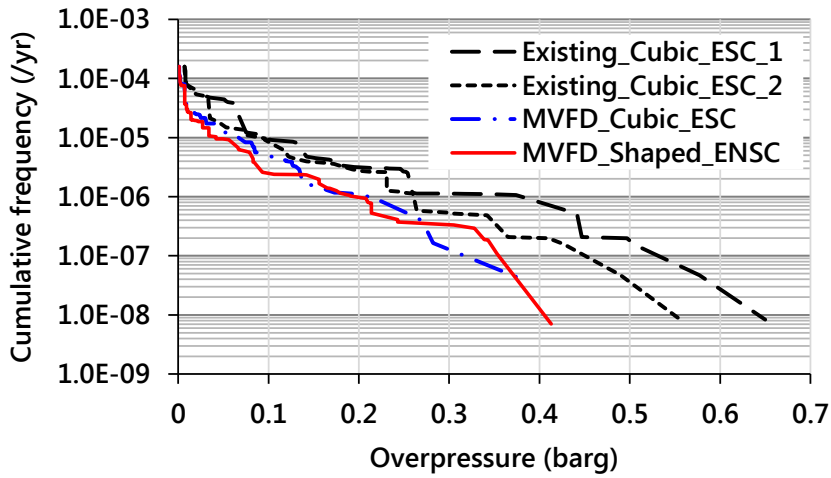

(b) S5-U-T

Fig. 76 Overpressure exceedance curves of S5 module

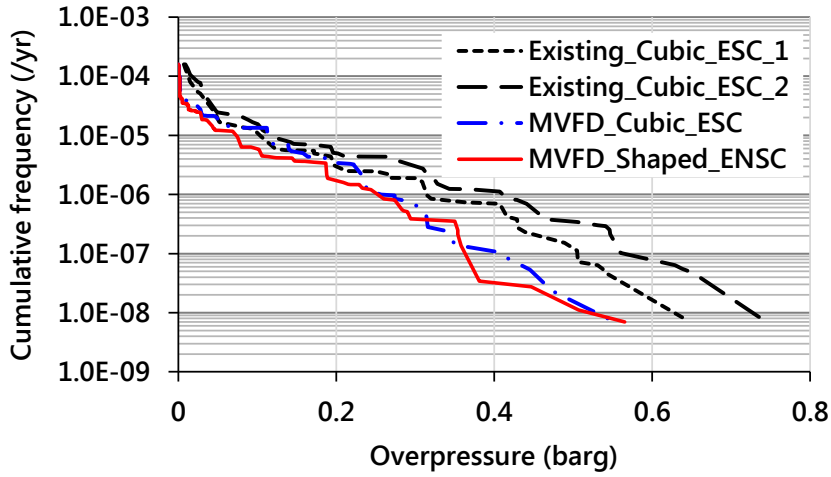

(a) S6-P-U

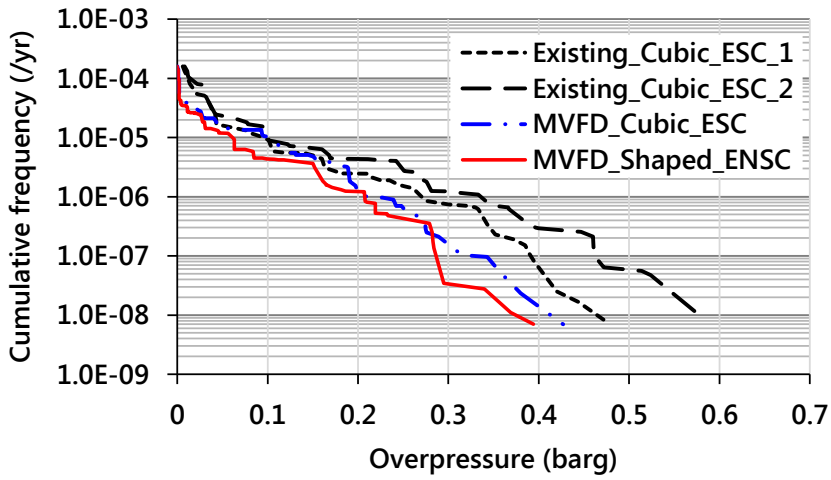

(b) S6-U-T

Fig. 77 Overpressure exceedance curves of S6 module

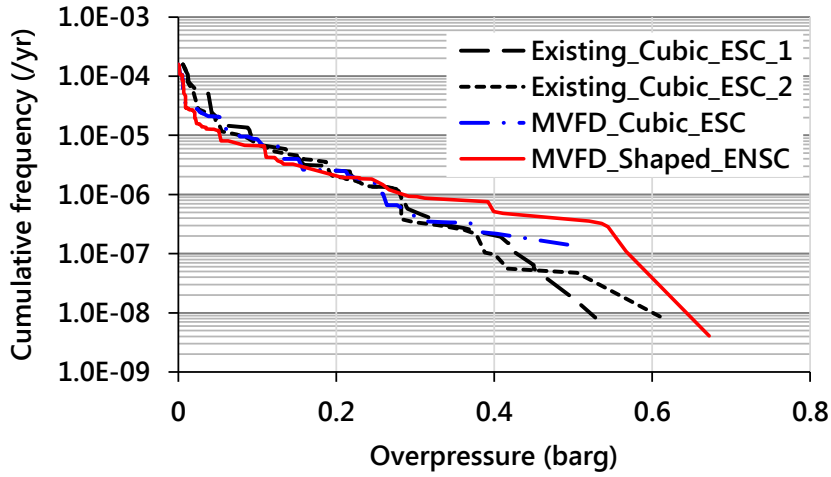

(a) P5-P-U

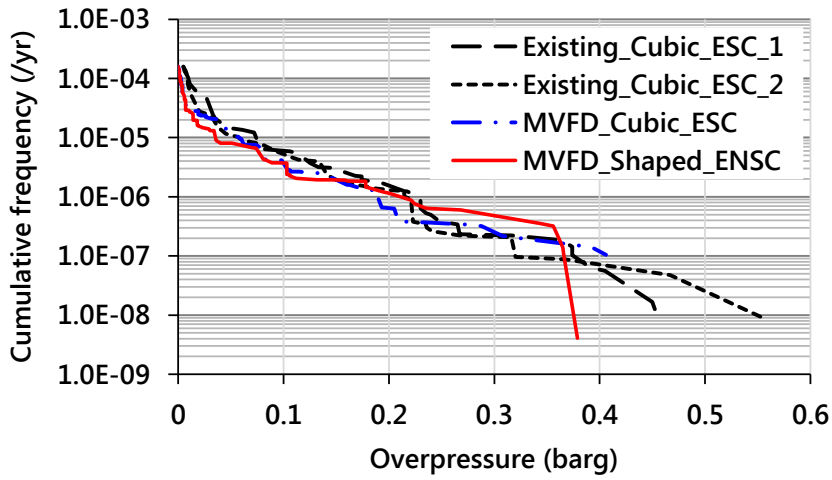

(a) P5-U-T

Fig. 78 Overpressure exceedance curves of P5 module

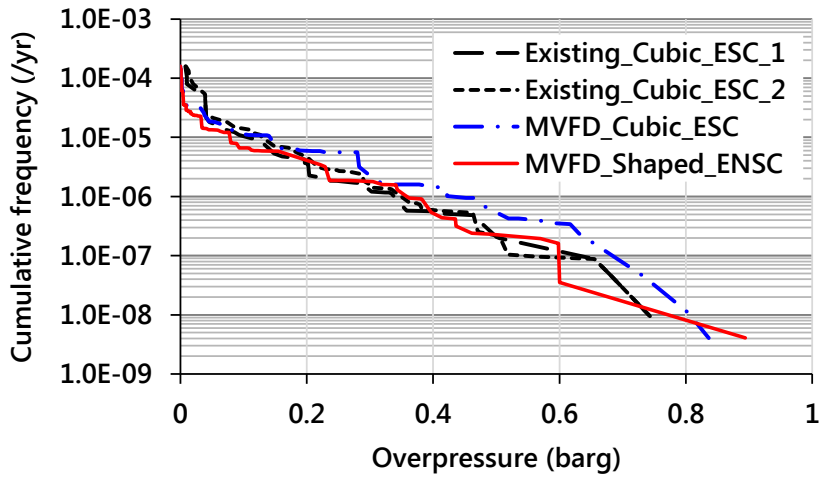

(a) P6-P-U

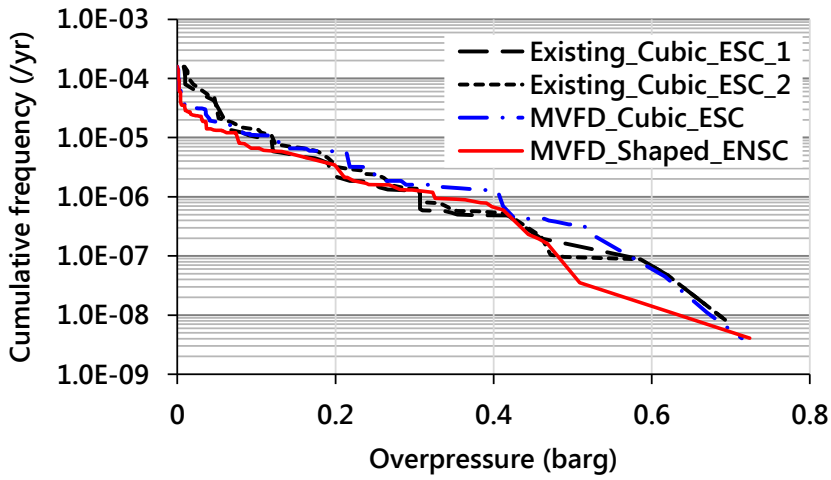

(b) P6-U-M

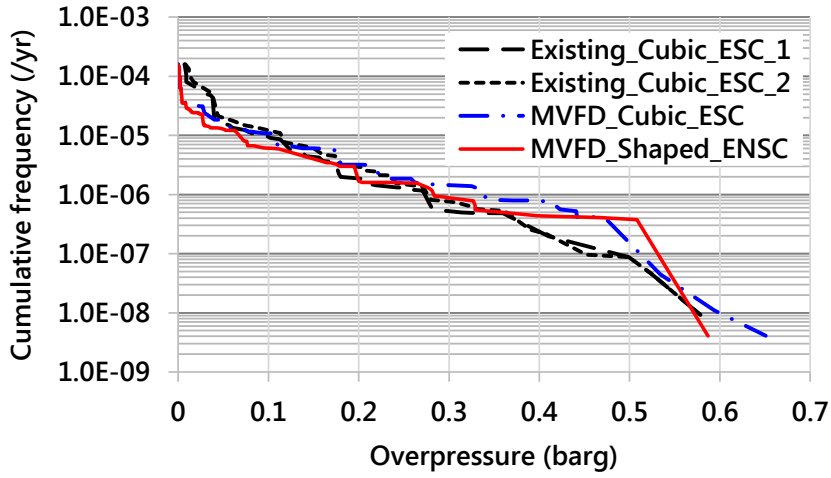

(c) P6-M-T

Fig. 79 Overpressure exceedance curves of P6 module

In general, the “MVFD_Cubic_ESC” and the “MVFD_Shaped_ENSC” tend to be similar compared to the existing two cases, and this implies that the effect of the gas cloud location is more dominant than the effect of the gas cloud shape globally. On the other hand, obvious local difference is observed as well between the “MVFD_Cubic_ESC” and “MVFD_Shaped_ENSC”, and the difference is mainly accounted by the effect of considering the gas cloud shape.

The conservative aspect of the proposed gas clouds (i.e. “MVFD_Cubic_ESC” proposed in Chapter 4, “MVFD_Shaped_ENSC” proposed in the present Chapter.) are also investigated in comparison with the existing gas clouds (i.e. the gas clouds presented in Chpater 3.). As illustrated in Table 14, for S5 and S6 modules, the exceedance curves evaluated with the two proposed gas clouds are generally less conservative than the existing gas clouds, and the reason can be explained by the consideration of gas cloud position as described above. Since the gas positions of the proposed gas clouds are determined according to the results of the dispersion simulations, they can represent the actual gas clouds more accurately. As a result, the less conservative aspects of the exceedance curves are inevitable. On the contrary, for P5 and P6 modules, the exceedance curves evaluated by the proposed gas clouds are more conservative for some specific deck spaces. Particularly, only taking into account the core region of the exceedance curve as shown in Fig. 80, such results become more obvious. For example, in Table 15, the “MVFD_Shaped_ENSC” is more conservative for the P5 module and “MVFD_Cubic_ESC” is more conservative for the P6 module.

Table 14 Overall comparisons with the existing gas clouds

Modules	MVFD_Cubic_ESC	MVFD_Shaped_ENSC
S5-P-U	Less conservative	Less conservative
S5-U-T	Less conservative	Less conservative
S6-P-U	Less conservative	Less conservative
S6-U-T	Less conservative	Less conservative
P5-P-U	Less conservative	More conservative
P5-U-T	Less conservative	Similar
P6-P-U	More conservative	Similar
P6-U-M	More conservative	Similar or less conservative
P6-M-T	More conservative	More conservative

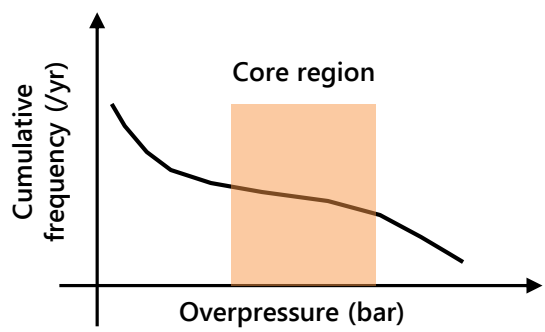

Fig. 80 Core region of overpressure exceedance curve

Table 15 Comparisons with the existing gas clouds (Core region)

Modules	MVFD_Cubic_ESC	MVFD_Shaped_ENSC
S5-P-U	Less conservative	Less conservative
S5-U-T	Less conservative	Less conservative
P6-P-U	Less conservative	Less conservative
P6-U-T	Less conservative	Less conservative
P5-P-U	Similar	More conservative
P5-U-T	Similar	More conservative
P6-P-U	More conservative	Similar
P6-U-M	More conservative	Similar
P6-M-T	More conservative	More conservative

The occurrence of such opposite trends is also due to the consideration of the shape of the gas cloud. As illustrated in Fig. 81, considering the shape, a longer flame propagation is expected with the “Shaped_ENSC” in P6 module, which results in more conservative exceedance curves for the P5 module. On the contrary, without considering the shape, the gas cloud volume is more concentrated in the P6 module when using the “Cubic_ESC” and therefore the “MVFD_Cubic_ESC” is likely to provide a more conservative exceedance curve for the P6 module. Currently, the ignition location is only considered at the center of the gas cloud, but if the edge ignition is also taken into account, the less conservative aspects may be improved.

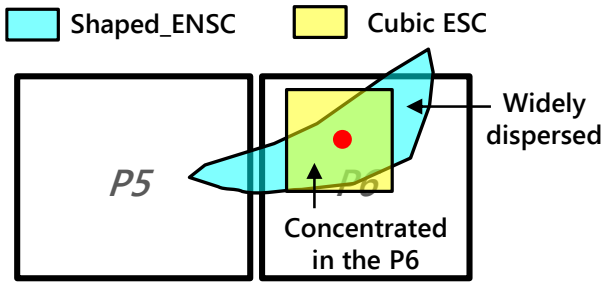

Fig. 81 Comparison of gas cloud shape between “Shaped_ENSC” and “Cubic_ESC”

5.7. Summary

The validations and case studies discussed in the current chapter prove that the resulting overpressure or the exceedance curve can be incorrectly estimated without considering the shape of the gas clouds. When using the proposed gas cloud, i.e. “Shaped_ENSC”, the accuracy of the ERA results can be improved, but the results may not be always conservative. Generally, for most targets, the proposed gas cloud yields less conservative results than the existing gas clouds. In order to improve the accuracy of the ERA results, however, the low conservatism is enviable and can be acceptable.

Conclusion

The concept of using the gas cloud frequency distribution to investigate explosion scenarios is an important aspect in the probabilistic ERA methodology. However, the existing approaches have some limitations in investigating the explosion scenarios, which consequently affect the accuracy of ERA results. The limitations can be summarized in three points as below. In response to the limitations, several solutions have been proposed, each discussed in Chapter 3 to 5.

i. Incomplete consideration of the entire gas cloud propagation,
ii. Conservative determination of the gas cloud position and shape.
iii. The possibility that the ERA results may vary depending on the determined gas cloud position and shape.

In the existing approaches, the simplifications in CFD application cause many problems for deriving the frequency cloud distribution. These problems are embodied in the issues with respect to the accuracy of CFD gas dispersion modelling itself, and the possibility of reflecting the entire transient process of gas cloud propagation. Among them, the latter can form a key part in the whole ERA process, which may influence the accuracy of ignition probability as well as the resulting gas cloud frequency distribution. Focusing on this, in Chapter 3, a new type of gas cloud frequency distribution, i.e. ignited gas cloud frequency distribution is proposed by introducing a concept of individual frequency. The proposed distribution can afford to fully reflect a transient process of gas

cloud propagation whilst without raising the problem of having heavy computational demands for the CFD simulations. The key point resides in finding a proper CFD simulation duration using the magnitude of the individual frequency. Regarding this, case studies for validation are presented, and in general good results are seen when discarding the 3rd phases in time-varying leak rates. Therefore the corresponding proposed approach is very worthwhile for reflecting the time-varying leak rates.

On the other hand, using the ignited gas cloud frequency distribution, it is also possible to look into the importance of the transient process of gas cloud propagation. For that, another case study is also carried out in Chapter 3, in which the gas clouds are both partially and fully monitored by varying the time interval. The results are investigated in terms of the proposed distribution as well as overpressure exceedance curves. It can be observed that when the clouds are partially monitored using a time interval greater than 1s, the resultant distribution and the exceedance curves may generally be overestimated. In particular, when the clouds are monitored very coarsely, considerable differences from the fully monitored case (i.e. the base case) are expected in the high-level categories. As a result, it is concluded that using a certain number of clouds to derive the gas cloud frequency distribution is not reasonable and is not recommended.

Considering the gas cloud position, an upgraded version of the ignited gas cloud frequency distribution, i.e. MVFD is proposed in Chapter 4. The MVFD is designed to automatically determine the cloud position without the conservative engineering judgment. The key point resides in quantifying the cloud position and reflecting it into the previous ignited gas cloud frequency distribution. In this

regard, a specific methodology using the volumetric center of the ESC is proposed. In order to demonstrate the advantage and rationality of the proposed distribution, case studies are carried out and as expected the ERA results evaluated by the proposed distribution are observed better than those evaluated by the existing distribution. With respect to the existing approach, the study described in Chapter 4 proves that the ERA results can vary with the choice of the gas cloud position. In addition, the differences in the ERA results evaluated by both the existing and proposed approaches have proven to be primarily responsible for the size–position mismatched clouds. As a result, it is concluded that the MVFD is more reasonable for investigating the explosion scenario than the existing gas cloud distribution.

Considering the shape of the gas cloud, the concept of shaped equivalent gas cloud shape is proposed in Chapter 5. In association with the MVFD proposed in Chapter 4, the shaped equivalent gas cloud is designed to be determined for each joint category that has an explosion frequency greater than zero. The key point of the methodology is to represent a gas cloud using a certain number of CVs applied to the gas dispersion simulation. The shaped equivalent gas cloud is determined by selecting a certain number of CVs based on the severity calculation. Case studies are also performed to investigate the importance of considering the shape. It has been observed that there is an obvious difference between the case of considering the shape and the case of not considering it. The difference is mainly caused by the different flame propagation paths that determine the explosion consequence, i.e., overpressure distribution. As a result, it is concluded that the accuracy of the

ERA results can be improved if the shape of the gas cloud is taken into account.

In consequence, the overall advantages of the proposed methodology can be summarized into three points:

- Improve the accuracy of ERA results by increasing the utilization CFD gas dispersion simulation results (i.e. the entire gas cloud propagation, the gas cloud position and shaped)
- The time-varying leak rate is taken into account without increasing the computing costs significantly.
- The entire process of investigating the explosion scenarios can be fully automated and thus the ERA results can be uniquely determined.

Compared to the existing approaches, however, the proposed methodology may be less conservative in some cases, but this is inevitable in order to improve the accuracy of the ERA results. The validation work carried out in the present study is limited and the proposed methodology still lacks practical application to other models and input conditions. From an application point of view, the ERA procedure may be much more complex than before, but it can be supplemented by the fact that the proposed methodology can be fully automated. In future studies, the proposed methodology should be improved more accurately through more applications.

References

[1] Alonso, F.D., Ferradás, E.G., Pérez, J.F.S., Aznar, A.M., Gimeno, J.R., Alonso, J.M., 2006. Characteristic overpressure–impulse–distance curves for vapour cloud explosions using the TNO Multi–Energy model. J. Hazard Mater. 137, 734–741.

[2] Alghamdi, S.S.S., 2011. Development a Vapor Cloud Explosion Risk Analysis Tool Using Exceedance Methodology. Texas A&M University, M. Sc.

[3] Azzi, C., Rogstadkjernet, L., Wingerden, K., Choi, J.W., Ryu, Y.H., 2016. Influence of scenario choices when performing CFD simulations for explosion risk analyses: focus on dispersion. J. Loss Prev. Process. Ind. 41, 87–96.

[4] Bakke, J.R., Hansen, O.R., 2003. Probabilistic analysis of gas explosion loads. FABIG Newsletter (34), 22–29.

[5] Dadashzadeh, M., Khan, F.I., Hawboldt, K., Amyotte, P., 2013. An integrated approach for fire and explosion consequence modelling. Fire Saf. J. 61, 324–337.

[6] Dadashzadeh, M., Ahmad, A., Khan, F.I., 2016. Dispersion modelling and analysis of hydrogen fuel gas relased in an enclosed area: a CFD–based approach. Fuel 184, 192–201.

[7] Dan, S.K., Lee, C.J., Park, J.P., Shin, D.G., Yoon, E.S., 2014. Quantitative risk analysis of fire and explosion on the top–side LNG–liquefaction process of LNG–FPSO. Process Saf Environ 92, 430–441.

[8] Davis, S., Hansen, O.R., Rogstadkjernet, L., Bratteteig, A., Berthelsen, I., Davidsen, T.,Holm, J.V., 2011. Benefits of risk–based design through probabilistic consequence

modeling. In: Proceedings of the 7th Global Congress on Process Safety, Chicago, IL, USA.

[9] Det Norske Veritas (DNV), 1998. Ignition Modeling Time Dependent Ignition Probability Model. Report No. 96-3629.

[10] Gexcon, 2015. FLACS User's Manual. Revision 10.4, GexCon A.S., Bergen, Norway.

[11] Gupta, S., Chan, S., 2016. A CFD based explosion risk analysis methodology using time varying release rates in dispersion simulations. J. Loss Prev. Process. Ind. 39, 59-67.

[12] Hansen, O.R., Middha, P., 2007. CFD-based risk assessment for hydrogen applications. In: Proceedings of the AIChE Spring National Meeting & Forty-first Annual Loss Prevention Symposium, Houston, US, pp. 235-258.

[13] Hansen, O.R., Talberg, O., Bakke, J.R., 1999. CFD-based methodology for quantitative gas explosion risk assessment in congested process areas: examples and validation status. In: Proceedings of the International Conference and Workshop on Modeling the Consequences of Accidental Releases of Hazardous Materials. San Francisco, CA, USA, pp. 457-477.

[14] Hansen, O.R., Gavelli, F., Davis, S.G., Middha, P., 2013. Equivalent cloud methods used for explosion risk and consequence studies. J. Loss Prev. Process. Ind. 26, 511-527.

[15] Hansen, O.R., Kjellander, M.T., Martini, R., Pappas, J.A., 2016. Estimation of explosion loading on small and medium sized equipment from CFD simulations. J. Loss Prev. Process. Ind. 41, 382-398.

[16] Hoorelbeke, P., Bakke, J.R., Renoult, J., Izatt, C., 2006. Vapor cloud explosion analysis of onshore petrochemical facilities. In: Proceedings of the ASSE-MEC 7th Professional Development Conference and Exhibition, Kingdom of Bahrain, pp. 248-261.

[17] HSE, 2002. A Review of the State-of-the-art in Gas Explosion Modeling. Health and Safety Laboratory Report CM/00/04.

[18] Jin, Y.L., Jang, B.S., 2015. Probabilistic fire risk analysis and structural safety assessment of FPSO topside module. Ocean Eng. 106, 725-737.

[19] Jin, Y.L., Jang, B.S., 2016. Fire risk analysis procedure based on temperature approximation for determination of failed area of offshore structures: Living quarters on semi-drilling rig. Ocean Eng. 126, 29-46

[20] Jin, Y.L., Jang, B.S., 2018a. Probabilistic explosion risk analysis for offshore topside process area. Part I : A new type of gas cloud frequency distribution for time-varying leak rates. J. Loss Prev. Process. Ind. 51, 125-136.

[21] Jin, Y.L., Jang, B.S., 2018b. Probabilistic explosion risk analysis for offshore topside process area. Part II : Development of gas cloud multivariate frequency distribution (MVFD). J. Loss Prev. Process. Ind. 51, 150-168.

[22] Jin, Y.L., Jang, B.S., 2018c. Ignition probability modeling based on CFD gas dispersion simulations for probabilistic explosion risk analysis in congested offshore process areas. FABIG Newsletter (73), 20-25.

[23] Khan, F.I., Sadiq, R., Husain, T., 2002. Risk-based process safety assessment and control measures design for offshore process facilities. J. Hazard Mater. 94, 1-36.

[24] Li, J.D., Abdel-jawad, M., Ma, G.W., 2014. New correlation for vapor cloud explosion overpressure calculation at congested configurations. J. Loss Prev. Profess. Ind. 31, 16-25.

[25] NORSOK Z-013., 2010. Risk and Emergency Preparedness Analysis. NORSOK Standard, Oslo, Norway Latest version 2010.

[26] Park, S.Y., Jeong, B.G., Lee, B.S., Oterkus, S., Zhou, P.L., 2018. Potential risk of vapour cloud explosion in FLNG liquefaction modules. Ocean Eng 149 , 423-437.

[27] Pula, R., Khan, F.I., Veitch, B., Amyotte, P.R., 2006. A Grid based approach for fire and explosion consequence analysis. Process Saf Environ 84, 79-91.

[28] Qiao, A., Zhang, S., 2010. Advanced CFD modeling on vapor dispersion and vapor cloud explosion. J. Loss Prev. Process. Ind. 23, 843-848.

[29] Ramírez-Marengo, C., Diaz-Ovalle, C., Vázquez-Román, R., Sam Mannan, M., 2015. A stochastic approach for risk analysis in vapor cloud explosion. J. Loss Prev. Process. Ind. 35, 249-256.

[30] Rathnayaka. S., Khan, F.I., Amyotte, P., 2011. SHIPP methodlogy: predictive accident modelling approach. Part I: methodology and model description. Process Saf Environ 89, 151-164.

[31] Rathnayaka. S., Khan, F.I., Amyotte, P., 2011. Accident modeling approach for safety assessment in an LNG processing facility. J. Loss Prev. Process. Ind. 25, 414–423.

[32] Talberg, O., Hansen, O.R., Bakke, J.R., 2000. Recent Advances in CFD-based Probabilistic Explosion Risk Assessment. Major Hazard Offshore, London, UK.

[33] Talberg, O., Hansen, O.R., Bakke, J.R., van Wingerden, K., 2001. Application of a CFDbased probabilistic risk assessment to a gas-handling plant. In: Proceedings of the International ESMG Symposium.

[34] Tauseef, S.M., Rashtchina, D., Abbasi, T., Abbasi, S.A., 2011. A method for simulation of vapour cloud explosions based on computational fluid dynamics (CFD). J. Loss Prev. Process. Ind. 24, 638-647.

[35] Total, 2011. Technological Risk Assessment Methodology. General Specification, GE EP SAF 041.

[36] Villa, V., Paltrinieri, N., Khan, F.I., Cozzani, V., 2016. Towards dynamic risk analysis: a review of the risk assessment approach and its limitations in the chemical process industry. Safety Science 89, 77-93.